Battery Repurposing of Plug-in Electric Vehicles: A Framework for the Integration of Renewable Energy and Electrified Transportation

by

Shahab Shokrzadeh

A Thesis submitted to the Faculty of Graduate Studies of

The University of Manitoba

in partial fulfilment of the requirements of the degree of

Doctor of Philosophy

Department of Mechanical Engineering
University of Manitoba
Winnipeg, Canada

Abstract

A comprehensive framework is presented for the integration of electrified transportation and renewable energy through repurposing batteries of plug-in electric vehicles towards a sustainable energy future. The framework considers future market penetration scenarios of plug-in electric vehicles, availability of batteries at their vehicular end of life, and the storage capacity required to generate base-load wind power in the region of study. The objective is to develop a model that can be used as a policy tool to investigate how different scenarios and pertinent parameters can effectively meet the challenges of sustainability in the energy and transportation sectors when the ultimate goal is to simultaneously displace fossil fuels with new generation of low-cost intermittent renewable energy. A sample case study is performed for Canada to investigate and verify the performance of the model. The analysis shows that the proposed approach can further improve the energy sustainability performance of Canada in 2050 by 1.65–4.11%, depending on the confidence level and in addition to electrification of transportation.

In the framework, a statistical algorithm is developed to calculate the capacity of an energy storage system required for delivering base-load electricity for a wind farm in the future electric grids. The algorithm contributes towards the goal of utilizing low-cost intermittent wind energy to base-load power generation in the future electric grids. The introduced algorithm presents three methods to perform the sizing calculations each representing a scenario associated with the stages of the wind energy industry. The results of the studied case are applied to estimate the cost of wind energy to produce rated power at different confidence levels, which show cost-effectiveness and less intermittency on the power systems allowing for larger penetrations of renewables.

Advanced statistical methods are used to more accurately characterize the operational wind power output versus manufacturer's power curve. This is essential for effective integration of wind power into the power systems. Four parametric and nonparametric models are applied to estimate the power curve of wind turbines based on the available operational wind power data. The results of this study suggest that the penalized spline

regression method presents a better performance over the other analyzed methods.

Finally, an experimental testing is performed in laboratory to show the proof of concept of the capacity degradation of used batteries of plug-in electric vehicles in stationary applications using a 25 kWh repurposed energy storage system obtained from a taxi fleet in their “as-is” condition.

The proposed comprehensive framework herein presents an approach leading to a sustainable transportation system by providing low-cost renewable energy, and can be used as a gold standard to compare other policies like hydrogen energy technologies.

Contributions

This thesis focuses on the development of a framework for the integration of renewable energy and electrified transportation through repurposing batteries of the emerging plug-in electric vehicles towards a sustainable energy system. The presented work also makes a significant contribution to the wind energy industry by developing a statistical algorithm for electric energy storage sizing when the goal is to generate base-load wind power for greater penetration of intermittent renewable energy in the future electric grids. Advanced statistical methods are applied for more accurate estimation of power curves based on operational power data.

Following is the list of particular contributions achieved.

- A comprehensive framework is proposed for the integration of energy and transportation when the ultimate objective is to simultaneously displace fossil fuels in transportation with new generation of renewable energy.

- A simulation model is developed that encompasses the pertinent components of the proposed battery repurposing framework. The developed model can be used to investigate how different scenarios and parameters can effectively meet the challenges of sustainability in the energy and transportation sectors.

- A measure of energy sustainability is introduced and applied to investigate the performance of the proposed framework to develop sustainable energy policy based on addressing energy drivers in its totality.

- A new cost model is proposed to properly assess the cost of delivering base-load power from renewables when they rely on intermittent sources.

- A statistical algorithm is developed for sizing the capacity of energy storage system required for delivering base-load electricity for a wind farm. The presented energy storage sizing algorithm contributes towards the goal of utilizing intermittent wind to base-load generation for a sustainable energy future.

- Advanced statistical models are applied to estimate wind turbine manufacturer's power curves based on operational wind power data. The estimated power curve can be used for the performance monitoring of turbine, power forecasting, and for more realistically sizing the energy storage system.

- An experimental testing is performed in laboratory to show the proof of concept and investigate the capacity degradation of repurposed batteries of plug-in electric vehicles in stationary applications.

Acronyms

The following tables provide a summary of the commonly used acronyms presented in this thesis in the areas of renewable energy, transportation, and the statistical methods used in the analyses. These acronyms are tabulated in the order of their appearance in the text.

Acronym	Description
GHG	Greenhouse gas.
IEA	International energy agency.
2DS	2 degrees (Celsius) scenario.
ICE	Internal combustion engine.
LDV	Light duty vehicle.
PHEV	Plug-in hybrid electric vehicle.
BEV	Battery electric vehicle.
PEV	Plug-in electric vehicle.
GW	Gigawatt.
PV	Solar photovoltaic.
LCOE	Levelized cost of electricity.
MWh	Megawatt hour.
kWh	Kilowatt hour.
EOL	End-of-life.
RER	Renewable energy ratio.
RED	Renewable efficiency demand.
kW	Kilowatt.
ESS	Energy storage system.
EMS	Energy management system.
DOD	Depth of discharge.
$MtCO_2e$	Million tonnes of CO_2 equivalent.
EDV	Electric drive vehicle.
CARB	California air resource board.
ZEV	Zero emission vehicle.
HEV	Hybrid electric vehicle.
FCV	Fuel cell vehicle.
AER	All-electric range.
EV	Electric vehicle.
FEV	Full electric vehicle.
AEV	All electric vehicle.
EVSE	Electric vehicle supply equipment.
AC	Alternating current.
DC	Direct current.
SAE	Society of automotive engineers.

Acronym	Description
EPRI	Electric and power research institute.
OEM	Original equipment manufacturer.
GWh	Gigawatt hour.
NiMH	Nickel-metal hydride.
Mtoe	Million tonnes of oil equivalent.
O&M	Operation and maintenance.
DOE	Department of energy.
NREL	National renewable energy laboratory.
PDF	Probability distribution function.
RSS	Residual sum of squares.
MSPE	Mean squared prediction error.
GCV	Generalized cross-validation.
WPP	Wind power plant.
MET	Meteorological tower.
IEC	International electrotechnical commission.
RMSE	Root mean squared error.
NMAPE	Normalized mean absolute percentage error.
sMAPE	Symmetric mean absolute percentage error.
MAE	Mean absolute error.
PR	Polynomial regression.
LR	Local regression.
CS	Cubic spline.
PS	Penalized spline .
ML	Maximum likelihood.
MM	Method of moments.
CDF	Cumulative distribution function.
LS	Least square.
CEF	Clean energy fund.
BMS	Battery management systems.
BBM	Battery bank module.
GUI	Graphical user interface.
Ah	Ampere hour.
CanWEA	Canadian wind energy association.

Acknowledgments

First and foremost, I would like to thank my academic advisor, Dr. Eric Bibeau, for his direction, support, guidance, and friendship. Dr. Bibeau has shown me how to look at energy issues from a different viewpoint and find effective pathways leading to global sustainability.

Also, I am indebted to Dr. Mohammad Jafari Jozani for all his expertise, guidance, support, and friendship. Thank you for pushing me beyond what I thought I am capable.

I wish to extend my thanks to my PhD examining committee: Dr. David Kuhn, Dr. Ani Gole, and Dr. Jose Etcheverry for their valuable comments and efforts in the evaluation of this work.

I would also like to thank Tom Molinksi at Soft White 60, and Robert Yonza and Jeff Blais at Manitoba Hydro for their support and valuable discussions and comments regarding my work. I also would like to acknowledge the Manitoba Hydro HVDC Center for providing the opportunity of experimental testing; special thanks to Dexter Williams and Dr. Farid Mosallat. Thanks to colleagues at the Renewable Energy Research Group of the University of Manitoba. Special thanks to my friends for their encouragement and support.

I also would like to acknowledge the Natural Sciences and Engineering Research Council of Canada, Canada's AUTO21 Network of Centres of Excellence, and the Manitoba Hydro Chair in Alternative Energy for the financial support.

Finally, I wish to extend my deepest thankfulness to my family, especially to my dear parents for their endless love and support, my dear grandma "Fakhri", and my uncle "Ali" who has been a true mentor in my life.

To Roja, for all her love, inspiration and support!

Contents

List of Tables

List of Figures

Chapter 1

Introduction

This thesis develops an energy sustainability framework for the integration of intermittent and low-cost renewable energy and electrified transportation. Batteries of plug-in electric vehicles are repurposed to be integrated with intermittent wind power after their vehicular end-of-life to obtain a higher share of renewable energy towards a sustainable transportation system. An algorithm is presented for predicting the capacity of energy storage system required to integrate wind energy for base-load power generation at different stages of the wind energy industry. Furthermore, advanced statistical methods are used to model wind turbine power curves based on operational power data. Herein, we first present the problem statement, and briefly review the challenges in the energy and transport sectors. The proposed concept of battery repurposing is then introduced, and the components of the framework are described. The objectives as well as the research questions are presented followed by the the methodology developed to accomplish the proposed objectives. Finally, the outline of the thesis is presented.

1.1 Problem statement

Current trends in global energy supply, energy consumption and environmental emissions are not sustainable, and require substantial investments to promote towards a sustainable energy future [1, 2, 3]. Global energy drivers—peak oil, energy security, climate change, growing demand, emissions—have resulted in adoption of strategic policies that can mitigate risks from a business-as-usual approach. The finite resources of conventional energy and the consequent greenhouse gas (GHG) emissions urge decisive actions towards clean alternatives with less environmental impacts. Electrification of transportation and renewable energy are the key solutions to put the globe on a sustainable foundation.

Transportation is one of the major contributing sectors to the global energy consumption, and has significant environmental impacts as it mostly relies on internal combustion engines (ICEs) driven mainly by fossil fuels. In 2012, transportation accounted for 20% of the global primary energy consumption, and was responsible for 25% of the energy related GHG emissions [4]. The International Energy Agency (IEA) has proposed the 2 degrees scenario (2DS) in which the increase of the earth's average temperature should be limited to 2 °C by 2050. In the 2DS, the transport sector accounts for 21% of CO_2 reductions in 2050 [5]. To achieve such targets and to develop a sustainable approach for light duty vehicles (LDVs), electrification of transportation is emerging as the promising solution [6, 7]. Automakers have started mass production of new technologies like plug-in hybrid electric vehicles (PHEVs) and battery electric vehicles (BEVs), collectively known as plug-in electric vehicles (PEVs), which provide higher fuel efficiency and extended electric range [8, 9]. Also, many governments and policymakers have set ambitious targets for these vehicles in the new sales of LDVs that highlight the critical role of electric mobility in their transportation systems [8, 3].

However, the high cost of propulsion batteries of PEVs and the public perception of electric mobility are among the challenges that should be addressed [3].

The other strategic path towards clean energy alternatives with less environmental impacts is to incorporate more renewable energy in the global energy mix. Expansion of intermittent sources, like wind and solar energy, is the crucial component to the growth of electricity generations from renewables. The global installed capacity of wind power has approached 300 gigawatt (GW) in 2013, *i.e.*, almost double the cumulative capacity in 2008 [10, 11]. The global installed capacity of solar photovoltaic (PV) has also drastically increased reaching more than 95 GW in 2012 [12]. Higher penetration of intermittent wind and solar, however, has technical and economic implications, and can be limited by their stochastic nature. Moreover, according to the IEA's World Energy Outlook 2013, the share of fossil fuels in the global energy mix has remained constant at 82% for the last 25 years. The report also predicts that with significant adoption of renewable energy this figure will only drop to around 75% in 2035 [13]. Besides, huge investments are required to minimize the environmental impacts of fossil fuels and minimize the climate change effects. According to a study by Bloomberg New Energy Finance, the annual world's investment required to avoid more climate damages should be increased from $300 billion in 2014 to $600 billion in 2019 [14].

These statistics highlight the necessity of effective sustainable initiatives which can impact the current trend of the global energy and related emissions status. More important, wind energy is now confirmed to have the lowest levelized cost of electricity (LCOE) in most jurisdictions, where LCOE is an overall competitiveness measure of electricity generation costs by different sources reported in dollar per megawatt hour ($/MWh), or cent per kilowatt hour (¢/kWh) [15, 16]. Therefore, sustainable transportation has to integrate low-cost intermittent renewable energy.

Many studies have attempted to develop a sustainable approach for LDVs in the transport sector while achieving relatively poor performance results, even acting contrary to sustainable objectives. Scenarios that advocate low efficiency or high cost approaches need to move to sustainability, *e.g.*, discussions in [17, 18, 19, 20]. Therefore, real sustainable approaches need to be formulated to impact global energy policy, and provide economically affordable and environmentally sensible energy resources.

1.2 Sensible solution

To address energy challenges, the sensible approach is to simultaneously replace fossil fuels with ***R***enewable energy sources, increase energy ***E***fficiency, and reduce energy ***D***emand, collectively referred to as the RED approach [21, 22]. In compliance with the RED approach that can change the current unsustainable path is the electrification of transportation while addressing the electric energy demand by incorporating intermittent renewable energy sources.

This thesis proposes battery repurposing of PEVs as a sustainable energy framework for the integration of energy and transportation. We investigate how electrified transportation can support higher share of renewable energy to mitigate fossil fuels in the transport sector. Batteries of PEVs can be repurposed for use in different stationary applications when they reach their vehicular end-of-life (EOL), and before being recycled. The goal is to accommodate greater amount of wind power while the energy conversion efficiency of vehicles improves by electrification of the powertrain. The use of existing renewable energy to address new PEV electric loads is not considered, as this has no impact on the renewable energy ratio (RER), and is contrary to the RED approach. More important, the LCOE for wind is the lowest, now reaching a record level of 3.7–8.1 ¢/kWh without subsidies [15]. To develop the repurposing model of PEV batteries for their vehicular and stationary applications, the framework considers plug-in electric vehicles market penetration, availability of batteries at their vehicular EOL, and the storage capacity required to generate base-load wind power in the region of study. Statistical and mathematical models are applied to establish an assembly of information through synthesizing a simulation that encompasses different elements of battery repurposing. To assess the sustainability performance of the proposed approach, RER is defined as the ratio of total renewable energy generated to the total primary energy used for a jurisdiction in a given year [23]. RER can be used as a critical indicator of sustainability and a policy tool that can govern technology implementation.

The proposed framework more closely focuses on wind energy and the integration of the intermittent source for base-load power generation to meet the energy requirements of emerging electric vehicles. Adding adequate energy storage system (ESS) to intermittent wind power can support greater penetration rates of wind energy. Higher share of electricity generation from intermittent wind in the electric grid also motivates the analysis of the performance of wind power generators as uncertainties in the generated output power can cause serious challenges in the energy management systems (EMS), and impact the reliability of the power grid [24]. Therefore, effective integration of wind power into the power systems requires appropriately sized ESS and accurate estimation of the turbine power curve for operational management of wind energy, as well as performance monitoring of turbines [25, 26, 27]. The major components of this framework and the life cycle of these batteries are illustrated in Figure 1.1.

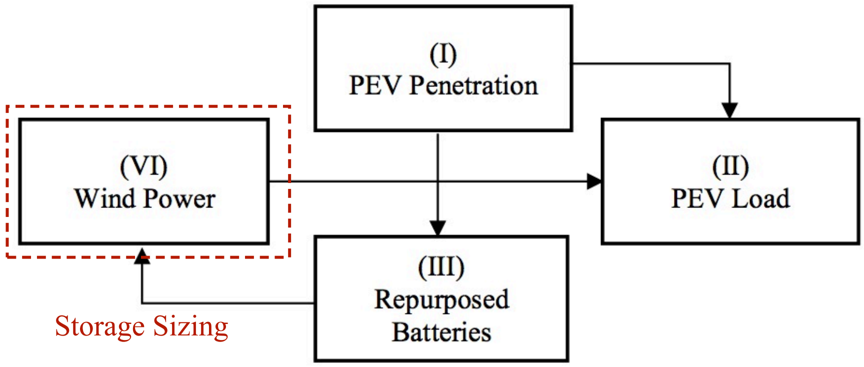

Figure 1.1: Components and the process steps of the proposed framework of plug-in electric vehicles battery repurposing.

1.3 Research objectives

The objectives of this research work are listed below.

1. Synthesize a simulation model to establish a framework that encompasses the components of battery repurposing to investigate how the proposed approach can effectively meet the challenges of sustainability in the energy and transportation sectors by simultaneously displacing fossil fuels in transportation with new generation of low-cost intermittent renewable energy. The model also investigates the performance of the proposed framework as a critical factor to develop sustainable energy policy based on addressing energy drivers in its totality.

2. Create a statistical algorithm for sizing the energy storage system required for delivering base-load electricity for a wind farm. The presented energy storage sizing algorithm contributes towards the goal of utilizing intermittent wind to base-load generation for a sustainable energy future.

3. Introduce a new cost model to establish a proper baseline for economic assessment of base-load power generation of intermittent renewable energy sources that

require storage.

4. Apply advanced statistical models to estimate wind turbine manufacturer power curves based on available operational wind power to more realistically demonstrate the performance of wind power generators.

5. Perform an experimental testing in laboratory using a 25 kWh repurposed energy storage system to monitor and show the proof of concept of the capacity degradation of repurposed batteries of PEVs in stationary applications.

To achieve the objectives of this thesis, the following research questions need to be addressed:

1. What are the market penetration scenarios for the future adoption of PEVs to realistically represent the diffusion rates? What are the other identified parameters to be included in the framework model? What is the annual electric energy demand required for charging the emerging PEVs?

2. How to calculate the required energy storage capacity when the goal is to generate base-load power from intermittent renewables? What is the cost of producing continuous power when the source is intermittent and requires storage?

3. What statistical methods can be used to provide an efficient estimate of a wind turbine power curve when the operational wind power data are available?

4. How to assess and verify the capacity degradation of PEVs used batteries repurposed for stationary applications in their post-vehicular life? What are the test conditions and the facility requirements to achieve this?

5. How to evaluate the sustainability performance of the jurisdiction of study by implementing the proposed concept as a policy tool?

1.4 Methodology

To implement the battery repurposing framework, the components illustrated in Figure 1.1 need to be developed. A simulation code is built for the pertinent components of proposed framework in MATLAB®. To this end, the model first adopts a penetration scenario of the diffusion of PEVs in the market over the time horizon of the study. Predicting a realistic adoption scenario of PEVs in the automotive market is complex and influenced by various socio-economic parameters [28, 29]. Several studies have attempted to forecast the future diffusion rates of the technology in many jurisdictions worldwide. The PEVs future market forecasts are studied and a benchmark is adopted as the input to the model. The consequent electric energy loads due to introduction of PEVs to the market is also required to be studied within the framework. The framework requires to calculate the available electric energy storage capacity available from retiring batteries of PEVs at their EOL. To achieve this objective, the model considers a life span of the vehicular period, battery life at the EOL, and partial damages and losses. Next task is to develop a sizing model of the required storage capacity for wind power integration to generate a more reliable output of the intermittent source. Based on recent studies, *e.g.* in [30, 31], most robust grid systems today, no matter what the supply mix is, can likely accommodate up to approximately 25% intermittent sources such as wind power without any changes to the electric grid. Penetrations greater than approximately 25% wind and solar renewables on an energy basis will require the use of ESS to integrate these intermittent renewables. The future electric grid can be made 100% renewable with utilizing high penetration of intermittent renewables like wind and solar, that are available just about anywhere in the world, if their intermittent nature is addressed by the addition of an appropriate amount of ESS. These intermittent renewables can be converted to base-load generation by using appropriately sized

ESS to smooth out their intermittency, allowing penetration of up to 100% base-load intermittent renewables for a more sustainable future due to CO_2 and other harmful emissions.

A statistical algorithm is therefore developed for sizing the energy storage system required for delivering base-load electricity to a selected confidence level for a wind farm. There is limited literature on ESS sizing to generate base-load power for a target confidence level. Three methods are presented to perform the ESS sizing calculations each representing a scenario associated with (*i*) wind farm project conception, or, (*ii*) wind farm operation. In each method, statistical models are used to calculate the required ESS energy capacity using wind resource assessment data, operational power data and wind power generator's specifications. Furthermore, effective integration of wind power into the power systems requires accurate estimation of the wind turbine power curve for operational management of wind energy and performance monitoring of turbines. Moreover, accurate estimation of the wind turbine power curve is required to more realistically size the storage capacity for wind energy integration [32]. Advanced statistical models are also used for power curve modeling of a wind turbine for the storage sizing algorithm. Four parametric and nonparametric statistical methods are used to fit the empirical power curve of a wind turbine, and the associated modeling codes are implemented in the R programming environment.

Degradation rates of repurposed batteries in their post-vehicular life is the other challenge that needs considering in the framework model. Many studies have attempted to investigate capacity loss and degradation of Li-ion batteries utilized in electric vehicles, for example in [33, 34, 35]. Various parameters may impact the life of batteries such as depth of discharge (DOD), charging rate, temperature, and calendar age [36, 37, 38]. However, degradation of Li-ion batteries in their automotive life, and then in stationary applications is still under study and needs validating experimental information. To obtain an indication of how electric vehicles used batteries degrade with charging cycles, a short-duration experimental analysis is performed at the test facility at Manitoba Hydro HVDC Center. Repurposed batteries were obtained from a taxi fleet demonstration in Baltimore in the U.S. using Electrovaya batteries. For this purpose, 2 battery packs are used each consisting of 4 modules wherein 24 battery cells are accommodated. The approximate voltage of each repurposed battery pack is 400 V.

Finally, the overall energy sustainability performance of the proposed framework for the studied case is assessed by quantifying the fossil fuel displacement in transportation with base-load wind energy accommodated by PEVs repurposed batteries.

1.5 Outline of the thesis

Chapter 2, presents the development and implementation of the comprehensive model of the PEV battery repurposing framework. A review of the literature on the contributing elements of the proposed battery repurposing framework is provided in this chapter. The review includes technology study, market status and future adoption scenarios of PEVs; energy storage technologies and specifically, electric vehicles propulsion batteries technology; overview of renewable energy technologies with the focus on wind power and its integration in the electric grid; and overall status of studies and publications on PEV repurposed batteries. Major blocks of the proposed repurposing framework are described by identifying related parameters, and building and implementing contributing sub-systems. MATLAB® is also used for programming the related algorithms and calculations in the model.

Chapter 3, presents advanced statistical methods for wind turbine power curve modeling. Four parametric and nonparametric methods are applied to estimate the wind turbine power curve. The results of the simulated methods are applied to an operational wind power data set of a wind farm in North America. The code of the simulation is developed in R programming language. This development is used to determine the required ESS for wind turbines.

Chapter 4 develops a general statistical algorithm for sizing the energy storage system required for delivering base-load electricity to a selected confidence level for a wind farm in the future electric grids. In this chapter, we develop three methods based on parametric and nonparametric statistical models using wind resource assessment data and available wind turbine information representing different stages of a wind farm project–from site selection to operational status. The models associated with the presented methods of sizing algorithm are developed and implemented using R programming language.

Chapter 5 describes the experimental setup of the test facility and specifications of the two battery packs used for the short-duration experimental analysis, and provides the results of monitoring that how repurposed batteries degrade with charging cycles.

Chapter 6 provides the results of the framework simulation for a case study of Canada followed by a discussion on the results and on the energy sustainability performance of the proposed concept.

Finally, Chapter 7 concludes the thesis by providing a summary of accomplishments, the outline of the suggested future work that can be followed upon this research.

Chapter 2

Battery Repurposing Framework

In Canada, transportation has been the major consumer of the total energy consumption 2601.1 PJ in 2010 [39]. In the latest available report by Transport Canada [40], road transportation accounts for approximately 80% of the transportation-related GHG emissions, *i.e.*, equal to 137.5 million tonnes of CO_2 equivalent ($MtCO_2e$) or approximately 19.6% of the total GHG emitted in Canada in 2011. The proposed framework of battery repurposing of PEVs for the integration of electrified transportation and renewable energy is presented in this chapter. The objective is to investigate how electric mobility can support greater share of renewable energy to mitigate fossil fuels in the transport sector. In this framework, repurposed batteries, obtained from PEVs are used at their automotive EOL, as stationary electric storage systems to integrate with intermittent wind power generation. The framework considers PEVs market penetration, annual energy demand for vehicles charging, availability of batteries at their vehicular EOL, and the storage capacity required to generate base-load wind power in the region of study. The simulation model of the proposed framework is coded and a case study is performed to show the results. The developed model of the framework can be extended to various applications and scenarios. A new cost model is proposed to calculate and compare the cost of delivering base-load power from renewables when they rely on intermittent sources. The renewable energy ratio is used as a measure of the energy sustainability to evaluate the performance of the proposed framework,. While this analysis identifies complexities and uncertainties in predicting the outcome of the proposed approach, the results suggest a self-sufficiency of the integrated system to address concerns regarding the impact of vehicular charging energy requirements with renewable energy. This study shows that the battery repurposing framework is a sensible approach that addresses energy drivers simultaneously by displacing fossil fuels with new renewable energy generation, and solves energy and environmental issues in transportation effectively rather than looking at aspects in isolation. The proposed model can be used as a policy tool to investigate the outcome of various scenarios in the energy and transport sectors.

Section 2.1 describes the components of the framework and explains the life cycle of batteries in their vehicular and post-vehicular life. Section 2.2 presents a review of the literature associated with various components of the battery repurposing framework. Section 2.3 describes the MATLAB® code developed to perform the simulation of the proposed framework. Section 2.4 provides a summary of the chapter; and the results of the simulation are presented in a case study in Chapter 6.

2.1 Description of the framework

Battery repurposing of PEVs is an approach in compliance with the RED approach that can address energy and environmental issues simultaneously. The proposed con-

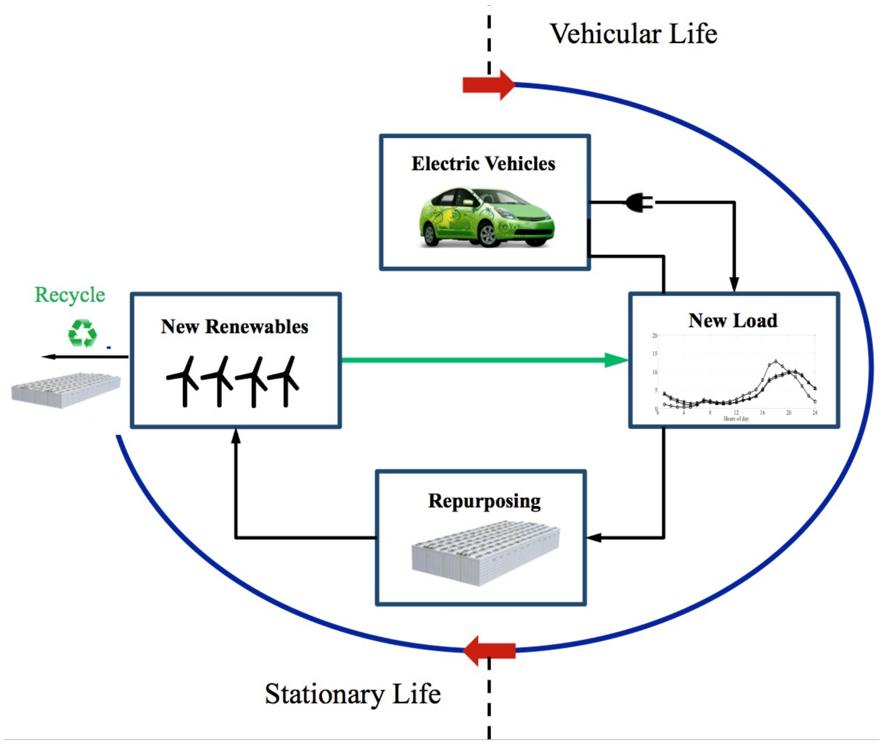

Figure 2.1: Illustration of the battery repurposing concept where the battery life cycle begins with the installation on vehicle where uses electricity for its propulsion. The secondary life begins when the used battery is repurposed for new stationary applications before being recycled.

cept has the potential to increase the share of renewable energy sources in electric power generation, and displace fossil fuels by clean electricity in transportation through electric mobility. Moreover, while the relatively high cost of batteries of PEVs may act as a limiting factor for the wide market adoption of these vehicles [41, 42, 43], battery repurposing has the potential to reduce the initial cost of batteries by creating new market for the used batteries. Several studies investigated the potential value for the traction battery of PEVs at their vehicular EOL [44, 45, 46]. In the repurposing framework, PEV batteries can be reused from electric vehicles after reaching the end of their on-board useful performance, then will be tested, refurbished and employed in different stationary storage applications. Figure 2.1 illustrates the concept with the specific application of supporting intermittent renewables.

The life cycle of batteries begins with the installation of manufactured batteries in electric vehicles, then repurposing for stationary applications, and finally recycling. The components associated with the proposed framework are developed, and the simulation code is built in MATLAB®(see Section 2.3). By implementing the simulation code, the proposed concept model is executed for Canada as a case study. The model selects an annual market penetration rate representing the new sales of electric vehicles in the region of study. Annual aggregate energy demand due to introduction of PEVs to the grid is then calculated to determine the energy impact of the growing market of electric cars. To calculate the storage capacity available from PEV batteries in their post-vehicular life, a benchmark degradation rate is assumed based on the available literature. A wind-storage sizing model is next required to estimate the required capacity of the ESS to support wind farm to generate base-load wind power. Therefore, the proposed framework more closely focuses on a storage sizing algorithm towards the objective of wind power base-load generation for the future smart electric grids. The theory and algorithm of this component of the framework are developed in Chapters 3 and 4. The framework then investigates how the improved quality wind energy addresses new PEVs charging load to increase the RER and address energy drivers simultaneously. Also, a general expression is proposed for the capital cost of renewable energy that includes the cost of storage when they are intermittent.

The results of the model of the proposed framework for the studied case of Canada in 2050 show that while electrification of transportation improves the energy efficiency in the transport sector and increases the RER by 0.91%, repurposing batteries of PEVs to support base-load wind power can further increase the RER by 1.65–4.11%, depending on the confidence level selected for ESS sizing. The difference is that new charging loads are exclusively addressed by renewable energy, that results in a more effective energy policy.

2.2 Relevant literature

In this section, a review of the literature associated with the various elements of the battery repurposing framework is presented. The presented literature fills in the framework blocks to describe the related field of technology depicted as a core in Figure 2.2. The electric vehicles element includes the technology, market status, and market penetration rates of PEVs. The electric storage elements include storage technologies and applications, technologies of PEV traction batteries, and degradation rates in vehicular and in stationary applications. The renewable energy element includes an overview of renewable energy technologies with the emphasis on intermittent wind power. Power curve modeling of wind turbines and storage sizing for base-load power generation are more closely addressed in Chapters 3 and 4.

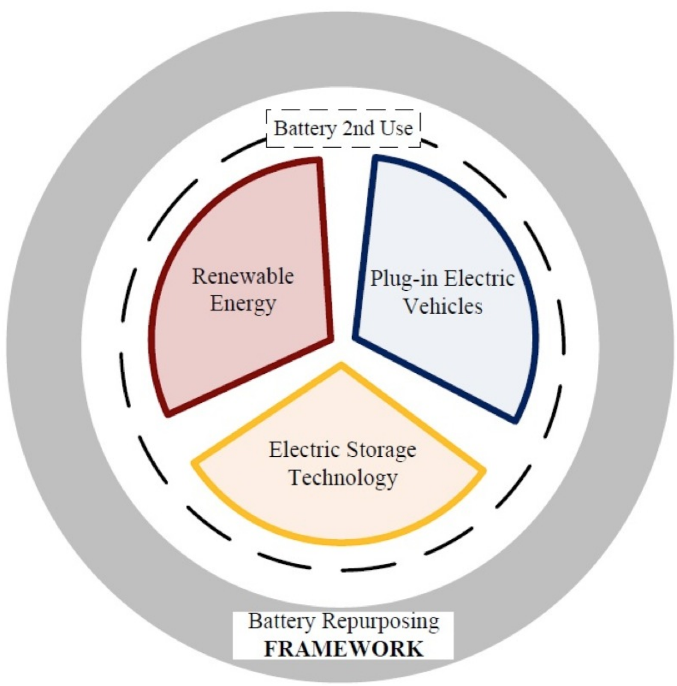

Figure 2.2: Illustration of the literature related to the components of the proposed framework creating the core of this research.

2.2.1 Electric vehicles

Electric drive vehicle (EDV) is a vehicle that uses at least one electric motor for traction purposes [47]. After the first demonstration of an electric vehicle in the 1830s using non-rechargeable batteries [48], the first road electric vehicle was made in 1881 in France by G. Trouve powered by a secondary Plante battery [49]. The second era of electric vehicles happened in the period of 1951-2000 due to high oil prices and environmental emissions [3]. In the 1990s, the California Air Resource Board (CARB) mandated large automotive manufacturers to start producing zero emission vehicles (ZEVs). The regulation sparked a new era in electric vehicle development when Toyota successfully launched Prius as the first commercial hybrid electric vehicle (HEV) in the world in 1997. By commercial introduction of PEVs in the late 2010, the new age of electric transportation has begun. According to a report by [50], the global annual sales of these vehicles will reach 3.8 million in 2020.

EDVs can have different technologies for their propulsion, and can be categorized as HEV, PHEV, BEV, and fuel cell vehicle (FCV). This research aims to study reusing traction batteries of electric vehicles and develop a sustainable approach for transportation from an energy perspective; and therefore, this work does not include FCVs (see Appendix A). Moreover, unlike fuel cells, the Lithium chemistry has a significant potential to improve further and the Li-ion batteries have only reached a small percentage of their theoretical limit [51]. Also, due to the small size batteries of HEVs, they are not of interest to this study, and only are briefly introduced and discussed here. Hybrid electric is a type of electric vehicles that has both an engine and an electric motor powered by a battery for its traction. Due to smaller battery capacity compared to other electric powered vehicles, and the drivetrain architecture, HEVs are not capable of driving the full range on electricity [8]. The batteries of HEVs typically have 1 kWh to 4 kWh of capacity. A PHEV is a hybrid electric car that uses an engine and an electric motor with larger batteries which can be recharged through an external electric power source [52, 53]. The key point about HEV and PHEV technologies is that they rely on fossil-fuel combustion engines. BEVs—also known as electric vehicles (EVs), full electric vehicles (FEVs), or all-electric vehicles (AEVs)—are pure electric vehicles with no engine onboard. These vehicles need to be recharged at the end of their driving range. These vehicles are equipped with batteries, and are propelled solely by an electric machine that is controlled by a motor drive. In these vehicles, the battery is the only source for propulsion [46, 52]. The battery capacity in BEVs can vary from 20-35 kWh allowing them to have highest AER [52]. Appendix B provides more details on different drivetrains of EDVs.

2.2.1.1 Market status

Mass commercial production of PEVs gained momentum by commercial launch of the PHEV Chevrolet Volt and the BEV Nissan Leaf in the U.S. in 2011 [54]. The Volt and Leaf were launched in December 2010 where the giant automakers, Chevrolet and Nissan, had delivered 2,510 Volts and Nissan 2,186 Leafs by the spring 2011 [55]. The Volt was the first PHEV available for purchase while other companies like Toyota started to develop their PHEV line by mass producing the plug-in version of Prius hybrid [54]. Battery capacity of the Volt is 16 kWh that enables an electric range of about 60 km. The plug-in Prius has a battery capacity of 4.4 kWh that provides an electric range of 18 km. The Leaf has a battery pack of 24 kWh providing an electric range of 118 km. In February 2013, Nissan announced that the automaker has passed 50,000 sales units since its launch in 2010 [56]. Ford Focus and i-MiEV are the other two popular BEVs in the current plug-in vehicles market. The battery electric i-MiEV was introduced by Mitsubishi in Japan late 2009 where the production of the vehicle has jumped from 1,710 in 2009 to 14,795 units in 2011 [57]. The Mitsubishi i-MiEV is benefiting from a 16 kWh Li-ion battery with an expected range of 100 km in the U.S. The Ford Focus was launched in 2012 as the first plug-in vehicle by Ford Motor Company. The Focus battery capacity is 23 kWh that enables an electric range of 122 km. The annual sale of the Focus in 2012 has been 685 units [58].

2.2.1.2 Market penetration forecasts

The future of electric transportation as a promising solution in addressing energy and climate issues has been the subject of many research studies. Consumers, automakers, governments and electric utilities are among the stakeholders in the market of PEVs. Several studies have attempted to forecast market penetration rates for electric vehicles under different scenarios [8, 52, 28, 59, 60]. Various models have been developed to forecast the penetration rates of different technologies of PEVs. The main simulation techniques for the penetration forecast models include diffusion and time-domain models, consumer choice models and agent-based models [61]. Many governments in the world have implemented decisive policies and stimulating plans such as tax incentives to consumers, and financial supports for auto manufacturers to favor higher market adoptions of PEVs. Targets for the future of PEVs are set for different penetration scenarios from low to high in the near-term future. Table 2.1 summarizes the PEV sales targets for a number of countries and regions around the world. Although market forecast of a new product is a mature subject of study, the outlook of PEVs future market is highly diverse, complex and subject to numerous parameters. This can be reasoned by different assumptions and simulation approaches these studies adopt [63]. Depending on the simulation technique, these parameters include vehicles sales price,

Table 2.1: Governments announcements for PEVs future sales market in the near-term future [8, 9, 62].

Country/Region	Target Sales	Report Date
World	3,000,000 in sales of PEVs in 2020	2012
Europe	3,000,000 total stock of PEVs in 2020	2012
USA	1,000,000 total stock of PEVs in 2015	2011
Canada	500,000 total stock of PEVs in 2018	2009
Germany	1,000,000 total stock of PEVs in 2020	2013
China	10,000,000 total stock of PEVs in 2020	2012

electric range of the vehicle, gasoline and electricity prices, and governmental subsidies and tax policies resulting in a diverse outcome.

2.2.1.3 Charging characteristics

For widespread introduction of PEVs, charging infrastructure to provide electric charge to these vehicles is a crucial aspect of their operation. Electric vehicle supply equipment (EVSE) is the equipment that all PEVs need to have available at their residential or workplace parking locations. These two locations are of the highest priority as vehicles spend 66% and 14% at these spots, respectively [54]. There are different power levels at which PEVs can be recharged while parked. The charging operation is categorized as alternating current (AC) or direct current (DC) charging based on whether the delivered electricity is AC or DC [54]. In DC charging, also named as fast charging, the AC electricity is converted in a stationary converter to DC to directly charge the vehicle. AC charging can be performed at different levels as level 1 or 2. The charging power is primarily dictated by the rated power of the line that is the product of the line voltage and the maximum rated current of the line. The time period of charging then will be determined by the capacity of battery. According to the Society of Automotive

Engineers (SAE) recommended standard [64], electrical rating for North America for level 1 AC charging is 120 volts, 1 phase at maximum current of 12 or 16 Amps where the circuit breaker ratings are 15 and 20 Amps, respectively. For level 2 AC charging the nominal voltage is 208 or 240 volts, 1 phase at maximum current of 32 or 80 Amps with the circuit breaker rating of 40 and 100 Amps, respectively.

2.2.1.4 Vehicle charging load

It is important to evaluate and estimate the profile of charging load imposed by the fleet of PEVs. Many studies attempted to develop charging profile models to determine the growing electricity demand from PEV charging *e.g.* [65, 66, 67, 68, 69]. The key factor for plug-in time of electric vehicles is when drivers recharge their vehicles. When the optimum time for electricity providers is overnight charging, drivers prefer recharging at their convenience [70]. By conducting different approaches, many studies present that although different vehicles may charge at different times during the day, the aggregate charging profiles follow similar distribution with most occurrence probability during night. The Electric and Power Research Institute (EPRI) creates a scenario for charging profile of electric vehicles where 74% of charging load is distributed from 10:00 p.m. to 6:00 a.m. [28]. PHEVs and BEVs are expected to be capable of charging at different levels. Level 2 charging is expected to be more desirable due shorter charging time. Although BEVs with higher battery capacity may prefer level 3 charging, costly equipment and installation can impede wide adoption of level 3 charging at residential locations [52]. Several stochastic analyses have attempted to determine the likelihood of plug-in vehicles charging at a specific time and develop charging profiles [69, 71]. The framework assumes a worst-case scenario to calculate the energy demand of charging in which PHEVs and BEVs charge at the same time.

The imposed load of electric vehicles is of interest to this study to investigate how base-load wind power with repurposed batteries can contribute to the charging electricity of PEVs. The total daily energy requirement by PEVs depends on the vehicle's energy efficiency in kWh per driven distance per day. A daily energy demand of PEVs is calculated based on an average daily commute for a typical average populated city.

2.2.2 Propulsion batteries of PEVs

There are different chemistries used for EDVs propulsion batteries such as Nickel-metal hydride (NiMH) and Lithium-ion (Li-ion) and lead-acid [45, 72]. These batteries are used for different levels of automotive applications. For example, stop-and-start electric vehicles use lead-acid while HEVs and PEVs mostly use NiMH and Li-ion batteries. Li-ion battery is widely accepted to be the leading technology for both PHEV and BEV technologies, and shows advantages over other major chemistries [73, 74]. The selection of electrode materials and electrolytes of a Li-ion battery has a significant impact on its useful life of the battery [75, 76, 77]. The main advantages of Li-ion batteries are the high energy density in kWh/kg, high power density in kW/kg, long cycle life, and low weight and volume [72], achieving between 150 to 180 Wh/kg energy density. The major issues of Li-ion technology are high cost, moderate calendar life and poor performance in cold temperatures [8]. The manufacturing scale of Li-ion batteries is anticipated to be approximately 35 GWh by 2015 [73]. A module of a battery is composed of several cells containing electrodes and electrolytes in a container. A battery pack is made by assembling several modules together. In electric vehicles battery modules are typically 10-30 volts [45]. For PEVs, the battery pack can typically be composed of 10-40 battery modules. The pack usually operates in the range of 100-350 volts.

2.2.2.1 Battery degradation

The capacity of Li-ion battery decreases by charge-discharge cycling [78, 34]. A shallow discharge is when a small portion of stored energy is drawn while discharging most of the stored energy is a deep discharge. It is essential to quantify the degradation of PEV batteries over the time of their cycle life. Many studies have attempted to develop technical and economic battery life prediction models using different approaches under different aging factors such as cycle frequency, calendar life, ambient temperature, DOD, and charge voltages [79, 33, 35, 36, 38]. For the repurposing framework, it is important to (i) predict the life status of PEV battery at the vehicular EOL, and (ii) predict a degradation rate for the stationary life of the repurposed battery.

2.2.3 Renewable energy

Supporting higher share of renewable energy in the energy sector and in the transport is one of main objective of the battery repurposing concept presented herein. This section provides an overview of current technology and market status emphasizing on wind energy as the main technology of interest to the repurposing framework. In the world's current unsustainable energy context, renewable energy is the most promising solution that is becoming a viable component of the global energy supply [80]. The main benefits of renewables are mitigating environmental impacts by reducing GHG emissions, and reducing the reliance on finite fossilbased energy sources. According to the IEA's 2010 World Energy Outlook, the supply of main renewable energy technologies—wind, solar, hydro, geothermal, biomass and marine energy—increases from 840 million tonnes of oil equivalent (Mtoe) in 2008 to nearly 3,250 Mtoe in 2035. Wind and solar photovoltaic power generation are key technologies to address global energy drivers and achieve the world's objective of limiting the earth's temperature increase to 2 °C in 2050 [81]. The global installed capacity of wind power has almost doubled since 2008 approaching 300 GW in 2013, *i.e.*, 2.5% of the total electricity generation [11]. The world's installed capacity of solar PV has also drastically increased reaching more than 95 GW in 2012 [13]. In 2013, the electricity generation from wind in Denmark, England, Spain and Germany has been 30-, 25-, 25- and 20%, respectively [11]. On the other side, the cost of power generation from wind for onshore wind turbines has significantly dropped from $3000 in 2005 to $1500–2000 in 2013 per unit power (*i.e.*, $/kW).

2.2.3.1 Wind energy

Wind turbine is a generator that converts the kinetic energy of the mass flow rate of wind to electricity. Wind speed is the main parameter for the design of wind turbines for a region of study. Depending on the design of a wind turbine, wind speeds ranging from 4 m/s to 25 m/s are suitable for power generations [82, 83]. Wind farms usually require an average wind speed of at least 7 m/s. Assessment of available resources of wind is an important tool that allows to estimate the rated power and the generated energy of a wind farm. Wind energy is an intermittent source of energy which can have different time variations such as short-term, diurnal, annual, and even inter-annual [84]. Effective utilization of wind energy into the power systems requires accurate wind resource assessment as well as estimation of the turbine power curve for operational management of wind farm and for performance monitoring of turbines.

2.2.3.2 Cost of wind energy

To address global energy and environmental challenges, an "energy technology revolution" is required including solutions such as higher energy efficiency and greater share of renewable energy sources [85, 86]. The IEA's technology roadmap on wind energy targets that 12% of global electricity will be from wind power [86]. Availability of wind power throughout the world will result in less reliance on imported energy. In addition, reduction of CO_2 and other emissions is a major benefit of wind power. Also, wind power is highly attractive in areas where water sources are limited [86]. In several studies investigating the economics of wind energy the cost of wind power is assessed competitive with conventional power sources [86, 84]. However, the cost of wind power can increase significantly when the intermittent source requires storage to be comparable to constant power generation. In North America, the capital cost for wind energy generation–the cost that may include turbine, grid connections, foundations, and infrastructure–was estimated in 2008 to be between 1,400 and 1,900 $/kW [86]. The life cycle cost of wind energy can have large variances due to capital costs, wind resource availability, operation and maintenance (O&M) costs, life duration of the turbine, and etc. [86]. According to [87], the U.S. capacity weighted average of wind life cycle cost has been 4.7 and 6.7 cents per kilowatt (¢/kW), with and without tax credits, respectively. The O&M cost is calculated in [86] to range from 1.2 to 3.2 (¢/kW).

2.2.3.3 Integration of wind energy

The U.S. 2012 annual energy outlook projects more than 100% increase in non-hydro renewable energy capacity from 2010 to 2035 [88]. Many experts believe that even a higher share of wind power will be economically viable [73]. However, due to variable nature of wind, integration of wind power into the electric system is a more challenging task. Use of utility scale ESS is viable solution in effective integration of intermittent wind and solar energy. A comprehensive study by the U.S. Department of Energy (DOE) [78], discusses 17 electric grid-related applications, and analyzes potential benefits of various ESS technologies. These applications in the electricity market are categorized as grid system applications, ancillary services, as well as end-user and utility customer applications, and applications for renewable energy integration. Many studies have investigated the integration of ESS and intermittent wind power for higher penetration rates in the grid *e.g.*, in [73, 89, 90, 91]. The focus of this thesis is to integrate more wind energy for transportation without impacting dispatchable generation. Within the proposed framework, we specifically look at how repurposed batteries can increase the RER through improving the quality and reliability of wind energy to address the PEV charging energy load. Therefore, modeling of wind turbine power curve and sizing of the ESS capacity required to be integrated with wind power to generate base-load power based on wind farm operational data are discussed and developed in this thesis.

2.2.3.4 100% renewable energy scenario

Towards a sustainable energy system, and to mitigate the environmental impacts and climate change effects, a transition to 100% renewable energy is imperative. Several studies have analyzed pathways and scenarios to develop roadmaps and strategies at the local, national and global levels for fully displacing fossil fuels in the future energy mix [92, 93, 94, 95]. To achieve the goal of 100% renewable energy, a comprehensive conversion is required in all sectors of the energy system, *i.e.*, transportation, electricity generation, industry, and heating and cooling [96]. Electrification of transportation, replacing fossil fuel burning plants with the emerging wind and solar power, reducing end-user's energy demand, and improving energy efficiency are among the key solutions, that are in compliance with RED approach. Moreover, to ensure successful implementation of proposed solutions, proper policy orientations at the regional and national levels, and decisive action plans are inevitable. According to a report by Sustainable Canada Dialogues in 2015, Canada could achieve 100% reliance on low carbon electricity in 2035, which requires the country to implement a long-term plan to reduce at least 80% of the GHG emissions by 2050 [97]. This report presents 10 policy orientations for short-, middle-, and long-term targets as a possible pathway to achieve 26-28% reduction in emission below the level of 2005 in 2025, and 80% by 2050. The roadmap necessitates eliminating subsidies on fossil fuels, applying carbon tax programs, and electrification of transportation, among others,

2.2.4 Battery repurposing

Several studies in the literature have attempted to assess potential applications for the used batteries of electric vehicles in the electricity market [41, 45, 46, 98, 99, 73, 100]. These studies investigate technical and economic viability of applying used batteries in stationary applications in their post-vehicular life. The U.S. National Renewable Energy Laboratory (NREL) in [99, 41] have identified potential applications for PEV Li-ion propulsion batteries after their vehicular life to reduce cost and support further adoption of electric cars. This effort has recognized major barriers in their study such as battery degradation, application selection for used batteries, and cost and operational considerations. As the main focus of this research, capacity firming of renewable energy is accepted to have large market potential for secondary use of PEV batteries [45]. This thesis develops a simulation model for the integration of transportation and renewable energy through utilizing repurposed batteries of PEVs. The repurposing model looks at the framework at macro-level using certain parameters as described in the following sections.

2.3 The proposed framework model

The blocks of the proposed framework model associated with vehicular and post-vehicular life of the batteries are developed herein, and the parameters and assumptions are explained.

2.3.1 Vehicular life

The life of batteries on vehicles starts with the installation of manufactured batteries in electric vehicles. The vehicular lifetime of these batteries depends on various parameters such as their chemistry, charging approach, driving patterns, and weather conditions of where they serve [33]. The forecast of the market penetration of PEVs determines the projected annual sales of these vehicles, and consequently, the number of batteries that will be available on the market each year. Also, the annual charging load of PEVs should be calculated to determine the yearly energy demand required for charging these batteries. These two parts are discussed in the following sections.

2.3.1.1 PEV market penetration forecasts

Time-series market penetration models of a new product present the life cycle of that product over time. Many parameters can be included in the modeling that influence the adoption of a new product, $a(t)$, where t is the time horizon of the repurposing model. Any diffusion function of adoption of PEVs can be applied as the input to the battery repurposing model to investigate various scenarios in the future of electrified transportation. A penetration scenario of PEVs is adopted for a case study of Canada, and a time-series diffusion rate for PHEV and BEV technologies is applied where $t = 1, \ldots, 41$, corresponding to the calendar year from 2010 to 2050. The adopted $a(t)$ will be linked to the repurposing model predict when the batteries would be available for repurposing. The proposed framework predicts when the batteries become available on the market and how many hours of storage are available to support wind power in the next 10–20 years to address the new load.

2.3.1.2 PEV charging energy requirements

By adopting a market penetration rate for PEVs the framework model calculates the average annual energy required for PEVs in the location of study. To calculate the annual energy demand, the maximum power limited by the electric line, or the vehicles battery capacity can be used [101]. Alternatively, the electric energy required to meet the charging load of PEVs per year can be estimated using daily mileage driven by a passenger vehicle for a typical urban driving profile, electric vehicle fuel efficiency, and the predicted number of PEVs in the location of study. The annual aggregate energy demand for PEVs, E_l, in kWh per year, is therefore expressed as follows

$$E_l = R \times \eta_e \times N \times 365, \tag{2.1}$$

where R is the electric range driven daily in km per day, η_e is the electric range efficiency in kWh per km, and N is the number of plug-in electric vehicles—either PHEV or BEV—available per year.

To estimate R, Equation (2.1) uses the average daily driven distance for a LDV in a typical North American from the duty cycle study developed for a typical North American urban driving pattern for cities with the population of 1 million or less in [102]. To more realistically present the average commute distance by LDVs, the model also considers a coefficient to account for possible extra distance for rural driving. In this model, this extra driving distance is assumed to be fuelled by electricity in BEVs and by gasoline in PHEVs.

2.3.2 Post-vehicular life

In the life cycle of propulsion batteries of electric vehicles, after their automotive EOL, they can be utilized in stationary applications. As inputs to the repurposing framework, it is required to estimate the useful remaining life of repurposed batteries at the beginning of their stationary life, *i.e.* as well as the vehicular EOL, and to project the degradation rate of these batteries in the new application before being recycled. Moreover, the framework calculates the energy storage capacity required for integrating intermittent wind power to produce constant output power.

2.3.2.1 EOL and degradation of PEV battery

Degradation of Li-ion batteries in the automotive life, and then in stationary applications is influenced by parameters such as charging rate, the DOD, temperature, and calendar age, and needs validating experimental information. Important to the battery repurposing framework is to (i) estimate the remaining life of the battery at the time of removal from vehicles, and (ii) adopt a degradation rate in their secondary life before being recycled. These factors determine the hours of electric storage available to be repurposed for a new application. While predicting a realistic scenario for the capacity loss of Li-ion battery is complex and subject to several parameters, a base scenario is assumed for the capacity loss per year to represent the available capacity when the battery is removed from vehicles, and how it fades in the stationary life. In this study, and to calculate the capacity loss of the batteries in the stationary application, the results in [103] are used as a typical degradation pattern. Batteries service life on vehicles is assumed to be 8 years with remaining capacity of 80% at their vehicular EOL [99, 104, 105]. The framework model can apply degradation rates to study different scenarios of available repurposed storage capacity from PEVs in their post-vehicular life. In this work, we also perform a short-duration experimental testing to obtain an indication and to monitor the aging pattern of used batteries presented in Chapter 5.

2.3.2.2 Wind energy storage sizing

The proposed framework calculates the size of ESS required to integrate with wind energy towards the goal of converting intermittent wind to base-load generation. The goal is not to rely on available capacities for utilities to integrate intermittent renewable energy by using existing generators; but the goal is to use such capacity to increase the RER. Chapter 4 develops a statistical algorithm for ESS sizing for delivering base-load electricity to a user-selected confidence level. The algorithm proposes different methods based on parametric and nonparametric statistical models using wind resource assessment data and available wind turbine information representing different stages of a wind farm project—from site selection to operational status. The proposed methods can be used in the framework model to calculate the size of ESS for single or multiple locations for the region of study. For the case study in this chapter, method M_2 developed in Chapter 4 is used. To this end, the model needs to base the calculation on an actual site in the location of study. We use time-domain wind speed data available for the location of study. Next step is to calculate the time-domain power data using a selected wind turbine manufacturer power curve. Having known the power curve function, $f(\cdot)$, the time-domain wind power is obtained using $p_i = f(v_i)$. To obtain the size of ESS, the power rating imbalances between the generated wind power, P_w, and the desired dispatchable power output, P_d, are calculated:

$$P_{ESS}(t) + P_w(t) = P_d(t), \tag{2.2}$$

where P_{ESS} is the storage power ratings. For this analysis, where the objective is to produce base-load wind power at a given confidence level, $P_d(t)$ in Equation (2.2) can be replaced by the firm capacity, p^*. The histogram of the wind power values is constructed to obtain the relative frequency distribution of the fitted wind power values, $g(p)$. Therefore, p^* is computed by

$$p^* = \mathbb{E}(P) = \sum_p \ p \ g(p), \tag{2.3}$$

where $\mathbb{E}(\cdot)$ is the mean of the probability distribution function (pdf). Next step is to calculate the energy charges and discharges experienced by ESS in delivering the firm capacity of the turbine. To achieve this, the energy imbalances are calculated as the net difference between the firm capacity and the generated wind power over the span of individual time intervals given by

$$E_{_{ESS}}(t_i) = \Big(p^* - P_w(t_i)\Big) \cdot \Delta t_i \, , \tag{2.4}$$

where $E_{_{ESS}}(t_i)$ is the calculated state of energy of ESS at time t_i, and Δt_i is the span of the corresponding time interval. The sum of consecutive occurrences of individual energy imbalances forms the energy charges and discharges of ESS over the time period of study. To apply different confidence levels to the calculated ESS capacity, we use the probability distribution of the energy ratings. The histogram of the calculated ESS energy charges and discharges is created to test different statistical distributions. Chapter 4 shows that the best fit to the observed energy values of ESS is obtained using the Laplace distribution. By determining the parameters of the fitted distribution to the calculated energy values, different confidence levels can be applied to the size of ESS.

2.4 Chapter summary

We proposed the battery repurposing of PEVs that can effectively integrate electrified transportation and intermittent renewable energy. A review of the literature associated with the battery repurposing framework was provided in this chapter. The components of the framework and the development of the simulation model implemented in MATLAB® were explained. Chapter 6 provides the results of the framework simulation for a studied case of Canada followed by a discussion. The results will show that PEV battery repurposing further increases the RER by 1.65–4.11% in 2050 through addressing the new charging loads of PEVs by base-load wind power generation.

Chapter 3

Wind Power Curve Modeling

Wind turbine power curve modeling is an important tool in turbine performance monitoring and power forecasting. There are several statistical techniques to fit the empirical power curve of a wind turbine which can be classified into parametric and nonparametric methods. In this chapter, we study four of these methods to estimate the wind turbine power curve, which will be used in Chapter 4 to calculate the size of ESS. Polynomial regression is studied as the benchmark parametric model, and issues associated with this technique are discussed. The locally weighted polynomial regression method is then introduced, and shows its advantages over the polynomial regression. Also, the spline regression method is examined to achieve more flexibility for fitting the power curve. Finally, we develop a penalized spline regression model to address the issues of choosing the number and location of knots in the spline regression. The performance of the presented methods is evaluated using two simulated data sets as well as an actual operational power data of a wind farm in North America.

3.1 Wind turbine power curve

The power curve of a wind turbine presents the electrical power output ratings of the machine for different wind speeds [106]. A typical wind turbine power curve has three main characteristic speeds: cut-in (v_c), rated (v_r) and cut-out (v_s) speeds. The turbine starts generating power when the wind speed reaches the cut-in value. The rated speed is the wind speed at which the generator is producing the machine's rated power. When the wind speed reaches the cut-out speed, the power generation is shut down to prevent damage [107]. Theoretical power curves are supplied by manufacturers assuming ideal meteorological and topographical conditions. In practice, however, wind turbines are never used under ideal conditions, and the empirical power curves could be substantially different from the theoretical ones due to the location of the turbine, air density, wind velocity distribution, wind direction, mechanical and control issues as well as uncertainties in measurements. Figure 3.1 shows a typical wind turbine power curve with three main characteristic speeds.

There are several statistical methods to fit the empirical power curve of a wind turbine [108]. These methods can be classified into parametric and nonparametric techniques [109, 110]. Parametric techniques are based on mathematical models which are often built by a family of functions with a number of parameters to describe the turbine power curve [111]. Examples of these models include segmented linear models [112], polynomial regression [113, 114], and models based on probabilistic distributions such as four- or five-parameter logistic distributions [110, 115]. Parametric methods are usually restricted by their nature. Unlike parametric techniques, nonparametric methods do not impose any pre-specified model, and attempt to produce an estimate of the power curve that is as close as possible to the observed data subject to the smoothness of the fit. Such methods have major advantages over parametric methods as they can

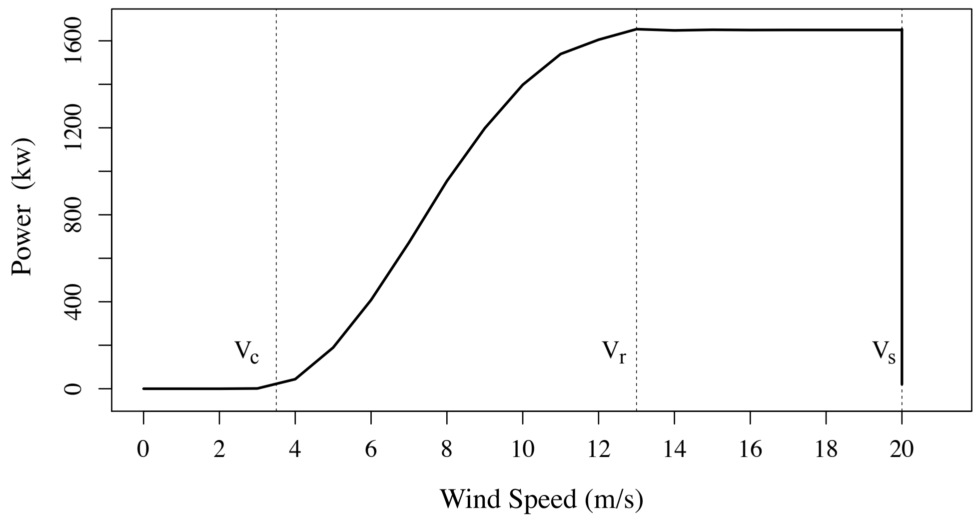

Figure 3.1: A typical wind turbine power curve with three main characteristic speeds. The turbine starts generating power when the wind speed reaches the v_c value, and produces the machine's rated power at v_r. The turbine is shut down when the wind speed reaches the v_s speed.

accurately model a wide range of possible shapes of power curves. Examples of nonparametric techniques include neural networks (*e.g.*, generalized mapping regressor, and feed–forward multi-layer perceptron [116]), fuzzy logic methods (*e.g.*, fuzzy cluster centre models [117]), and data mining methods (*e.g.*, the multi-layer perception, the random forest, and the k-nearest neighbour [118]). No one model fitting approach dominates all others over all possible observations obtained from different wind turbines. On a particular data set, a specific method might work best, but on other data sets other methods might be more applicable. Therefore, it is important to investigate the performance of different statistical procedures for power curve fitting, and decide which method produces better results for a given data set.

This chapter focuses on wind turbine power curve modeling based on available operational output power data using four parametric and nonparametric methods. We present polynomial regression as a benchmark parametric method for power curve fitting. This method has been used extensively in the literature, however, suffers from its global nature and sensitivity to anomalies within observations. In this method, one usually needs a high degree polynomial regression model to provide a good fit to the observed data set. Fitting a high degree polynomial regression model results in a good fit to the observed data set but may overfit the data points [119], and the fitted power curve will closely follow the noise of the power generating system. To avoid such problems, we propose using the locally weighted polynomial regression as a nonparametric method, and study some of its properties on simulated as well as real data sets. Cubic spline regression is another nonparametric method which has been introduced for wind turbine power curve fitting [120, 121]. However, there are a number of practical issues with this method such as choosing the number and the location of knots to fit the cubic spline model. In addition, while these models perform well for wind turbines with smooth power curves, their performance outside the boundary knots could be undesirable. Natural cubic spline regression is proposed to improve the performance of the cubic spline regression models outside the boundary knots. Finally, we develop a penalized spline regression model which provides an enhanced performance compared to the spline regression by addressing the challenge of choosing the number and the location of knots. We note that the nonparametric methods developed in this work are more flexible, less sensitive to anomalies within observations, easier to implement, and computationally more feasible compared to other methods in the literature. While our proposed methods show promising results for modeling the wind power generation, one might also be able to use our results to obtain efficient and easy-to-implement methods for characterizing wind turbine power curves which can be used in other applications such as wind power forecasting and on-line monitoring of power curves for detecting anomalies in a wind turbine power generation process.

Section 3.2, discusses different parametric and nonparametric power curve estimation methods by introducing two typical power curves and simulating two random data sets with normal errors. We then present the theoretical foundation of each method, and apply them to the simulated data sets. Section 3.3 presents actual operational data sets of a wind farm in North America, and investigate the performance of each method. The results of the proposed techniques and the evaluation metrics are also presented. Section 3.4 provides a summary of the chapter and some concluding remarks.

3.2 Power curve estimation

A wind turbine produces electrical power by converting the instantaneous power of wind to mechanical rotation of the turbine's rotor, which drives an electrical generator to produce electricity. The generated electrical power available from the mass flow rate of air through the turbine blades is given by

$$P_e = \frac{1}{2}\,\eta\, C_p\, \rho\, A\, V^3, \tag{3.1}$$

where P_e is the electrical power produced by the wind turbine in W, η is the machine's overall efficiency, C_p is the dimensionless power coefficient representing the theoretical amount of mechanical power that can be extracted by the turbine rotor, ρ is the air density in kg/m^3, A is the turbine rotor area in m^2, and V is the wind speed in m/s [82, 122]. The power coefficient is a function of turbine blade tip speed ratio, λ, and the blade pitch angle, θ [123]. The maximum theoretical mechanical power that can be extracted by wind turbines is 0.5926, and is known as the Betz limit [124].

In this section, we characterize the machine's power curve based on actual generated power data using four parametric and nonparametric methods. Wind speed and power data sets, (v_i, p_i), are simulated from the additive model $p_i = f(v_i) + \epsilon_i$ with contaminated noise, where $f(\cdot)$ represents the manufacturer power curve. In parametric regression models the function $f(v_i)$, which shows the expected value of power p_i at a given wind speed v_i, is specified in advance by a mathematical model that can be characterized by a number of parameters which should be estimated using the observed data. In nonparametric regression models, the function $f(\cdot)$ is left unspecified, other than being smooth and continuous. The objective of nonparametric regression analysis is to estimate $f(\cdot)$, rather than estimating some parameters. These methods are often called scatter plot smoothing in the statistical literature. Two wind turbines are studied to represent two different typical shapes of the power curve: wind turbine model V82 and model FL–255 with the rated capacity of 1650 kW and 250 kW, respectively, manufactured by Vestas Wind Systems A/S and Furlander AG. Figure 3.2 shows theoretical power curves for these turbines with the scatter plots of simulated observations from each power curve. For each case, the observed wind power at a given wind speed is generated from a normal distribution with the mean equal to the manufacturer power curve and a constant standard deviation σ_ϵ, where $\sigma_\epsilon = 100$ for turbine model V82 and $\sigma_\epsilon = 20$ for turbine model FL-255. Each data set consists of a total number of 720 pairs of observations, denoted by (v_i, p_i), $i = 1, \ldots, n = 720$. The wind speed data is generated from a Weibull distribution representing the hourly wind distribution of the wind farm studied in Section 3.3.

3.2.1 Polynomial regression

Polynomial regression has been extensively used in the literature to estimate the power curve of wind turbines. This model can be considered as a standard extension of the

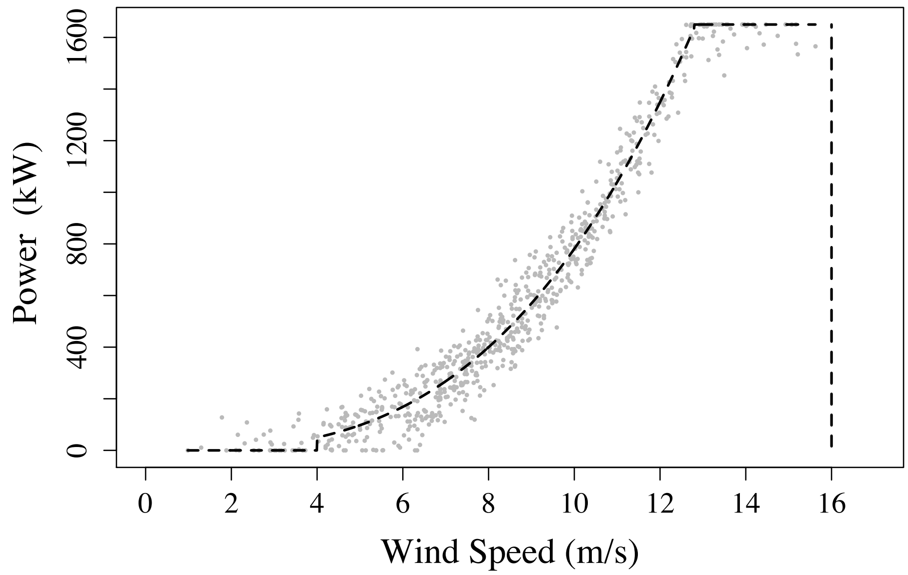

(a) Turbine V82

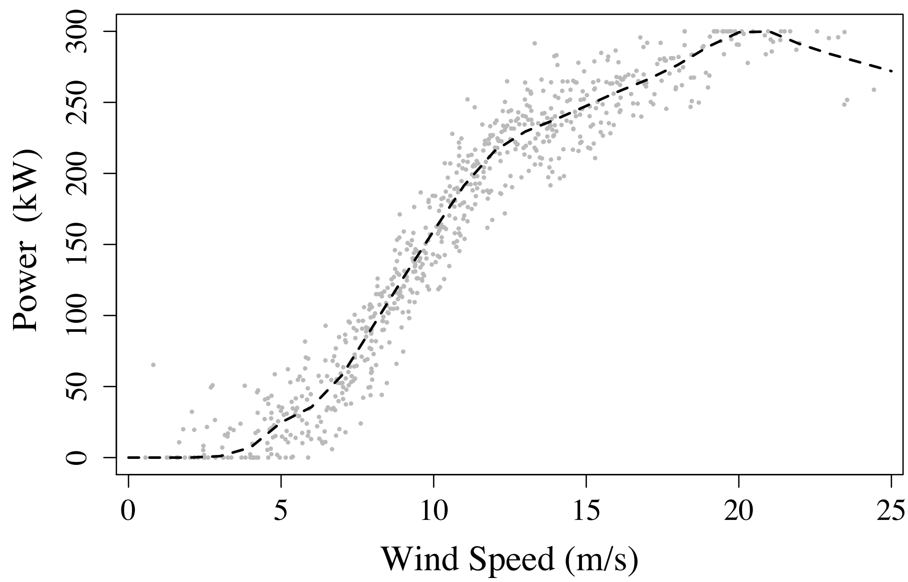

(b) Turbine FL-255

Figure 3.2: The manufacturer wind turbine power curves for (a) turbine model V82 and (b) turbine model FL-255 with the scatter plots of 720 generated wind speed and hourly produced power for 1 month, assuming normally distributed noises about the manufacturer power curves with standard deviations $\sigma_\epsilon = 100$ and $\sigma_\epsilon = 20$, respectively.

linear regression $p_i = \beta_0 + \beta_1 v_i + \epsilon_i$, with a polynomial function

$$p_i = \beta_0 + \beta_1 v_i + \beta_2 v_i^2 + \ldots + \beta_k v_i^k + \epsilon_i, \tag{3.2}$$

where ϵ_i is the error term. To estimate the parameters $\beta_0, \ldots, \beta_k$, based on a sample of size n, we can write the model in Equation (3.2) as

$$\mathbf{P} = \mathbf{V}\boldsymbol{\beta} + \boldsymbol{\epsilon}, \tag{3.3}$$

where $\mathbf{P}_{n\times 1} = (p_1, p_2, \ldots, p_n)^\top$, $\boldsymbol{\beta}_{(k+1)\times 1} = (\beta_0, \beta_1, \ldots, \beta_k)^\top$, $\boldsymbol{\epsilon}_{n\times 1} = (\epsilon_1, \epsilon_2, \ldots, \epsilon_n)^\top$, and

$$\mathbf{V}_{n\times(k+1)} = \begin{pmatrix} 1 & v_1 & \cdots & v_1^k \\ 1 & v_2 & \cdots & v_2^k \\ \vdots & \vdots & \ddots & \vdots \\ 1 & v_n & \cdots & v_n^k \end{pmatrix}.$$

The least squares method is used to estimate the unknown parameters $\boldsymbol{\beta}$ by minimizing the residual sum of squares (RSS):

$$\begin{aligned} \mathrm{RSS}(\boldsymbol{\beta}) &= \sum_{i=1}^{n} (p_i - \beta_0 - \sum_{j=1}^{k} \beta_j v_i^j)^2 \\ &= (\mathbf{P} - \mathbf{V}\boldsymbol{\beta})^\top (\mathbf{P} - \mathbf{V}\boldsymbol{\beta}), \end{aligned} \tag{3.4}$$

which is a quadratic function of the unknown parameters $\boldsymbol{\beta}$. Differentiating $\mathrm{RSS}(\boldsymbol{\beta})$ with respect to $\boldsymbol{\beta}$, we solve

$$\frac{\partial \mathrm{RSS}(\boldsymbol{\beta})}{\partial \boldsymbol{\beta}} = -2\mathbf{V}^\top (\mathbf{P} - \mathbf{V}\boldsymbol{\beta}) = 0, \tag{3.5}$$

where $\mathbf{V}^\top$ stands for the transpose of $\mathbf{V}$, and obtain the least squares estimator of $\boldsymbol{\beta}$ by

$$\widehat{\boldsymbol{\beta}} = (\mathbf{V}^\top \mathbf{V})^{-1} \mathbf{V}^\top \mathbf{P}. \tag{3.6}$$

The fitted power curve at a specific wind speed value v_i is $\widehat{f}(v_i) = \mathbf{V}_i \widehat{\boldsymbol{\beta}}$, where $\mathbf{V}_i = (1, v_i, v_i^2, \ldots, v_i^k)$ is the i-th row of the matrix $\mathbf{V}$. To obtain the degree of the polynomial regression, we use the cross-validation technique. The main idea of this technique is to divide the available observations into two sets: *a training set* and *a validation set*. First, observations in the training set are used to train the polynomial regression model how to estimate the power curve. Then, the validation set is used to test the model. Given the observed wind speed and power data, the use of a fitted polynomial model is warranted if it results in a low test error rate. We apply a 10-folded cross-validation by randomly dividing the observations into 10 folds of approximately equal sizes. Each time, a group of observation is considered as a validation set, and the remaining groups are used for the purpose of training a polynomial model of a specific degree for estimating the power curve. The 10-fold cross-validation is then computed by

$$\mathrm{CV}_{(10)} = \frac{1}{10} \sum_{i=1}^{10} \mathrm{MSPE}_i, \tag{3.7}$$

where MSPE_i is the mean squared prediction error associated with the i-th test group. Figure 3.3 shows the validation error rates for polynomials of degrees up to 10 for each turbine. We observe that for turbine model V82 10-fold cross-validation curve has a minimum at $k = 8$, while the $\mathrm{CV}_{(10)}$ curve is rather flat beyond $k = 5$. The one standard error rule is used in conjunction with cross-validation and choose a model with an error no more than one standard error above the error of the best model [119]. Here, to prevent overfitting the scatter plots, polynomial regression models with $k = 5$ and $k = 6$ are used for modeling the power curves of turbines V82 and FL-255, respectively. Figure 3.4 shows the fitted polynomial regression models for turbine model V82 with degrees 4 and 5, and turbine FL-255 with degrees 6 and 7.

3.2.2 Locally weighted polynomial regression

Polynomial regression is limited by its global nature where the fitted value of power at a given speed v_0 strongly depends on all data values even those v_is that are far from v_0. Also, it is not easy to achieve a functional form in a specific wind speed region without sacrificing the goodness of the fitted curve in other regions. In addition, polynomials are more sensitive to anomalies within the data. One way to avoid such problems is to fit a local regression model at a target point v_0. Locally weighted k-th order polynomial regression model solves a separate weighted least squares problem at each target wind v_0 by finding $\widehat{\boldsymbol{\beta}}(v_0)$ as follows

$$\begin{aligned}\widehat{\boldsymbol{\beta}}(v_0) &= \arg\min_{\boldsymbol{\beta}} \sum_{i=1}^{n} \mathcal{K}_s(v_0, v_i)(p_i - \beta_0 - \sum_{j=1}^{k} \beta_j v_i^j)^2 \\ &= \arg\min_{\boldsymbol{\beta}} (\mathbf{P} - \mathbf{V}\boldsymbol{\beta})^\top \mathbf{W}_s(v_0)(\mathbf{P} - \mathbf{V}\boldsymbol{\beta}) \end{aligned} \tag{3.8}$$

where $\mathbf{W}_s(v_0) = diag(\mathcal{K}_s(v_0, v_1), \ldots, \mathcal{K}_s(v_0, v_n))$ is a diagonal matrix, and $\mathcal{K}_s(v_0, v_i)$ is the smoothing kernel function. Using $\mathcal{K}_s(v_0, v_i)$, data points nearest to v_0 are given the highest weights and those farther away are given lower weights. This method is resistant against outliers by assigning low weights to observations which generate large

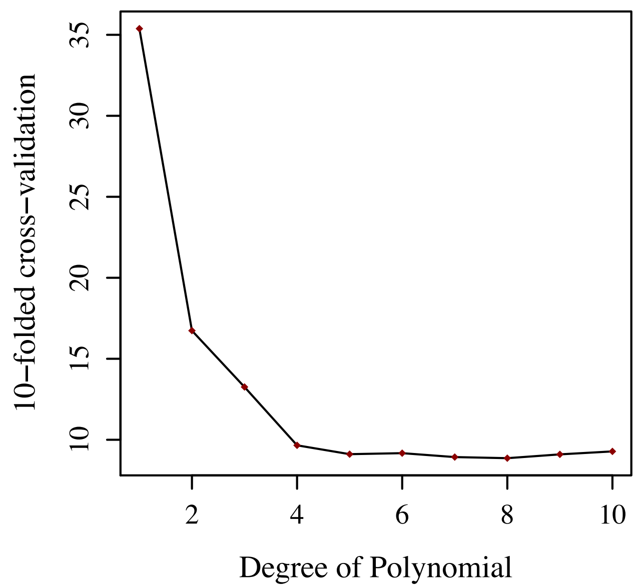

(a) Turbine V82

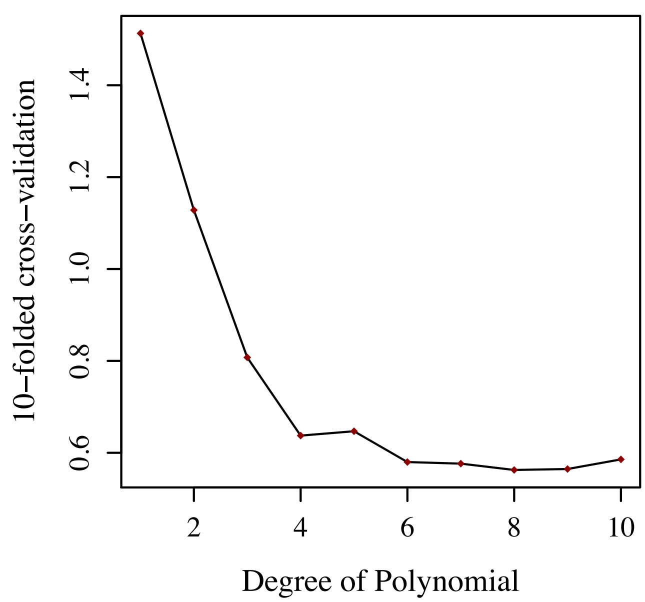

(b) Turbine FL-255

Figure 3.3: Cross-validation technique is used on each wind power data set in order to estimate the error rate that results in predicting the power using polynomial functions of wind speed. (a) shows a 10-fold cross-validation mean squared test error estimate for turbine V82, and (b) is that for turbine FL255.

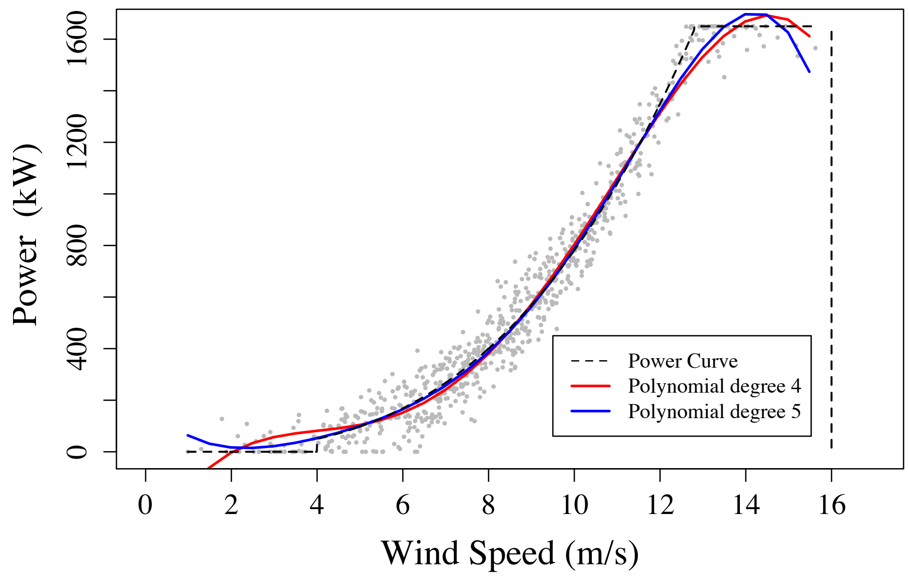

(a) Turbine V82

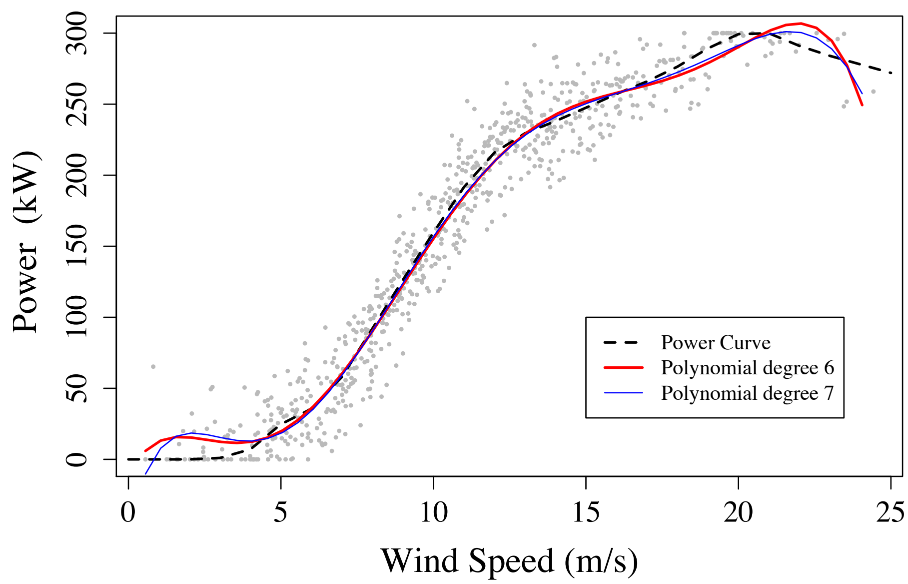

(b) Turbine FL-255

Figure 3.4: Fitted polynomial regression models for (a) turbine model V82 with degrees 4 and 5, and (b) for turbine model FL-255 with degrees 6 and 7. The black dashed curves are theoretical power curves from the manufacturers.

residuals [125]. For this analysis, we use the tri-cube smoothing kernel function

$$\mathcal{K}_s(v_0, v_i) = \begin{cases} \left(1 - \left|\frac{v_i - v_0}{s}\right|^3\right)^3, & \text{if } |v_i - v_0| \leq s, \\ 0, & \text{otherwise.} \end{cases} \tag{3.9}$$

However, one can also use other kernel functions such as the Gaussian kernel function. $\widehat{\boldsymbol{\beta}}(v_0)$ is computed for each v_0 as follows

$$\widehat{\boldsymbol{\beta}}(v_0) = (\mathbf{V}^\top \mathbf{W}_s(v_0)\mathbf{V})^{-1}\mathbf{V}^\top \mathbf{W}_s(v_0)\mathbf{P}. \tag{3.10}$$

Also, the corresponding estimated power at wind speed v_0 is

$$\begin{aligned} \widehat{f}(v_0) &= \mathbf{V}_0(\mathbf{V}^\top \mathbf{W}_s(v_0)\mathbf{V})^{-1}\mathbf{V}^\top \mathbf{W}_s(v_0)\mathbf{P} \\ &= \sum_{i=1}^{n} l_i(v_0; s)\, p_i, \end{aligned} \tag{3.11}$$

where $\mathbf{V}_0 = (1, v_0, v_0^2, \ldots, v_0^k)$ and the term $l_i(v_0; s)$ combines the local smoothing kernel $\mathcal{K}_s(v_0, \cdot)$ and the least squares operation for fitting the polynomial regression.

The most important component of this method is the choice of the span s which controls the flexibility of the non-linear fit. One can interpret s as the fraction of observations used in constructing the local fit at any point v_0. Small values of s will produce more local fits while large values results in more global fits using all the observations and the resulting model will be similar to the polynomial regression.

The cross-validation technique is used to obtain the optimum value of s for each data set, illustrated in Figure 3.5. In this figure, the optimum degree of the smoothness (span) parameter for linear and quadratic locally weighted polynomial regression models are obtained as the points resulting the minimum of the graphs.

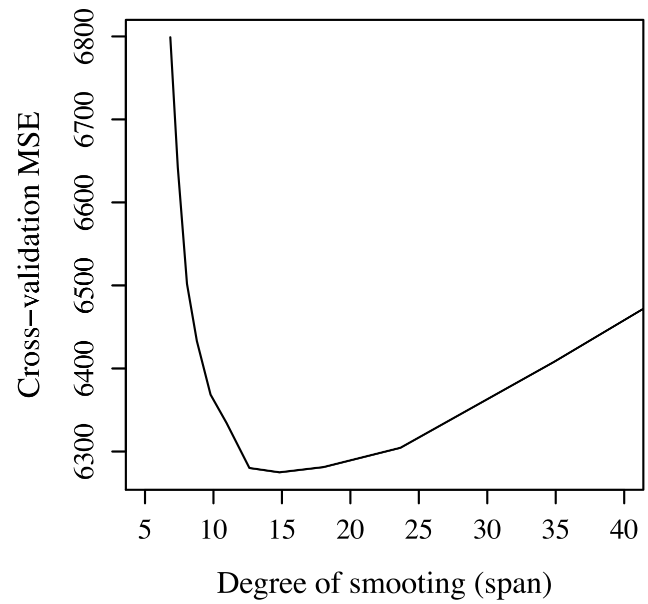

(a) Turbine V82

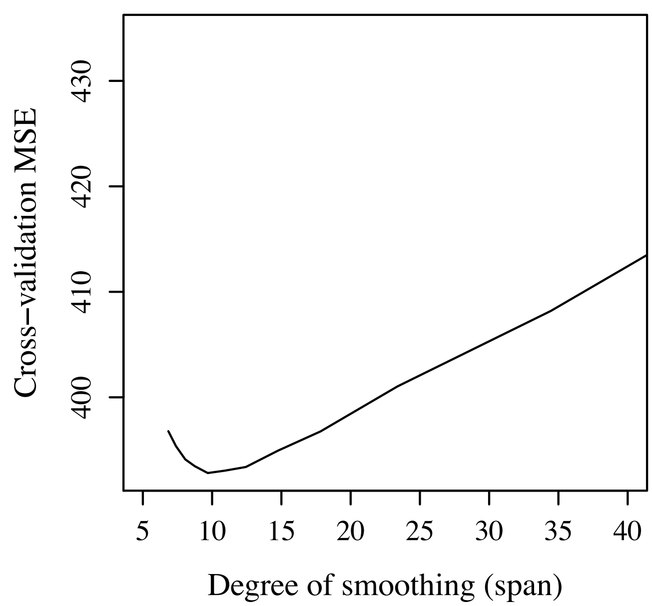

(b) Turbine FL-255

Figure 3.5: Cross-validation technique is used to find the optimum degree of smoothness (span) parameter for linear and quadratic locally weighted polynomial regression models for (a) turbine model V82, and (b) turbine model FL-255.

Figure 3.6 shows the locally weighted linear and quadratic regression models of power on wind speed for observations generated by turbines V82 and FL-255. By comparing Figure 3.4 with Figure 3.6, we observe that locally weighted polynomial regression models reduce the bias of polynomial regression models, especially at the boundaries. This is a well known property of locally weighted regression models over their corresponding polynomial regression models [126, 125]. To be more specific, by using the Taylor expansion of $\widehat{f}(v_0)$, one can show that the bias of $\widehat{f}(v_0)$ will only have components of degree $(k+1)$ and higher. For example, local linear regression fits tend to be biased in regions of curvature of true $f(\cdot)$, and locally weighted quadratic regression is generally able to correct this bias [127]. However, the bias reduction is obtained at a cost of variance increase. To see this, one can show that assuming $Var(\epsilon_i) = \sigma^2$ and that ϵ_i's are independent with mean zero, then $Var(\widehat{f}(v_0)) = \sigma^2 \sum_{i=1}^{n} l_i^2(v_0; s)$, where $l_i(v_0; s)$ is the vector of equivalent kernel weights at v_0 and $\sum_{i=1}^{n} l_i^2(v_0; s)$ increases with the degree of polynomial k. Therefore, for choosing k, one needs to pay careful attention to the bias-variance tradeoff of the fitted models.

3.2.3 Spline regression

Locally weighted polynomial regression method could result in an appropriate approximation to the manufacturer power curve. However, in practice, we might not have enough control on the curvature of the fitted power curve to provide a desirable approximation to the nonlinear nature of the relationship between the generated power and the wind speed. One way to achieve more flexibility and provide more control on the curvature of the fitted power curve is to use piecewise polynomials. A piecewise polynomial regression involves fitting separate low-degree polynomials over different regions of the wind speeds. To this end, we need to specify K different breakpoints,

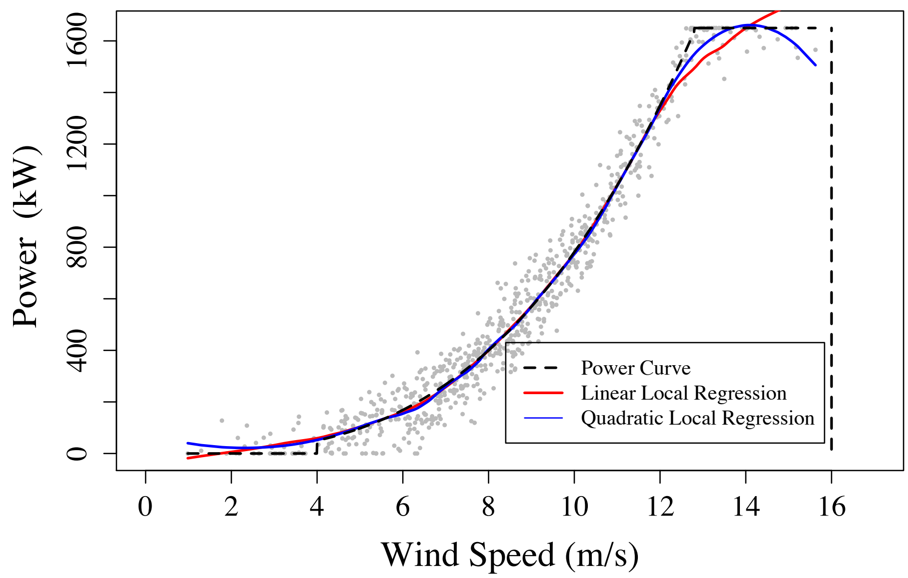

(a) Turbine V82

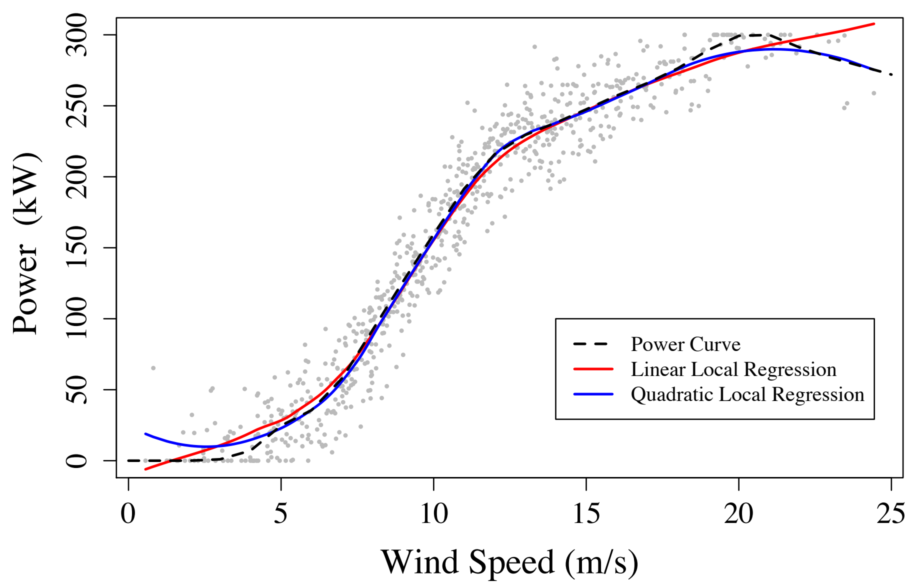

(b) Turbine FL-255

Figure 3.6: Locally weighted linear and quadratic regression models for the power data sets generated from the theoretical power curves of (a) turbine model V82, and (b) turbine model FL-255. The black dashed curves are theoretical power curves from the manufacturers.

known as knots, throughout the range of the wind speeds; and then fit $K + 1$ different polynomial regression models. To fit a smooth and continuous piecewise degree-k polynomial regression, we need to put the constraints that the first $k-1$ derivatives of the fitted power curve to be continuous. This can be achieved by using the polynomial spline regression function which is defined as:

$$p_i = \beta_0 + \sum_{r=1}^{k} \beta_r v_i^r + \sum_{j=1}^{K} \beta_{k+j}(v_i - \zeta_j)_+^k + \epsilon_i, \tag{3.12}$$

where $k \geq 1$ is the order of spline, $\zeta_1, \ldots, \zeta_K$ are a set of pre-specified knots, and the function $(\cdot)_+^k$ denotes a truncated power function as follows

$$(v_i - \zeta_j)_+^k = \begin{cases} (v_i - \zeta_j)^k, & v_i > \zeta_j, \\ 0, & \text{otherwise.} \end{cases} \tag{3.13}$$

The most popular spline regression is the cubic spline corresponding to the choice of $k = 3$ in Equation (3.12). Cubic spline regression models have been used for power curve modeling by [128], and are reliable to predict wind turbine power with smooth power curves. A cubic spline is a curve made up of sections of cubic polynomial joined together so that they are continuous in value as well as the first and second derivatives. As in Equation (3.12), the basic way to represent a cubic spline is to start off with power function basis v, v^2 and v^3 for cubic polynomial, and then add one truncated power series basis function per knot. Figure 3.7 shows truncated linear, cubic and quintic power function basis for spline regression on [0, 1] with knots at $\{0.1, 0.3, 0.5, 0.7, 0.9\}$. Note that for a sample of size n, the general spline regression model in Equation (3.12) can be written as

$$\mathbf{P} = \mathbf{Z}\boldsymbol{\beta} + \boldsymbol{\epsilon}, \tag{3.14}$$

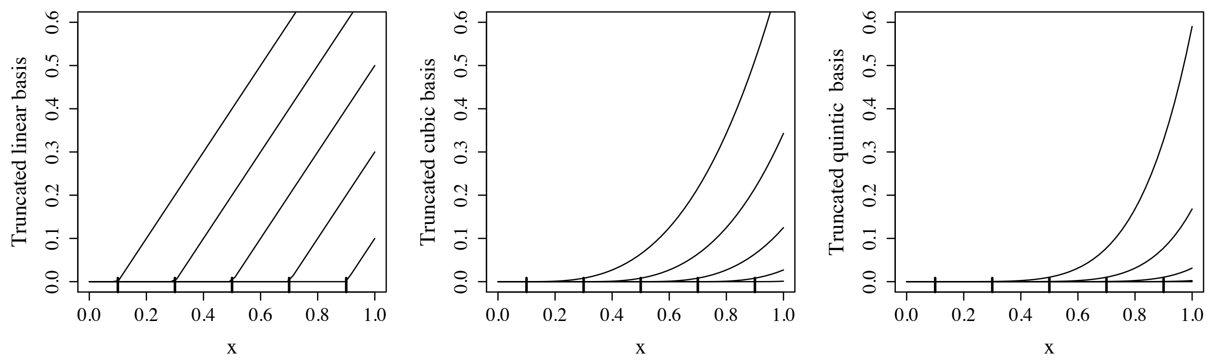

Figure 3.7: Truncated linear, cubic and quintic power function basis on [0,1] for a cubic spline regression model with knots at $0.1, \ldots, 0.9$ with the step of 0.2.

with $\mathbf{Z}_{n\times(K+k+1)} = (\mathbf{V}_{n\times(k+1)}, \mathbf{U}_{n\times K})$, where $\mathbf{U}_{n\times K}$ is a matrix with elements $(v_i - \zeta_j)_+^k$, $i = 1, \ldots, n$ and $j = 1, \ldots, K$, as follow

$$\mathbf{U}_{n\times K} = \begin{pmatrix} (v_1-\zeta_1)_+^k & (v_1-\zeta_2)_+^k & \cdots & (v_1-\zeta_K)_+^k \\ (v_2-\zeta_1)_+^k & (v_2-\zeta_2)_+^k & \cdots & (v_2-\zeta_K)_+^k \\ \vdots & \vdots & \vdots & \vdots \\ (v_n-\zeta_1)_+^k & (v_n-\zeta_2)_+^k & \cdots & (v_n-\zeta_K)_+^k \end{pmatrix}.$$

Hence, the model parameters can be estimated by the least squares method to obtain

$$\widehat{\boldsymbol{\beta}} = (\mathbf{Z}^\top\mathbf{Z})^{-1}\mathbf{Z}^\top\mathbf{P}, \tag{3.15}$$

and the fitted power curve at speed v_i is $\widehat{f}(v_i) = \mathbf{Z}_i\widehat{\boldsymbol{\beta}}$, where $\mathbf{Z}_i = (1, v_i, , \ldots, v_i^k, (v_i - \zeta_1)_+^k, \ldots, (v_i - \zeta_K)_+^k)$ is the i-th row of the matrix $\mathbf{Z}$.

The normal equations associated with the truncated power basis are highly ill-conditioned resulting in inaccuracies in the calculation of $\widehat{\boldsymbol{\beta}}$. For computational purposes, we use

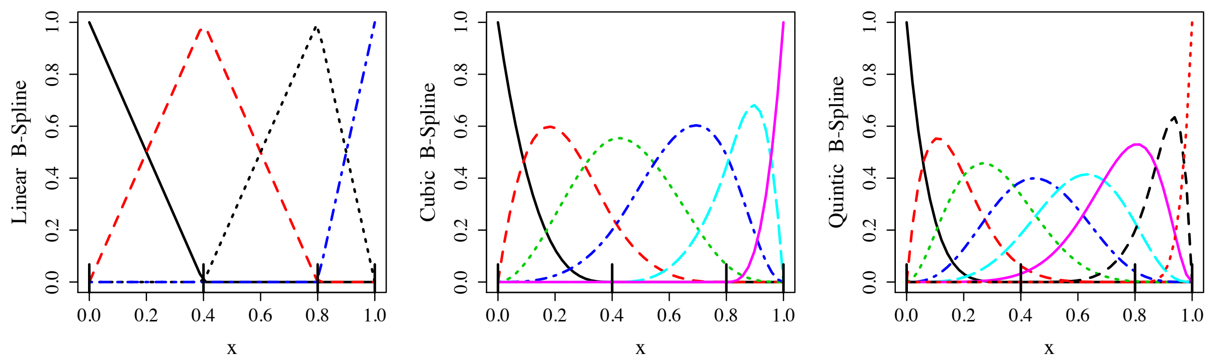

Figure 3.8: Linear, cubic and quintic B-splines on [0, 1] corresponding to knots 0.4, 0.8.

the B-spline basis and re-formulate Equation (3.12) as

$$p_i = \sum_{j=0}^{k+K} \beta_j B_j^k(v_i) + \epsilon_i, \tag{3.16}$$

or equivalently, $\mathbf{P} = \mathbb{B}\boldsymbol{\beta} + \boldsymbol{\epsilon}$, where $\mathbb{B}$ is a matrix with its (i, j)-th element being $B_j^k(v_i)$ where

$$B_j^k(v_i) = \tfrac{(v_i - \zeta_j)}{(\zeta_{j+k} - \zeta_j)} B_j^{k-1}(v_i) + \tfrac{(\zeta_{j+k+1} - v_i)}{(\zeta_{j+k+1} - \zeta_{j+1})} B_{j+1}^{k-1}(v_i),$$

for $j = -k, -k+1, \ldots, K$, $\zeta_0 = \zeta_{-1} = \ldots = \zeta_{-k} = \min\{v_i, i = 1, \ldots, n\}$ and $\zeta_K + 1 = \max\{v_i, i = 1, \ldots, n\}$. Also $B_j^0(v_i)$ are the natural basis for piecewise constant functions. Figure 3.8 shows samples of linear, cubic and quintic B-splines on [0,1] when there are two knots at points 0.4 and 0.8.

The least squares estimates of $\boldsymbol{\beta}$ is then given by

$$\widehat{\boldsymbol{\beta}} = (\mathbb{B}^\top \mathbb{B})^{-1} \mathbb{B}^\top \mathbf{P}, \tag{3.17}$$

which is more feasible for computational purposes. For other formulations of the spline regression see [129]. As depicted in Figure 3.9, spline regression often leads to superior results over polynomial regression. This is because spline regression introduces flexibility by increasing the number of knots but keeping the degree of polynomial fixed. If the function $f(\cdot)$ changes rapidly in a region of v, one can add more knots to capture the change. However, spline regression tends to behave erratically beyond the boundary knots compared with the corresponding global polynomial regression in those regions [127]. Natural spline regressions, which are constrained to be linear beyond the boundary knots, provide a useful tool to overcome this problem. Figure 3.9 shows the natural cubic spline power curve models fitted to the power data for turbines V82 and FL-255 when using 3, 10, and 20 equally spaced knots. One can observe that, if the the number and location of knots are chosen badly, spline regression will result in a poor fit. Several methods are proposed in the literature to obtain algorithms for optimizing over the number and location of knots, as shown by [130].

3.2.4 Penalized spline regression

To address the challenge of choosing the number and the location of knots in the spline regression, we propose to use a penalized spline regression model for fitting wind turbine power curves. The idea is to use spline regression with a fixed basis dimension at a size slightly larger than it is necessary (*e.g.*, fixed quantiles of wind variable), but to control the power curve smoothness by adding a penalty to the least squares fitting objective. In other words, we fit a power curve to the data points by minimizing

$$\frac{1}{n}\sum_{i=1}^{n}(p_i - f(v_i))^2 + \lambda \int \{f^{''}(t)\}^2 \, dt, \tag{3.18}$$

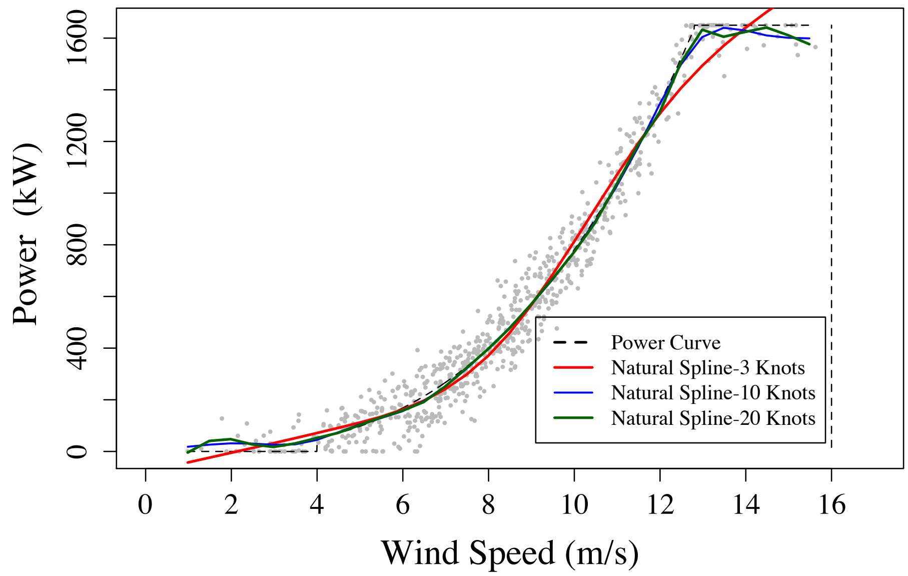

(a) Turbine V82

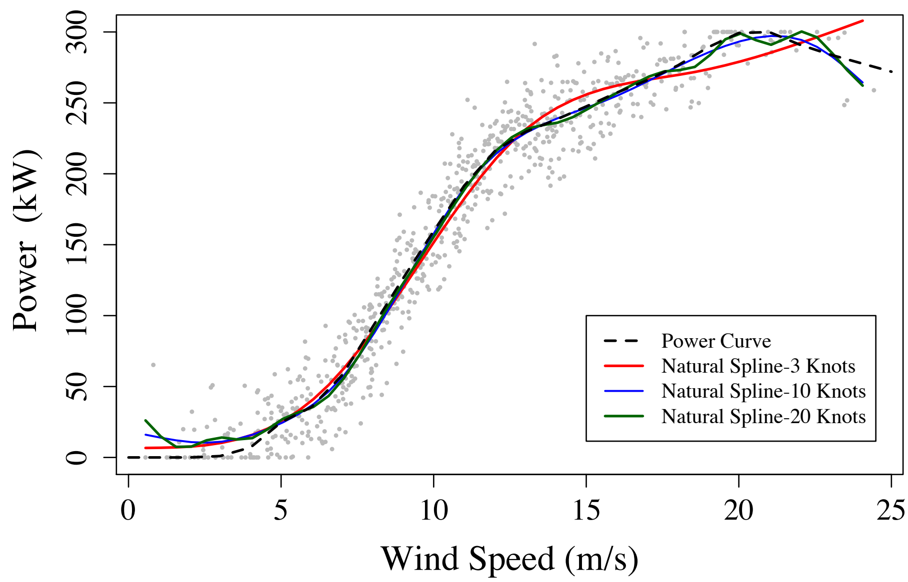

(b) Turbine FL-255

Figure 3.9: Natural cubic spline fits the power curves with 3, 10, and 20 knots for the power data generated from turbines V82 (a) and FL-255 (b). The black dashed curves are theoretical power curves from the manufacturers.

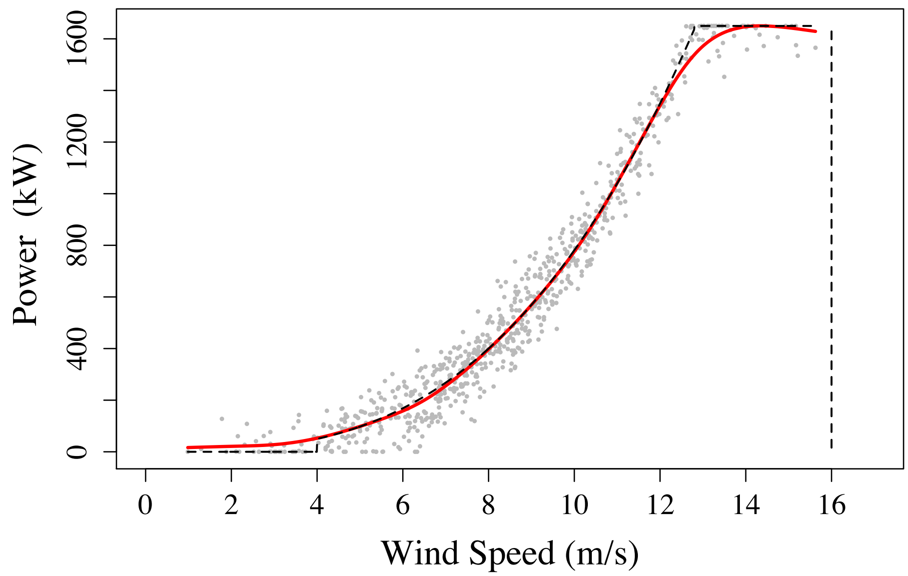

(a) Turbine V82

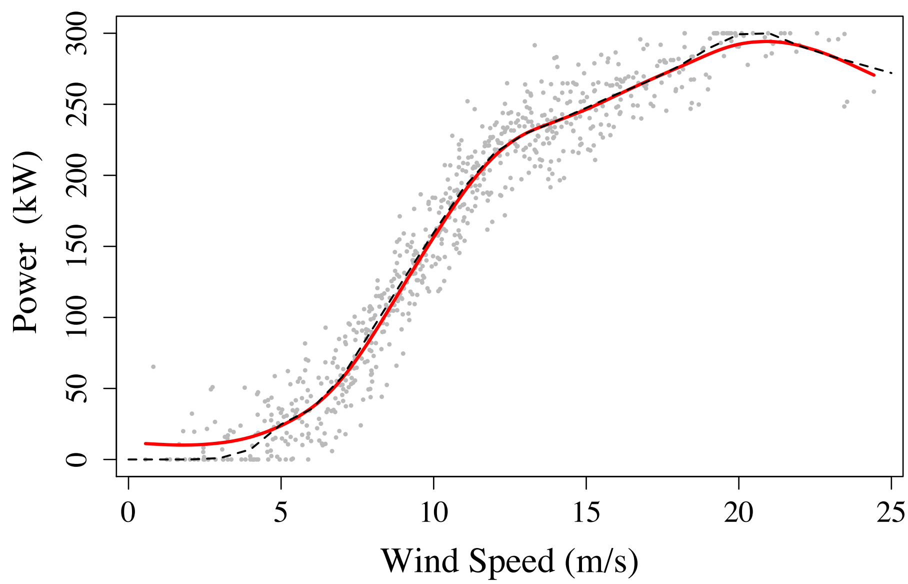

(b) Turbine FL-255

Figure 3.10: Fitted power curves (solid red curve) for (a) turbine V82 and (b) turbine FL-255 using penalized smoothing spline with the theoretical power curves (black-dashed curve).

where λ is a fixed smoothing parameter and $f''(\cdot)$ is the second derivative of $f(\cdot)$. The first term in Equation (3.18) measures the goodness of fit of the curve while the second term measures the roughness of $f(\cdot)$. The smoothing parameter λ balances the trade-off between goodness of fit and roughness of the curve. If the penalty is zero, we obtain a curve that interpolates the data points. If the penalty is infinite, we obtain an ordinary least squares fit to the data. The common way of choosing λ is by cross-validation. In many cases, the penalty term can be written as a quadratic form of $\boldsymbol{\beta}$, *i.e.*, $\int \{f''(t)\}^2\, dt = \boldsymbol{\beta}^\top \mathbf{D}\boldsymbol{\beta}$, where $\mathbf{D}$ is a matrix of known coefficients. The estimated model parameters under penalized spline regression are given by

$$\hat{\boldsymbol{\beta}}(\lambda) = (\mathbf{Z}^\top \mathbf{Z} + \lambda \mathbf{D})^{-1} \mathbf{Z}^\top \mathbf{P}, \tag{3.19}$$

and, the fitted power curve is

$$\hat{\mathbf{P}}(\lambda) = \mathbf{Z}\hat{\boldsymbol{\beta}}(\lambda) = \mathbf{Z}(\mathbf{Z}^\top \mathbf{Z} + \lambda \mathbf{D})^{-1} \mathbf{Z}^\top \mathbf{P} = \mathbf{H}(\lambda)\mathbf{P}, \tag{3.20}$$

where $\mathbf{H}(\lambda)$ is the hat matrix. Here, we choose the penalty function to be $\sum_{j=1}^{K} \beta_{p+j}^2$, which results in $\mathbf{D} = diag(\mathbf{0}_{p+1}, \mathbf{1}_K)$ [131]. To obtain a suitable value of λ, the generalized cross-validation statistic is used:

$$\text{GCV}(\lambda) = \frac{\text{MSE}(\lambda)}{[1 - \lambda n^{-1} trace\{\mathbf{H}(\lambda)\}]^2}\,, \tag{3.21}$$

where

$$\text{MSE}(\lambda) = \frac{1}{n} \sum_{i=1}^{n} (p_i - \hat{p}_i(\lambda))^2$$

and $\hat{p}_i(\lambda)$ is the i-th element of $\hat{\mathbf{P}}(\lambda)$ in Equation (3.20). Here, $trace\{\mathbf{H}(\lambda)\}$ is called the effective degrees of freedom of the fit. We choose a suitable value of λ by computing GCV(λ) for a grid of λ values and choosing the minimizer over the grid. Figure 3.10 depicts the power curves fitted to the simulated observations from turbines V82 and FL-255 using penalized smoothing spline when the smoothing parameter is obtained using generalized cross-validation technique. As shown in this figure, penalized smoothing spline provides the best fit, and the obtained power curves are similar to the manufacturer's. In the proposed method, the difficulty of choosing the number and the location of knots in cubic spline regression is reduced to a simple problem, and can be solved by cross-validation technique.

3.3 Real data application

In this section, we apply the methods in Section 3.2 to proprietary wind power data of a wind farm in North America. The wind power plant (WPP) includes over five dozen identical wind turbines with the rated capacity of 1.7 MW and the hub height of 80 m spread over an area of over 90 km^2. The cut-in, rated, and cut-out speeds of the turbines are 3.5, 13, and 20 m/s, respectively. There are three meteorological (MET) towers located in the WPP collecting wind speeds, wind directions, air density and humidity at 10-minute average. We have selected four wind turbines ($T_1, \ldots, T_4$) of the WPP to analyze the performance of the presented methods. To more accurately represent the wind data, turbines T_1, T_2, and T_3 are chosen near the MET towers, while the turbine T_4 is away from the towers. Two raw data sets of 4320 pairs are used representing 1 month 10-minute averaged data in June-July 2006, and 1 month in December-January 2007. This offers a more realistic representation of the performance of the turbines. To investigate the influence of the resolution of the available data, we also perform the analysis based on the hourly averaged data for the associated time spans.

Table 3.1: Classification of the wind power and speed raw data at the location of study.

Type	Data Description
1	Data points following the pattern of turbine's power curve.
2	Data points with high wind speed and low power values.
3	Data points with low wind speed and high power values.
4	Data points with negative wind speed values.
5	Data points with negative wind power values.

Figure 3.11 shows that the measured data of wind power versus wind speed do not exactly follow the power generation curve provided by the manufacturer. A wind turbine power curve is created by manufacturer through test measurements and under a standard procedure. The standard procedure is provided by the International Electrotechnical Commission (IEC) for measuring the power performance characteristics of turbines [132]. The deviation of actual measured wind power data from the turbine's power curve can be explained by the difference between the standard test conditions and the conditions of the actual site. The standard atmospheric test conditions as well as wind direction, vertical wind speed profile, horizontal uniformity of the wind speed across the face of the turbine, and aging components are among the influencing factors [133]. Another influencing parameter is the distance between the MET tower and the wind turbine where the actual wind speed experienced by the generator may not exactly match the measured data at the tower. Sensor and other data collection equipments can also cause erroneous measurements resulting in misrepresentation of the wind and power data.

Similar to [134], we observe different types of data points in our raw data set that can be classified as per Table 3.1. Data processing is required to filter the invalid data points. According to Table 3.1, data type 1 are the desired data points. Types 4 and 5 of data, where negative values for wind and for power observed, are filtered. To filter out the data types 2 and 3, for each wind speed datapoint, only the power values

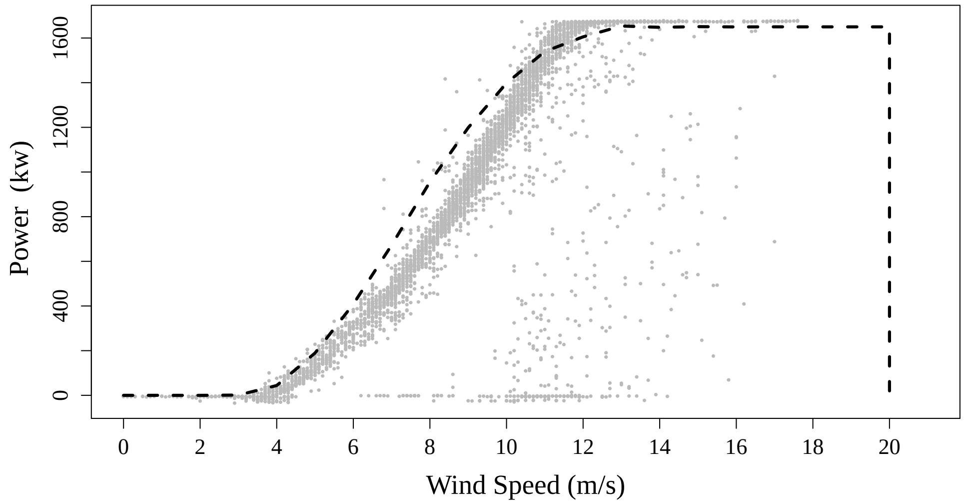

Figure 3.11: Turbine T_1 10-minute measured power data *vs.* measured wind speed. The manufacturer power curve is shown in dashed line with characteristic speeds: cut-in ($v_c = 3.5$), rated ($v_r = 13$) and cut-out ($v_s = 20$).

which lie within three standard deviations of the average power value at that speed are included.

Figure 3.12 shows the obtained scatter plot of 3663 data points from turbine T_1 for one month in winter after performing the filtering procedure. This figure also depicts the marginal histograms associated with the wind speed distribution on the horizontal axis and the generated power distribution on the vertical axis are. Figure 3.13 shows the four models proposed in this thesis applied to the filtered wind speed and the generated wind power data.

There are several statistical metrics which can be used as appropriate measures of performance for the fitted power curves such as the root of the mean of squared error (RMSE), normalized mean absolute percentage error (NMAPE), symmetric mean absolute percentage error (sMAPE), the mean absolute error (MAE), and the coefficient

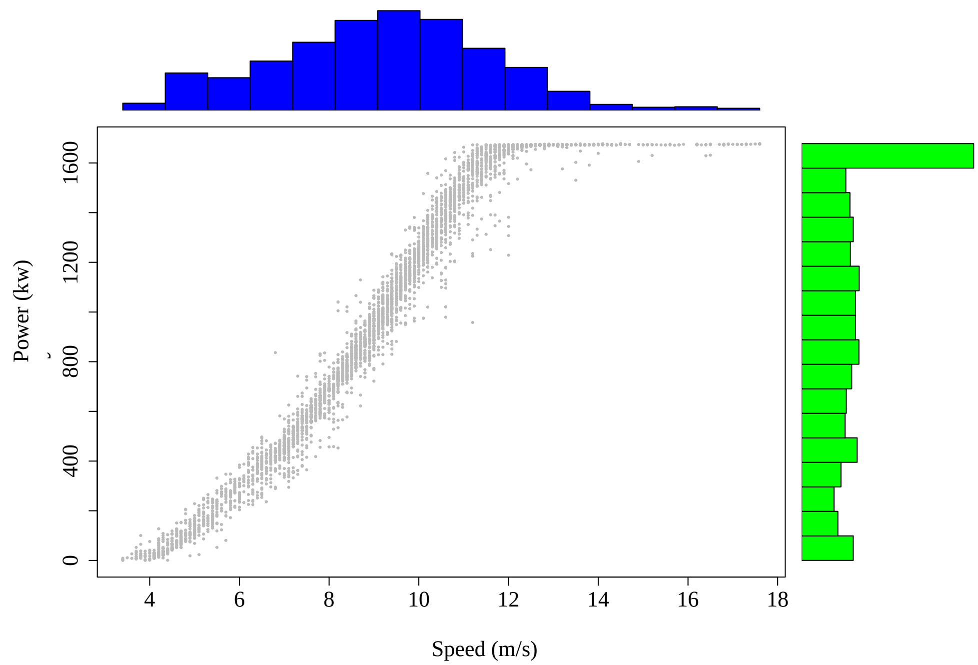

Figure 3.12: The scatter plot of the wind speed and the generated power with the marginal histograms associated with each variable by turbine T_1 for one month in winter.

of determination (R^2) [116, 135]. In this work, we use three measures to investigate the performance of the proposed models. The RMSE is the square root of the mean of the squared difference between the estimated and the actual power values given by

$$\text{RMSE} = \sqrt{\frac{1}{n}\sum_{i=1}^{n}(p_i - \widehat{p}_i)^2}\,, \tag{3.22}$$

where p_i is the observed wind power and $\widehat{p}_i$ is the estimated value of the power using the underlying method.

The NMAPE is the percentage of the mean of sum of the difference between the estimated and the actual power values over the maximum value of the estimated wind

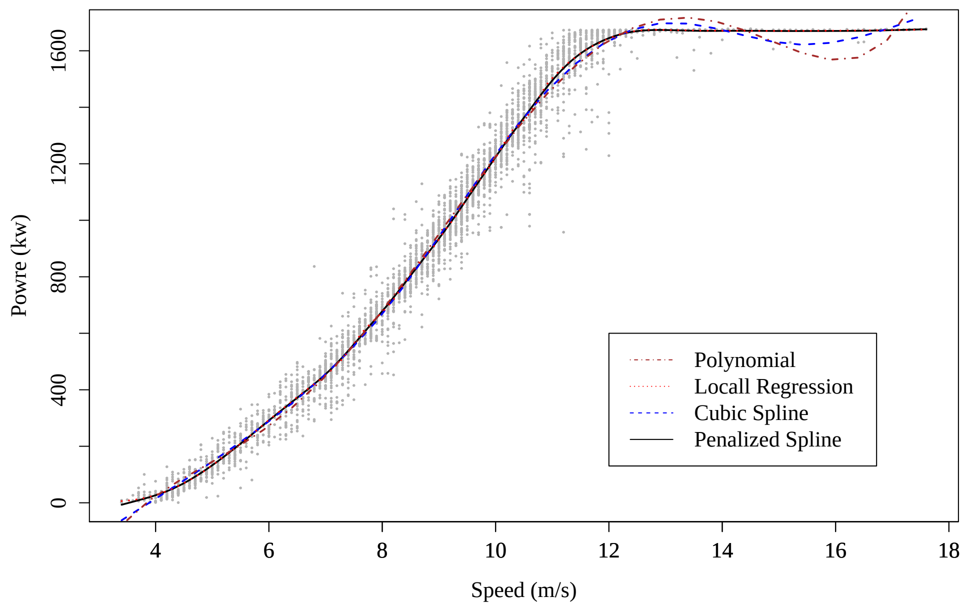

Figure 3.13: The scatter plot of the wind speed and the generated power by turbine T_1 for one month in winter with the fitted power curves using proposed methods.

power data. The NMAPE is given by

$$\text{NMAPE} = \frac{1}{n}\sum_{i=1}^{n}\frac{|p_i - \widehat{p}_i|}{\max_{j=1}^{n}\{\widehat{p}_j\}} \times 100\,, \tag{3.23}$$

and, the MAE is the mean of the absolute of the difference between actual and estimated values of power given by

$$\text{MAE} = \frac{1}{n}\sum_{i=1}^{n}|p_i - \hat{p}_i|. \tag{3.24}$$

By performing the error analysis, the values of RMSE, NMAPE, and MAE for the polynomial regression, locally weighted polynomial regression, cubic spline, and penalized spline methods are presented here. Table 3.2 shows the results of the analysis for two data sets representing 1 month 10-minute data in June-July 2006, and 1 month in December-January 2007. In this table, the values are obtained for the turbines T_1, T_2, and T_3 which are located near the three MET towers in the WPP. For the hourly data, the same data sets are used, and are averaged hourly to investigate the influence of data resolutions on the error measures. Table 3.2 ranks the performance of all four methods based on the calculated measures, where the smaller values are desirable. The ranking numbers are shown in the parenthesis next to the RMSE, NMAPE, and MAE values. We also provide the overall performance ranking of each method. As shown in the table, penalized spline regression method outperforms all other methods addressed in this study. Table 3.2 also suggests that locally weighed polynomial regression is dominating polynomial regression and cubic spline methods. Comparing the values of RMSE, NMAPE, and MAE for summer and winter shows the error measures are greater in the winter data for the same generator. This can be explained by the impact of weather condition and cold temperature on the atmospheric parameters, and on the mechanical and overall efficiency of the machine.

Similar to Table 3.2, the values of RMSE, NMAPE, and MAE are shown in Table 3.3 for the proposed methods of the same turbines. In this table, the same data sets are used, but the 10-minute data are averaged hourly to investigate the influence of data resolutions on the error measures. As shown in Table 3.3, the overall performance of the presented models for the hourly data sets is similarly following the performance ranking of the 10-minute data sets in Table 3.2.

Table 3.4 provides the values of of RMSE, NMAPE, and MAE for turbine T_4, which is the one located away from the MET towers. In this table, the 10-minute and hourly averaged data sets are used to investigate the influence of data resolution on the error measures for the proposed methods in the summer and winter periods. As shown in Table 3.4, the overall performance of the error metrics for turbine T_4, similarly follows

Table 3.2: Results for the summer and winter 10-minute data for turbines T_1, T_2 and T_3 for the polynomial regression (PR), locally weighted regression (LR), cubic spline (CS), and penalized spline (PS) methods.

Time	Method	Turbine T1			Turbine T2			Turbine T3			Final
		MAE	RMSE	NMAPE	MAE	RMSE	NMAPE	MAE	RMSE	NMAPE	Rank
Summer	PR	32.17 (4)	46.58 (3)	1.922 (4)	28.39 (4)	43.44 (4)	1.748 (4)	31.71 (4)	45.93 (4)	1.896 (4)	4
	LR	27.65 (2)	38.34 (1)	1.651 (2)	26.86 (3)	36.29 (2)	1.484 (2)	28.28 (2)	42.99 (2)	1.689 (2)	2
	CS	28.01 (3)	38.67 (2)	1.673 (3)	25.08 (2)	36.63 (3)	1.497 (3)	28.32 (3)	43.04 (3)	1.693 (3)	3
	PS	27.60 (1)	38.34 (1)	1.648 (1)	24.79 (1)	36.28 (1)	1.480 (1)	28.16 (1)	42.89 (1)	1.682 (1)	1
Winter	PR	47.95 (3)	69.23 (4)	2.858 (3)	37.63 (4)	49.05 (4)	2.217 (4)	47.95 (4)	63.23 (1)	2.575 (4)	4
	LR	42.87 (1)	67.74 (3)	2.555 (1)	28.24 (1)	41.93 (2)	1.682 (1)	42.88 (1)	65.74 (3)	2.281 (1)	2
	CS	45.39 (2)	67.37 (1)	2.705 (2)	33.91(3)	45.04 (3)	2.019 (3)	45.39 (3)	67.37 (4)	2.396 (3)	3
	PS	42.87 (1)	65.62 (2)	2.555 (1)	28.25 (2)	41.87 (1)	1.683 (2)	42.89 (2)	65.62 (2)	2.301 (2)	1

Table 3.3: Results for the summer and winter hourly data for turbines T_1, T_2 and T_3 for the polynomial regression (PR), locally weighted regression (LR), cubic spline (CS), and penalized spline (PS) methods.

Time	Method	Turbine T1			Turbine T2			Turbine T3			Final
		MAE	RMSE	NMAPE	MAE	RMSE	NMAPE	MAE	RMSE	NMAPE	Rank
Summer	PR	28.13 (4)	48.69 (4)	1.805 (4)	29.62 (4)	47.86 (4)	1.777 (4)	28.13 (4)	48.69 (4)	1.715 (4)	4
	LR	27.55 (2)	47.79 (1)	1.647 (2)	26.87 (2)	45.11 (3)	1.612 (2)	27.55 (2)	47.70 (1)	1.680 (2)	2
	CS	27.69 (3)	47.91 (3)	1.668 (3)	26.99 (3)	45.10 (2)	1.619 (3)	27.69 (3)	47.91 (3)	1.689 (3)	3
	PS	27.51 (1)	47.81 (2)	1.626 (1)	26.59 (1)	44.89 (1)	1.595 (1)	27.51 (1)	47.81 (2)	1.678 (1)	1
Winter	PR	62.53 (4)	99.88 (4)	3.723 (4)	37.31 (4)	60.45 (4)	2.226 (3)	60.84 (4)	104.21 (4)	2.789 (4)	4
	LR	59.80 (2)	96.24 (2)	3.408 (1)	33.78 (2)	57.12 (1)	2.016 (2)	57.11 (1)	102.89 (2)	2.681 (2)	2
	CS	59.84 (3)	98.96 (3)	3.430 (3)	34.63 (3)	57.46 (3)	2.016 (2)	57.47 (3)	103.47 (3)	2.786 (3)	3
	PS	58.66 (1)	95.93 (1)	3.424 (2)	32.85 (1)	54.38 (2)	1.960 (1)	57.36 (2)	102.26 (1)	2.386 (1)	1

the performance ranking of models for turbines $T_1, \ldots, T_3$ in Table 3.2 and Table 3.3.

3.4 Chapter summary

Accurate modeling of the wind turbine power curves is an important tool in the wind energy industry that can be used for assessment and monitoring of the turbine's performance, power forecasting as well as sizing the storage capacity for wind power integration. We have presented parametric and nonparametric regression models for estimating wind turbine power curves. Polynomial regression was used as the benchmark parametric method for power curve fitting. We have shown that polynomial regression models are limited by their global nature, and are very sensitive to outliers. Also, finding a good fit to the empirical data requires a high degree polynomial regression model which can cause an overfitting to the observed data. Locally weighted polynomial regression was introduced to address the issues of the global nature in polynomial regression and its sensitivity to outliers within the observations. Spline regression method, which is based on piecewise polynomial regression models, was then examined to achieve more flexibility for fitting the power curve. In this method, an important issue is finding the number and the location of knots to provide a good fit to the empirical power curve. To this end, we proposed a penalized spline regression model which reduces these problems to a simple problem of choosing a single parameter which can be determined using a cross-validation technique. The performance of the proposed methods was evaluated based on two simulated random data sets with normal errors as well as an operational wind power data for a wind farm in North America. Four wind turbines were selected to analyze the performance of the presented methods, of which, three turbines are chosen near the MET towers while the last one is located away from the towers. The accuracy of each method is evaluated

Table 3.4: Results for the summer and winter 10-minute and hourly data for turbine T_4 for the polynomial regression (PR), locally weighted regression (LR), cubic spline (CS), and penalized spline (PS) methods.

Time	Method	Summer			Winter			Final
		MAE	RMSE	NPAME	MAE	RMSE	NPAME	Rank
10 min.	PR	41.35 (4)	64.69 (4)	2.461 (4)	58.56 (4)	93.40 (4)	3.398 (4)	4
	LR	39.55 (3)	63.51 (2)	2.356 (3)	53.29 (2)	89.25 (1)	3.079 (2)	2
	CS	39.48 (2)	63.62 (3)	2.352 (2)	56.64 (3)	92.37 (3)	3.389 (3)	3
	PS	39.43 (1)	63.38 (1)	2.349 (1)	53.00 (1)	90.22 (2)	3.071 (1)	1
1 hour	PR	32.17 (4)	46.58 (3)	2.898 (1)	28.39 (4)	43.44 (4)	3.539 (4)	4
	LR	27.65 (2)	38.34 (1)	2.968 (4)	26.86 (3)	36.29 (2)	3.441 (1)	2
	CS	28.01 (3)	38.67 (2)	2.910 (2)	25.08 (2)	36.63 (3)	3.514 (3)	3
	PS	27.60 (1)	38.34 (1)	2.914 (3)	24.79 (1)	36.28 (1)	3.471 (2)	1

using the RMSE, NMAPE and MAE metrics. The results of this study suggest that penalized spline regression method utilized in this study presents a better performance over the other analyzed methods. The outcome of this study can be used in various applications such as turbine performance monitoring, power forecasting as well as sizing the storage capacity for wind power integration.

Chapter 4

Storage Sizing Algorithm

In this chapter, a statistical algorithm is proposed for predicting the size of the energy storage system required for delivering base-load electricity to a selected confidence level for a wind farm. The proposed algorithm can be utilized by utilities to assess wind integration and to investigate better capacity credits for wind farms connected to the grid, by wind farm operators to potentially increase their return on investment by designing a base-load wind farm to a selected confidence level, and by financial institutions to calculate the confidence level for base-load wind farm projects. Methods introduced are based on parametric and nonparametric statistical models using wind resource assessment data and available wind turbine information that reflect different stages of a wind farm project—from site selection to operational status. The proposed methods apply to isolated and grid connected wind farms. To study the performance of each method, we apply these to a North America operational wind farm data set. Averaged 10-minute data are used to calculate the firm capacity of the wind turbine for each proposed method. The size of the storage system is obtained by calculating the energy imbalances in each time interval and integrating these over the study time horizon. The probability distributions for the values of the occurred charges and discharges are constructed to enable applying different desired confidence levels. The results show that for different stages of the wind farm development, and depending on the available information, the proposed algorithm can properly predict and estimate size of the energy storage required to deliver constant output power to a user selected confidence level. We also compare the results the hourly averaged data to investigate the influence of time intervals on the model output. The comparison shows that while the results follow a similar pattern, the size of storage varies for different confidence levels. Similar to Chapter 3, the statistical methods are coded in R programming software.

4.1 Wind energy and ESS integration

Utilities that have a significant portion of their generation from fossil fuel sources have realized that a move away from these sources will be required for a more sustainable future due to CO_2 and other harmful emissions [24]. Several studies have investigated high penetration of intermittent wind power into the electric grids, and have addressed the main challenge of accommodating high penetration of the intermittent sources, *i.e.*, the variability imposed on the power system [136, 137, 138, 139]. Most robust grid systems today, no matter what the supply mix is, can likely accommodate approximately 25–30% intermittent sources such as wind power without any major changes to the grid [140, 141]. Larger penetrations of wind and solar renewables on an energy basis may require the use of storage systems to integrate these intermittent renewables. The future electric grid can be made 100% renewable with utilizing intermittent renewables, if their intermittent nature is addressed by the addition of an appropriate amount of

ESS [141, 142, 143]. As postulated in this chapter, these intermittent renewables can be "converted" to base-load generation by using appropriately sized ESS to smooth out their intermittency, allowing penetrations of more renewables. Recent studies show that wind electricity generation is economically competitive, achieving the lowest levelized cost [11, 15]. The declining costs of ESS can further support utilization of large scale ESS in power systems. Accurate estimation of the required storage capacity also provides a more reliable economic analysis for effective integration of wind energy. This is also true for isolated remote communities who are looking at displacement of diesel generators due to high costs. The cost formula presented in Chapter 6 shows how the size and cost of storage system affects the total cost of wind power production as a base-load generator unit.

In this chapter, methods are presented to perform the ESS sizing calculations each representing a scenario associated with (i) wind farm project conception, or, (ii) wind farm operation. In each method, we use statistical models to calculate the required ESS energy capacity. A data set of wind speed and power values for a wind farm in North America is used representing 10-minute and hourly averaged data for a duration of 6 months in 2006 and 2007 to implement the methods and compare the influence of data resolution on the size of ESS.

Section 4.2 describes the proposed ESS sizing algorithm. In Section 4.3, the first method is introduced for the scenario where the theoretical power curve is derived from available wind speed data. Within this method, three different approaches are presented which require prior knowledge of wind turbine parameters. Section 4.4 presents the ESS sizing case when the turbine is selected and the manufacturer power curve is known. Section 4.5 considers the case when the wind farm is operational and the operational wind power data are available. In Section 4.6, we apply these methods

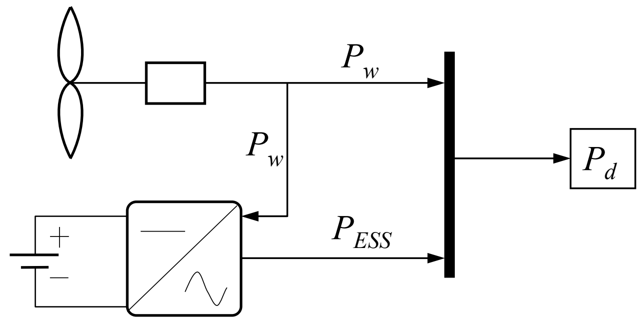

Figure 4.1: Schematic of integration of wind power, P_w, and power of energy storage system, P_{ESS}, to deliver a base-load or dispatchable power, P_d.

to wind resource and operation data of an actual wind farm. The summary of the chapter including a discussion on the future of electric grid with renewable energy is provided in Section 4.7 followed by some concluding remarks .

4.2 Storage sizing algorithm

This section presents the introduced general algorithm for calculating the size of ESS when the goal is to produce the base-load power of a wind generator in a given location. Figure 4.1 shows a schematic of integration of wind power, P_w, and power of energy storage system, P_{ESS}, to deliver constant and dispatchable power, P_d. We propose three different methods, denoted by M_1, M_2, and M_3, and expand on them using parametric and nonparametric statistical methods techniques that are introduced in Chapter 3. Each method represents a stage of development of a wind farm, from conception to operational.

The first method, M_1, is performed before the operation of the wind farm and uses only the wind resource assessment data of the location of study as well as some possible general information about the characteristics of a generic wind turbine such as v_c, v_s, and v_r wind speeds. In this method, M_{1A} represents the case where no information about the wind turbine is available. M_{1B} assumes that in addition to the time-domain wind data, v_c and v_s of a generic wind turbine are known. In M_{1C}, the rated speed of the generic turbine is also known.

The second method, M_2, is similar to M_1 except that we additionally have knowledge of the selected wind turbine power curve for the wind farm, which can be written as $p_i = f(v_i)$ where $f(\cdot)$ is known [106].

Method M_3 is performed when the actual operational data of the wind farm are available including the time series of the measured wind speeds and the corresponding generated power. Thus, these methods cover all possible scenarios for estimating the capacity of ESS to generate base-load wind power to a selected confidence level.

In the proposed algorithm, the storage sizing procedure is performed using the following steps:

i. *Wind turbine firm capacity calculation*: The firm capacity of the wind turbine, p^*, is determined as the reference value with respect to which, the size of ESS is calculated. This is the average output power that the generator is producing intermittently.

ii. *Power imbalances calculation*: The net difference between the firm capacity of the turbine p^*, and the wind power, P_w, is calculated.

iii. *Energy imbalances calculation*: For each time interval, the individual energy imbalances are calculated by integrating the net power rating over the span of time i.

iv. *ESS sizing calculation*: The size of each energy charges and discharges is obtained by summing over consecutive occurrences of individual energy imbalances.

v. *Confidence levels*: The histogram of ESS charges and discharges is created to fit a suitable pdf, and apply different statistical methods to obtain the size of ESS with different confidence levels. This represents a critical step in performing an economic assessment to determine the size of ESS.

4.3 M_1 based on wind resource assessment data

To obtain the firm capacity of the turbine, we first estimate the pdf of wind speeds by constructing the histogram of the wind speed data and estimating the parameters of the pdf of wind speeds. The Weibull distribution is often used to fit the wind speed data [144, 145, 146] as a unimodal, two parameter family of distribution functions with the following pdf

$$f_V(v) = \left(\frac{k}{c}\right)\left(\frac{v}{c}\right)^{k-1} e^{-(v/c)^k}; \quad v > 0, \tag{4.1}$$

where $c > 0$ is the scale parameter with the same unit as wind speed, and $k > 0$ is the dimensionless shape parameter of the distribution [147]. The notation $V \sim$ Weibull(c, k) is used to denote that V has the Weibull distribution with parameters c and k. The Weibull distribution with $c = 2$ reduces to the Rayleigh distribution which is widely used for fitting the wind speed data [148, 149]. The mean and the variance of a Weibull random variable are obtained in terms of gamma functions as follow

$$\mu_V = c\,\Gamma(1 + \frac{1}{k}) \qquad \text{and} \qquad \sigma_V^2 = c^2 \left\{\Gamma(1 + \frac{2}{k}) - \Gamma^2(1 + \frac{1}{k})\right\}, \tag{4.2}$$

where

$$\Gamma(t) = \int_0^\infty x^{t-1}\, e^{-x}\, dx, \quad t > 0.$$

There are several methods to estimate c and k in Equation (4.1), including the maximum likelihood (ML) method, the method of moments (MM), and the least square (LS) method [150, 151]. In this work, we use the ML method to estimate c and k which has several desirable theoretical properties such as asymptotic optimality and efficiency for large sample sizes [152]. The ML estimates of c and k are uniquely determined as follow [153]:

$$\widehat{c} = \left(\frac{1}{n} \sum_{i=1}^{n} {v_i}^{\widehat{k}} \right)^{\frac{1}{\widehat{k}}}, \tag{4.3}$$

$$\widehat{k} = \left(\frac{\sum_{i=1}^{n} {v_i}^{\widehat{k}} \ln v_i}{\sum_{i=1}^{n} {v_i}^{\widehat{k}}} - \frac{\sum_{i=1}^{n} \ln v_i}{n} \right)^{-1}. \tag{4.4}$$

Note that Equations (4.3) and (4.4) need to be computed numerically, or to be approximated using a Newton-Raphson algorithm [154].

By computing $\widehat{c}$ and $\widehat{k}$ of the fitted Weibull distribution, the pdf of the wind power is calculated using the theoretical wind power equation for the underlying wind turbine in the location of study. The wind power distribution can then be used to find the desired firm power capacity p^*, *i.e.*, the expected value (mean) of the power distribution. We now use M_{1A}, M_{1B} and M_{1C} to calculate the corresponding pdfs of the wind power. The idea is to estimate the required ESS capacity in a location prior to the selection or operation of the wind farm and study the sensitivity of ESS sizing with respect to the choice of p^*.

In M_{1A}, we first need to estimate the pdf of the theoretical wind power using the wind speed Weibull distribution [155, 156]. As shown in Section 3.2 of the previous chapter, the theoretical wind power from the mass flow rate of air through the turbine blades swept area is proportional to the cubic of the wind speed and is obtained by

$$P_w = \frac{1}{2}\ \rho(z,T)\ A\ V^3, \tag{4.5}$$

where P_w is the theoretical wind power in W, ρ is the air density in kg/m^3 as a function of the altitude z and the temperature T at the site, A is the turbine rotor's blades swept area in m^2, and V is the wind speed in m/s [107, 123]. In reality, the air density is stochastic but it is assumed to be known at the site of study, and it's variability is negligible. Hence, without loss of generality $\rho = \rho(z,T)$ is assumed constant. One can easily rewrite Equation (4.5) as $P_w = \alpha\, V^3$, and obtain

$$V = \sqrt[3]{\frac{P_w}{\alpha}}, \tag{4.6}$$

where $\alpha = \frac{1}{2}\,\rho\, A$ is known. Having known the distribution of wind speeds, the pdf of the wind power, $g(p)$, can be obtained as follows

$$g(p) = \frac{k}{3}\ \beta\ p^{\frac{k}{3}-1}\ e^{-\beta\ p^{\frac{k}{3}}}, \tag{4.7}$$

where $\beta = (\frac{1}{c}\ \sqrt[3]{\frac{1}{\alpha}})^k$. Also, the cumulative density function (cdf), $G(p)$, of generated wind power is given by

$$G(p) = \int_0^p\ g(t)\ dt = 1 - e^{-\beta\, p^{\frac{k}{3}}}. \tag{4.8}$$

Now, p^* can be calculated as follows

$$p^* = \mathbb{E}(P) = \int_0^{\infty} p \; g(p) \; dp = \frac{1}{\beta^{\frac{k}{3}}} \Gamma(\frac{3}{k} + 1), \tag{4.9}$$

where $\mathbb{E}(\cdot)$ is the expected value of the wind power probability distribution. p^* in Equation (4.9) can also be computed from the wind speed or its corresponding wind power frequency tables by replacing the integral with a summation over different values of power weighted by their corresponding relative frequencies.

In M_{1B}, in addition to the wind resource assessment data, we have knowledge of a generic wind turbine's v_c and v_s, and will apply the dimensionless power coefficient C_p, representing the theoretical amount of the mechanical power that can be extracted by the turbine rotor. The power coefficient is a function of turbine blade tip speed ratio, λ, and the blade pitch angle, θ [123]. The maximum theoretical power that can be extracted from wind is 0.5926 (the Betz limit [124]). Hence, in Equation (4.6) α is replaced by $\frac{1}{2}\, C_p \, \rho \, A$ to account for mechanical power of a generic wind turbine. In this method, the wind power pdf is modified with respect to the regions where the power is usable, *i.e.*, the regions before v_c ($V < v_c$), and beyond v_s ($V > v_s$) where a wind turbine does not generate power. This results in a new wind power distribution truncated at $p_c = \frac{1}{2}\, C_p \, \rho \, A \, v_c^3$ and $p_s = \frac{1}{2}\, C_p \, \rho \, A \, v_s^3$ as follows

$$g_{_T}(p) = \begin{cases} \frac{g(p)}{G(p_s) - G(p_c)} & \text{for} \quad p_c \leq p \leq p_s, \\ 0 & \text{for} \quad p < p_c \; \& \; p > p_s, \end{cases} \tag{4.10}$$

where the mean of the usable power under the truncated power distribution in Equation (4.10) can be obtained by

$$\mathbb{E}_{T}(P) = \int_{p_c}^{p_s} p\ g_{T}(p)\ dp = \frac{1}{G(p_s) - G(p_c)} \int_{p_c}^{p_s} p\ g(p)\ dp. \qquad (4.11)$$

Numerical techniques must be used to calculate Equation (4.11).

Note that the modified power distribution can be achieved either by directly truncating the wind speed pdf at v_c and v_s, or by truncating the power pdf at p_c and p_s. However, truncating the power distribution results in a more accurate estimation compared to first truncating the wind speed distribution [156]. As opposed to M_{1A}, the average usable power in Equation (4.11) should not be computed from the wind speed or its corresponding wind power frequency table by replacing the integral with the summation. This is because the values of v_c and v_s (or, p_c and p_s) can fall within the available frequency classes in the wind speed (or wind power) frequency table which result in inaccurate calculation of p^*.

In M_{1C}, as the rated speed of the generic wind turbine is available, we account for the regions where the wind turbine generates its rated capacity by inflating the truncated wind power distribution at $p_r = \frac{1}{2} C_p \, \rho \, A \, v_r^3$ corresponding to the rated wind speed. This results in the p_r–inflated truncated power distribution as follows

$$g_{IT}(p) = \begin{cases} 0 & \text{for} \quad p < p_c \ \& \ p > p_s, \\ g_{T}(p) & \text{for} \quad p_c \le p < p_r, \\ \frac{G(p_s) - G(p_r)}{G(p_s) - G(p_c)} & \text{for} \quad p_r \le p \le p_s. \end{cases} \qquad (4.12)$$

Note that $g_{IT}(\cdot)$ is a mixture of a continuous distribution and a mass point which can be rewritten as follows

$$g_{IT}(p) = g_T(p)\ \mathbb{I}_{[p_c,p_r]}(p) + \frac{G(p_s) - G(p_r)}{G(p_s) - G(p_c)}\ \mathbb{I}_{[p_r,p_s]}(p), \tag{4.13}$$

where $\mathbb{I}_A(p)$ is the indicator function given by

$$\mathbb{I}_A(p) = \begin{cases} 1 & \text{for} \quad p \in A, \\ 0 & \text{for} \quad p \notin A. \end{cases}, \qquad \text{for any } A \subset \mathbb{R}. \tag{4.14}$$

Now, the mean of the wind power distribution is obtained by

$$\mathbb{E}_{IT}(P) = \int_{p_c}^{p_r} g_T(p)\ dp\ + \frac{G(p_s) - G(p_r)}{G(p_s) - G(p_c)} p_r, \tag{4.15}$$

where using Equation (4.10), the above equation can be rewritten as

$$\mathbb{E}_{IT}(P) = \frac{1}{G(p_s) - G(p_c)} \int_{p_c}^{p_r} p\, g(p)\, dp + \frac{G(p_s) - G(p_r)}{G(p_s) - G(p_c)} p_r. \tag{4.16}$$

Similarly, numerical integrations are needed to compute Equation (4.16).

By way of example, suppose $V \sim \text{Weibull}(5.95, 3.05)$ represents the wind speed distribution of a location of study and assume that $\alpha = 1,350$ and $C_p = 0.45$. Also, suppose $v_c = 3.5$, $v_r = 13.5$ and $v_s = 24$ m/s. Calculating the output power capacity following M_{1A}, M_{1B} and M_{1C} approaches returns $p^* = 840.73$ kW for the wind power distribution, $p^* = 520.94$ kW for the truncated power distribution and $p^* = 517.59$ kW for the p_r-inflated truncated power distribution. It is worth noting how changing v_r affects the value of the output capacity factor in the p_r-inflated truncated power distribution. For example, if v_r is changed to 11.5 or 15.5 m/s, p^* will change to 507.99 or 520.24 kW, respectively, while the values of p^* under the power distribution as well as the truncated power distribution remain unchanged.

The next step in the ESS sizing process, after calculating p^*, is to calculate the power rating imbalances between the the wind power production P_w and the desired dispatchable power output P_d, assumed to be p^* for a flat base-load power by

$$P_{_{ESS}}(t) = p^* - P_w(t). \tag{4.17}$$

where $P_{_{ESS}}$ is the power rating of ESS at time t. To obtain the time-domain wind power data in M_1 since the power curve is not available, we use the theoretical formula in Equation (4.5) for M_{1A}, and apply $C_p = 0.45$ for M_{1B} and M_{1C}. Later, it is explained how one can modify Equation (4.17) to calculate p^* and accordingly, $P_{ESS}(t)$ for methods M_2 and M_3. Based on Equation (4.17), when the generated wind power is less (greater) than the desired capacity, $P_{_{ESS}}$ is positive (negative) and the storage system is discharged (charged).

Next is to obtain the energy capacity of the storage system. To achieve this, the size of the ESS energy charges and discharges over the time period of study should be calculated. Therefore, we require to calculate energy imbalances over the span of individual time intervals given by

$$E_{_{ESS}}(t_i) = \Big(p^* - P_w(t_i)\Big) \cdot \Delta t_i, \tag{4.18}$$

where $E_{_{ESS}}(t_i)$ is the energy of ESS at time t_i, and Δt_i is the span of the corresponding time interval. In other applications when the goal is to match a variable load, the term p^* will be replaced with the variable load $P_L(t_i)$, which is the power demand at time t_i. Next is the calculation of the size of each occurrence of energy charges and discharges experienced by ESS over the time horizon $\mathbb{T}$ as the sum of consecutive occurrences of

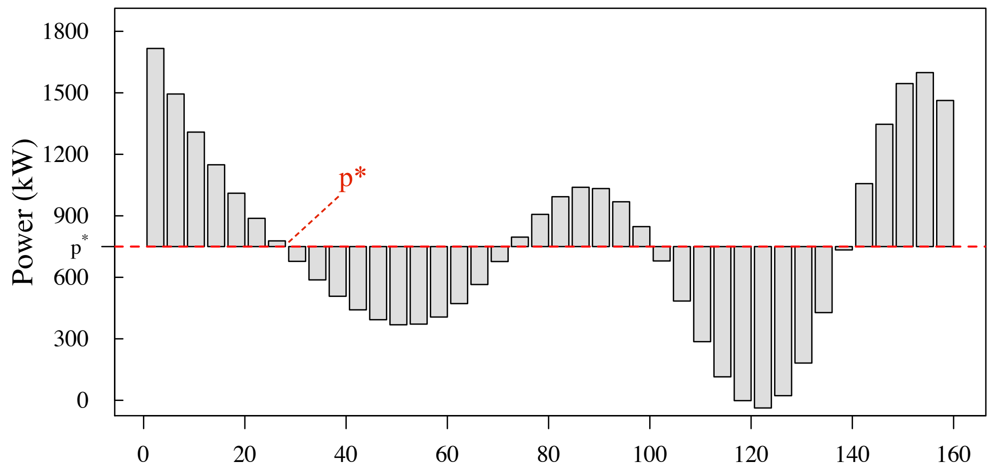

Figure 4.2: Example of intermittent wind power with individual charge and discharge occurrences realized by ESS each comprised of i and j energy imbalances in delivering constant output, p^*, over a sample time horizon $\mathbb{T}$ (hours).

individual energy imbalances given by

$$E_{ESS}(t) = \begin{cases} \sum_{i \in A} \Big(p^* - P_w(t_i)\Big) \cdot \Delta t_i & \text{for} \quad A = \Big\{i : (p^* - P_w(t_i)) > 0\Big\}, \\ \sum_{j \in B} \Big(P_w(t_j) - p^*\Big) \cdot \Delta t_j & \text{for} \quad B = \Big\{j : (p^* - P_w(t_j)) < 0\Big\} \end{cases} \tag{4.19}$$

Figure 4.2 illustrates an example of the individual charge and discharge occurrences each comprised of i and j energy imbalances.

By the above process, we obtain the ESS energy capacity required to deliver the firm capacity of the turbine or other grid integration requirements with a confidence of 100%. However, even when wind turbines are not utilized as base-load generators, the grid operator may need a back-up system for unexpected scenarios. Moreover, to be more economically competitive with other base-load power generation sources, it is more reasonable to apply lower confidence levels when deciding on the size of ESS. Section 4.6 explains how different confidence levels on the capacity of ESS can be obtained and then apply the methodology to a real data set.

Note that in method M_1, if the original speed data set from the wind assessment is proprietary or no longer available, one can directly calculate the total energy compensated by the ESS over any time span, *e.g.*, one year. This can be valuable for economic analysis as well as investment return study of a wind farm especially when the plant is combined with ESS for higher share of renewable into the electric grid. To this end, by having knowledge of v_c and v_s of a generic turbine, and a hypothetical wind speed, v^*, which corresponds to the turbine's firm output power capacity or is provided by an external source, the area under the obtained Weibull distribution is divided into four regions by the three wind speed values. ESS charging occurs when turbine is generating more power than v^*. ESS discharging occurs when the turbine is generating no power or less than desired. On the Weibull distribution, these happen at three regions: no power generation before v_c, no power generation beyond v_s, and between v_c and v^*. The size of ESS is calculated by multiplying the percentage of time where the desired power is not produced. The total capacity of ESS shows the economic value of the ESS in delivering base-load wind power.

4.4 M_2 based on the manufacturer power curve

In method M_2, the turbines are now selected for the wind farm, and we have access to the manufacturer power curve. Similar to M_1, this method follows the same steps of sizing ESS requirements, however, it is different in the first step for calculating the firm capacity of the turbine. M_2 relies on more specific information of a wind turbine and therefore, is expected to return a more realistic size for the ESS.

In M_2, we first calculate the time-domain power data by plugging in the values of wind speeds in the manufacturer power curve $p_i = f(v_i)$ where $f(\cdot)$ is known. The histogram of the wind power is then constructed to obtain the corresponding wind power probability distribution. By achieving the pdf of the wind power distribution, p^* is computed by

$$\mathbb{E}^*(P) = \sum_{p} p \; g^*(p) \tag{4.20}$$

where $\mathbb{E}^*(\cdot)$ is the mean, and $g^*(p)$ is the wind power relative frequency distribution obtained from calculated power values. The next steps are the same as M_1.

4.5 M_3 based on the empirical power curve

In method M_3, as the time-domain operational wind power data are available, we need to obtain an empirical wind power curve of the generator. Several parametric and non-parametric techniques can be used to fit the empirical power curve of a wind turbine. In this chapter, we use the locally weighted polynomial regression and penalized spline regression which are introduced in Sections 3.2.2 and 3.2.4 to be efficient methods for modeling wind turbine power curves proposed in [157]. For the sake of completeness of this chapter, the theories of these two regression models are briefly repeated for the ESS sizing method M_3. It is expected that M_3 provides more realistic results as it uses the actual power data of the operational wind farm.

4.5.1 Locally weighted polynomial regression

In this model, to estimate the wind turbine power curve, we solve a separate weighted least square polynomial regression problem at each target wind value v_0 by finding $\widehat{\boldsymbol{\beta}}(v_0)$ as

$$\widehat{\boldsymbol{\beta}}(v_0) = \arg\min_{\boldsymbol{\beta}} (\mathbf{P} - \mathbf{V}\boldsymbol{\beta})^\top \mathbf{W}_s(v_0)(\mathbf{P} - \mathbf{V}\boldsymbol{\beta}), \tag{4.21}$$

where $\boldsymbol{\beta} = (\beta_0, \ldots, \beta_k)^\top$, $\mathbf{P} = (p_1, \ldots, p_n)^\top$, $\mathbf{V} = (1, v_1, \ldots, v_n)^\top$, and $\mathbf{W}_s(v_0) = diag(\mathcal{K}_s(v_0, v_1), \ldots, \mathcal{K}_s(v_0, v_n))$ is a diagonal matrix. Here, $\mathcal{K}_s(v_0, v_i)$ is the smoothing kernel function that gives more weight to data points near v_0 and less weight to those farther from v_0, and hence is resistant against outliers [125]. In our analysis, we use the tri-cubic smoothing kernel function as in Equation 3.9, and compute $\widehat{\boldsymbol{\beta}}(v_0)$ for each v_0 as $\widehat{\boldsymbol{\beta}}(v_0) = (\mathbf{V}^\top \mathbf{W}_s(v_0)\mathbf{V})^{-1}\mathbf{V}^\top \mathbf{W}_s(v_0)\mathbf{P}$. The estimated power at wind speed v_0 is then obtained by

$$\widehat{f}(v_0) = \mathbf{V}_0(\mathbf{V}^\top \mathbf{W}_s(v_0)\mathbf{V})^{-1}\mathbf{V}^\top \mathbf{W}_s(v_0)\mathbf{P} \tag{4.22}$$

where $\mathbf{V}_0 = (1, v_0, v_0^2, \ldots, v_0^k)$. Cross-validation technique is used to obtain s and control the flexibility of the fit [157].

4.5.2 Penalized spline regression

This method suggests fitting separate low-degree polynomials over different regions of the wind speed using a polynomial spline regression model as $p_i = f(v_i) + \epsilon_i$, where

$$f(v_i) = \beta_0 + \sum_{r=1}^{k} \beta_r v_i^r + \sum_{j=1}^{K} \beta_{k+j}(v_i - \zeta_j)_+^k, \tag{4.23}$$

$k \geq 1$ is the order of spline, $\zeta_1, \ldots, \zeta_K$ are a set of pre-specified knots, and $(v_i - \zeta_j)_+^k = (v_i - \zeta_j)^k \, \mathbb{I}_{[\zeta_j, \infty)}(v_i)$.

Following [157], we use a fixed basis dimension at quantiles of the wind speeds, and control smoothness of the curve by adding a penalty to the least squares fitting objective, which can be represented as $\boldsymbol{\beta}^\top \mathbf{D} \boldsymbol{\beta} = \int \{f''(t)\}^2 \, dt$, where $\mathbf{D}$ is a matrix of known coefficients and $f''(\cdot)$ is the second derivative of $f(\cdot)$. This is done by the following minimization:

$$\frac{1}{n} \sum_{i=1}^{n} (p_i - f(v_i))^2 + \lambda \, \boldsymbol{\beta}^\top \mathbf{D} \boldsymbol{\beta}, \tag{4.24}$$

when λ is a fixed smoothing parameter. The estimated model parameters are obtained by $\hat{\boldsymbol{\beta}}(\lambda) = (\mathbf{Z}^\top \mathbf{Z} + \lambda \mathbf{D})^{-1} \mathbf{Z}^\top \mathbf{P}$. which result in the estimated power curve

$$\hat{\mathbf{P}}(\lambda) = \mathbf{Z} \hat{\boldsymbol{\beta}}(\lambda) = \mathbf{Z}(\mathbf{Z}^\top \mathbf{Z} + \lambda \mathbf{D})^{-1} \mathbf{Z}^\top \mathbf{P} = \mathbf{H}(\lambda) \mathbf{P}, \tag{4.25}$$

where $\mathbf{H}(\lambda)$ is the hat matrix. To obtain λ, as shown in Section 3.2.4 of Chapter 3, the generalized cross-validation technique is used [131].

Figure 4.3 illustrates the flowchart of the ESS sizing using methods M_1, M_2 and M_3 proposed in this chapter.

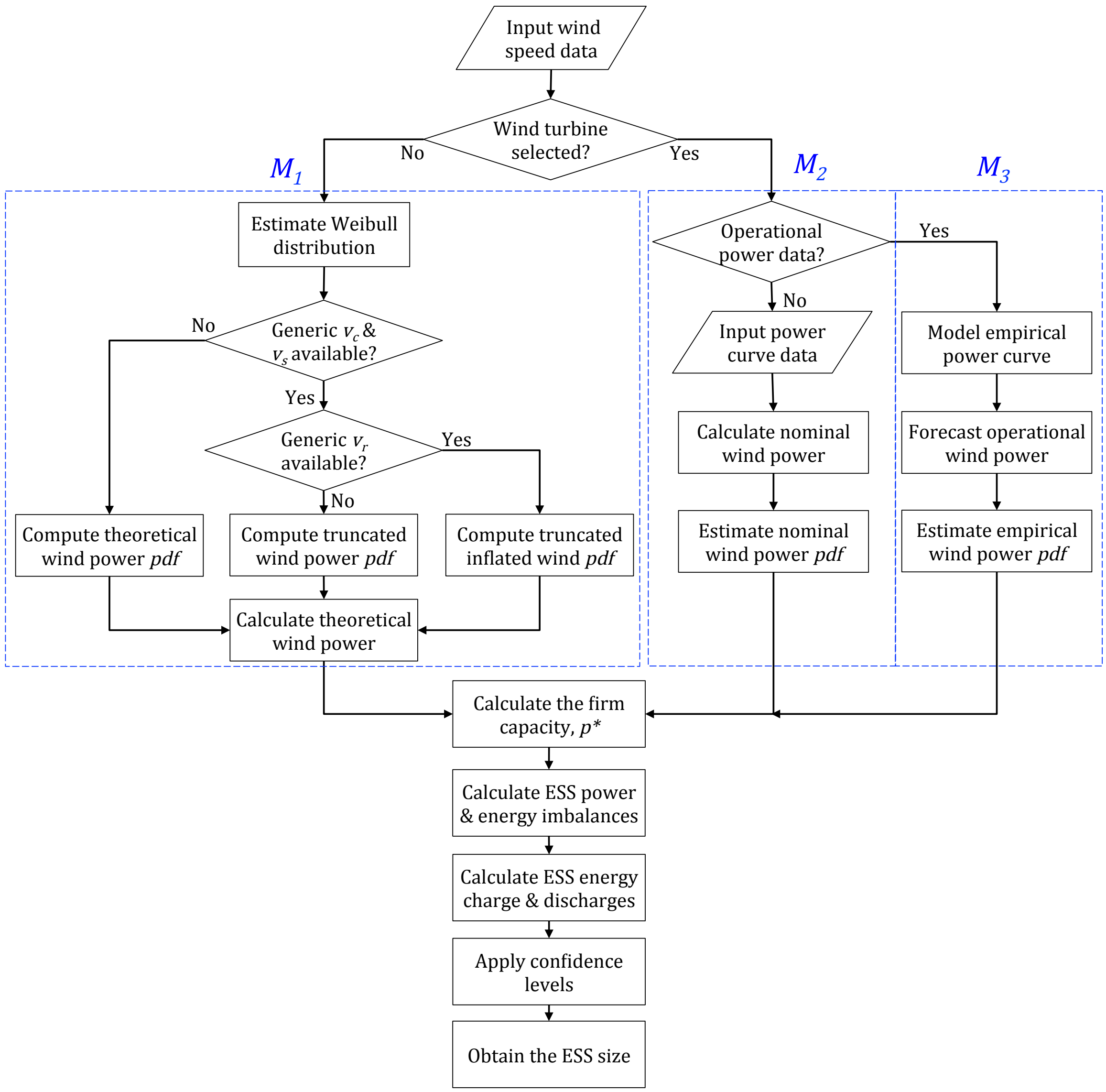

Figure 4.3: Flowchart of the procedures in the proposed methods of ESS sizing to cover all possible scenarios for a wind project. These methods allow to predict the capacity of ESS for base-load wind power generation for a given confidence level.

4.6 Real data application

We use a wind resource assessment data set as well as a proprietary operational wind power data to investigate the performance of each proposed method. The data set represents 10-minute averaged wind speed and wind power of 25920 points for a duration of 6 months in 2006 and 2007 of a wind farm in North America. We also use hourly averaged data and repeat the numerical analysis to assess the influence of data resolution on the size of ESS. Regarding the data set available for this analysis, it is recognized that industry standards usually require one year hourly wind data be used in an analysis of extreme wind variations over the life of a wind farm. Moreover, the data set are correlated to some longer term, *e.g.*, 20+ year wind data from a near-by MET tower to determine these extremes and thus the size of ESS to smooth out the power production. However, in this analysis and for the purpose of developing the methodology of the proposed statistical algorithm a 6 month data set is deemed acceptable. To start the ESS sizing with M_1, Equations (4.3) and (4.4) are numerically solved and the estimated parameters of the Weibull distribution ($\widehat{c}$ and $\widehat{k}$) associated with the histogram of the wind speed data are obtained as 2.55 m/s and 8.86 for the 10-minute data. We assume that the characteristic information of the generic turbine in M_1 are similar to those of the selected turbine's in M_2 and M_3 to more accurately account for the proposed methods' influence on the outcome. For M_{1A}, the turbine's blades swept area and the air density are input to Equation (4.5) which equal to $5,281$ m^2 and 1.225 kg/m^3. By setting $v_c = 3.5$ m/s and $v_s = 20$ m/s in M_{1B} as well as $v_r = 13$ m/s in M_{1C}, the theoretical pdfs of wind powers are obtained using Equations (4.7), (4.10) and (4.13). Using Equations (4.9), (4.11) and (4.16), the values of p^* are 2333, 1145, and 1107 kW for M_{1A}, M_{1B}, and M_{1C}, respectively. The theoretical time-domain wind power data are then computed using Equation (4.5) in M_{1A}, and where α is replaced by $\frac{1}{2}\, C_p\, \rho\, A$ in M_{1B} and M_{1C}.

In M_2, the manufacturer power curve of the generator is available. The selected wind turbine has the rated capacity of 1650 kW with the hub height of 80 m. The nominal wind power data are computed using $P(t) = f(V(t))$ where $f(\cdot)$ represents the manufacturer power curve which is known and $V(t)$ refers to the wind speed at time

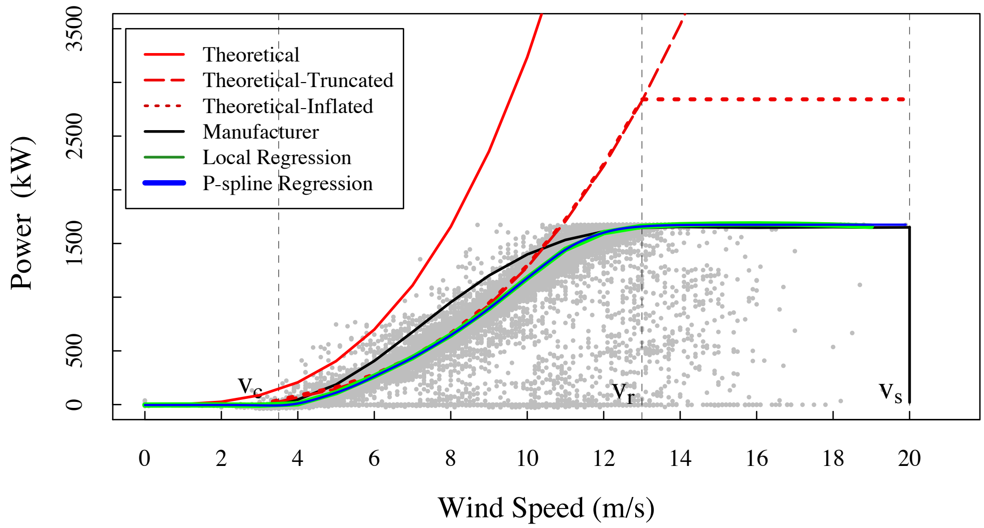

Figure 4.4: Comparison of wind turbine power curves in the theoretical, theoretical Betz limit power truncated at the generic v_c and v_s, and inflated at v_r, the manufacturer wind power, and the two empirical curves obtained by locally weighted polynomial and penalized spline regression.

t. The distribution of wind power is estimated using the nominal time-domain power data with the mean of the estimated distribution being 883 kW.

In M_3, we use the actual operational wind power data which are recorded at MET towers located in the wind farm. We select a wind turbine near one of the MET towers to more accurately present the wind speed as well as the power data. The empirical power curve is estimated using locally weighted polynomial and penalized spline regression methods described in Section 4.5. The firm capacity values of the turbine corresponding to each model are 716 kW and 715 kW, respectively.

Figure 4.4 shows the power curves for the theoretical power in wind (M_{1A}), theoretical Betz limit power truncated at the generic v_c and v_s (M_{1B}), and the inflated at v_r (M_{1C}), as well as the manufacturer wind power (M_2), and the two empirical curves obtained by LR and PS methods (M_3). To perform the ESS sizing methods, we need to calculate the power rating imbalances using Equation (4.17). The energy capacity of the ESS is obtained by Equation (4.19). Figure 4.5 shows the theoretical power outputs in methods M_{1A}, M_{1B} and M_{1C} *versus* the operational wind power 10-minute data. The figure also shows the calculated energy charges and discharges of the ESS for M_{1C}. Figure 4.6 shows similar results for M_2 and M_3. In practice, it may not be economically feasible to account for 100% of the capacity of ESS for integration with intermittent wind power. Hence, one needs to use the probability distribution of the energy ratings, and apply desired confidence levels. To this end, the histograms of the calculated energy capacity of ESS charges and discharges are created. By testing different statistical distributions, the best fits to the observed energy and power values of ESS are achieved using a Laplace(μ, σ) distribution with pdf

$$f_X(x; \mu, \sigma) = \frac{1}{\sigma}\, e^{-\frac{|x-\mu|}{\sigma}}; \quad x \text{ and } \mu \in R, \sigma > 0, \tag{4.26}$$

where μ is the location parameter and σ is a scale parameter. The ML estimation method is used to obtain the estimators of μ and σ as follow [158]

$$\widehat{\mu} = median(X_i) \;\text{ and }\; \widehat{\sigma} = \frac{1}{n}\sum_{i=1}^{n} |X_i - \widehat{\mu}|, \tag{4.27}$$

where X_i represent E_{EES} at time t_i.

The pdf of the energy values of ESS, and estimated values $\widehat{\mu}$ and $\widehat{\sigma}$ are then used to obtain different tolerance intervals for the size of ESS given by $[L, U]$, where $L = L(X_1, \ldots, X_n)$ and $U = U(X_1, \ldots, X_n)$ represent the lower and upper limits of the interval, respectively, with $L < U$. In general, an interval $[L, U]$ is a $(P, 1-\alpha)$-tolerance interval if it is constructed so that the fraction P of the population values

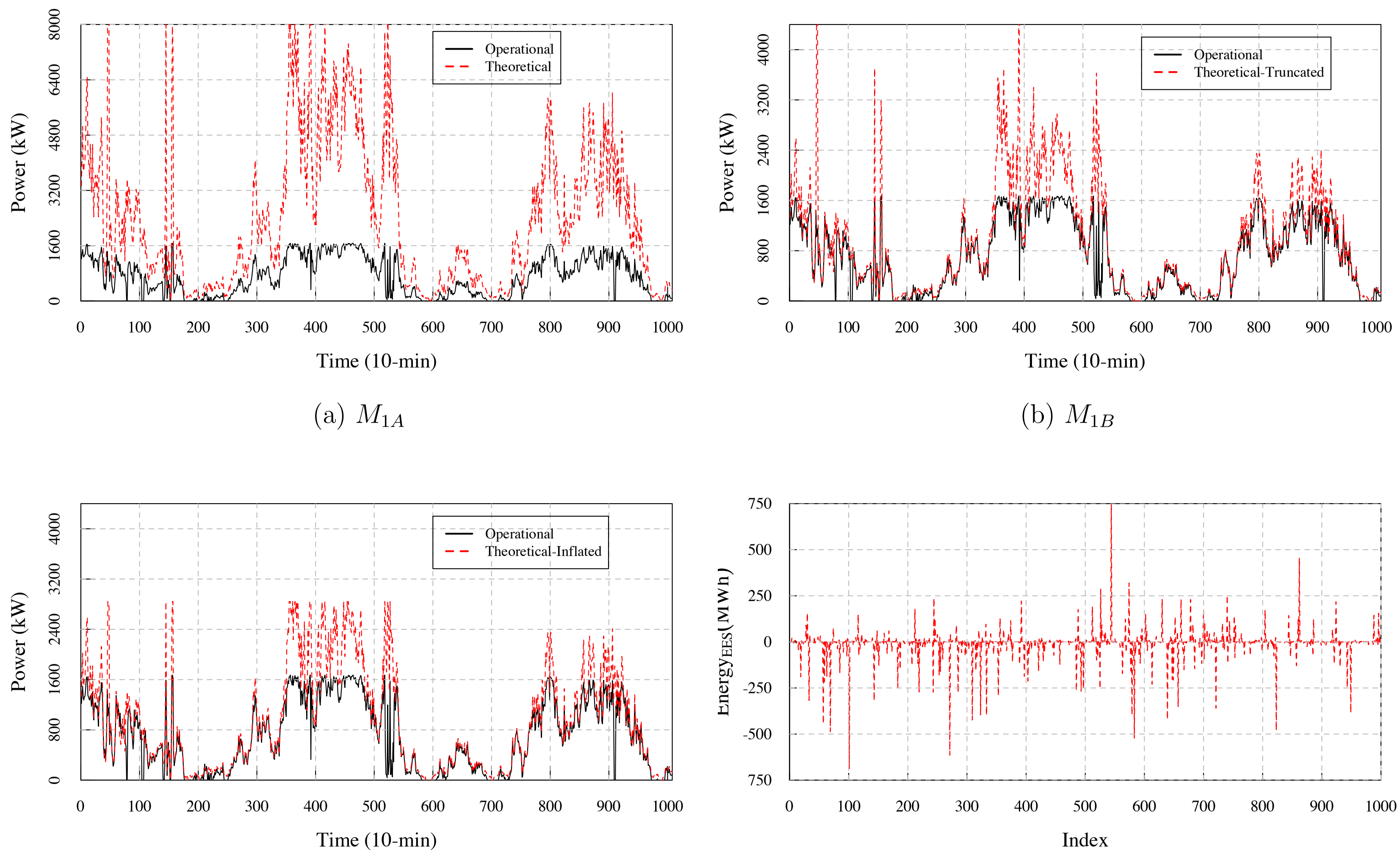

(a) M_{1A} (b) M_{1B}

(c) M_{1C} (d) ESS charges/discharges M_{1C}

Figure 4.5: The 10-minute theoretical power outputs using (a) theoretical power curve, (b) theoretical truncated power curve and (c) theoretical inflated power curve *versus* the operational wind power data. Figure (d) shows the energy charges/discharges of the ESS for M_{1C} when the theoretical power curve is truncated at v_c and v_s, and inflated at v_r.

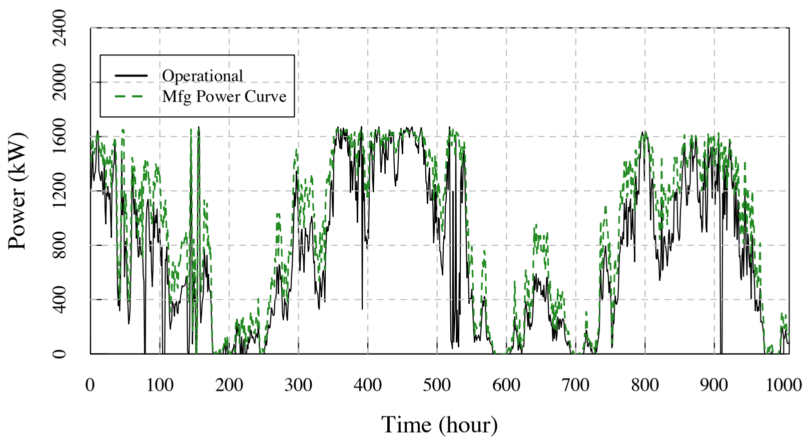

(a) M_2

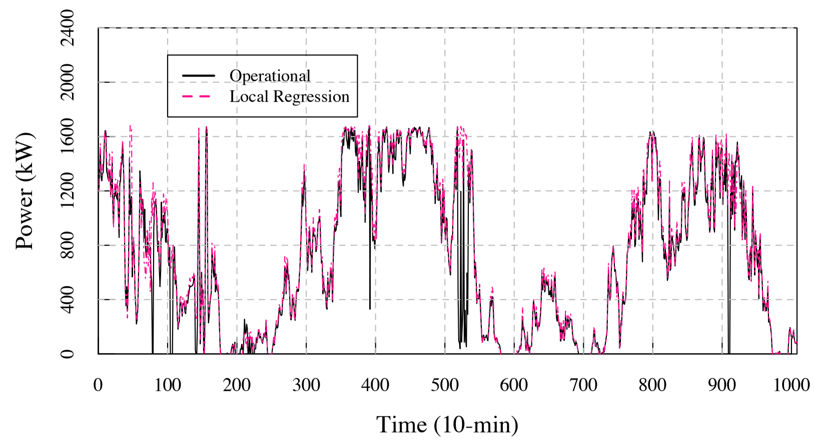

(b) M_3 (LR)

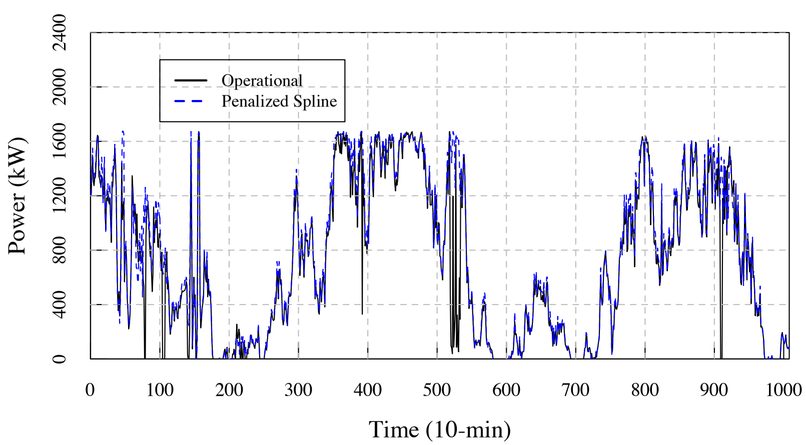

(c) M_3 (PS)

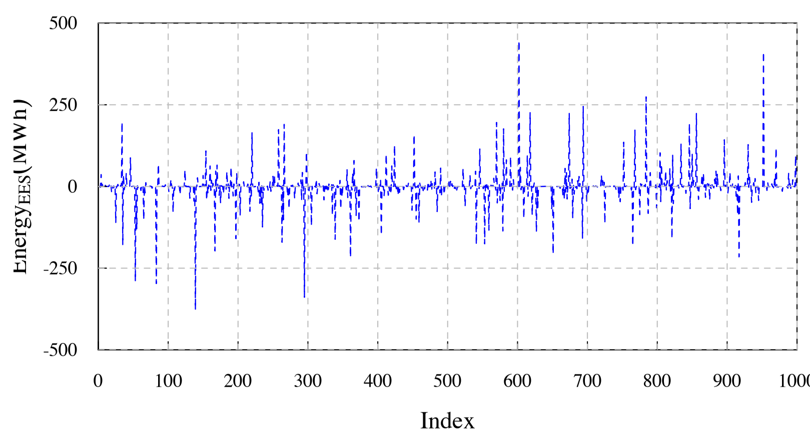

(d) ESS charges/discharges PS

Figure 4.6: The 10-minute theoretical power outputs using (a) manufacturer power curve, (b) LR power curve and (c) PS power curve *versus* the operational wind power data. Figure (d) shows the energy charges/discharges of the ESS using PS method.

lies within the interval with $100(1-\alpha)\%$ confidence, *i.e.*,

$$\mathbb{P}\left(\int_{L}^{U} f(x)\,dx \geq P\right) = 1-\alpha, \tag{4.28}$$

where P is called the content of the interval, and $[L, U]$ is referred to as a P-content tolerance interval with the confidence level $100(1-\alpha)\%$.

By having $\widehat{\mu}$ and $\widehat{\sigma}$, one can use the method proposed by [159] to obtain a $100(P, 1-\alpha)\%$ tolerance interval for the distribution of X as

$$L = \widehat{\mu} - \Lambda\ \widehat{\sigma} \ \text{ and } \ U = \widehat{\mu} + \Lambda\ \widehat{\sigma}\ , \tag{4.29}$$

where

$$\Lambda \approx -n\ \Lambda_p + \frac{z_{(1-\alpha/2)}}{n - z^2_{(1-\alpha/2)}} \times \sqrt{n\left(1+\Lambda_p^2\right) - z^2_{(1-\alpha/2)}},$$

such that n is the sample size, $z^2_{(1-\alpha/2)}$ is the $(1-\alpha/2)$-th quantile of a standard normal distribution, and $\Lambda_p = \ln\,(1-p)$. In our application, we use $\mu = \widehat{\mu} = 0$ as the Laplace distribution for ESS values should be centred around zero. Figure 4.7 shows the histogram of the calculated energy values fitted with a Laplace distribution, and a Q-Q plot to assess the goodness of the fitted Laplace distribution to the ESS energy values. Table 4.1 presents a summary of the calculated ESS energy capacities using 10-minute data set for the presented methods for 70-, 80-, 90- and 95%-content tolerance intervals. The confidence level $(1-\alpha)$ is chosen to be 90% and 95% for comparison.

To investigate the influence of the resolution of the available data on the calculated ESS sizes, we have repeated the methods presented in this work on 20-minute, 30-minute

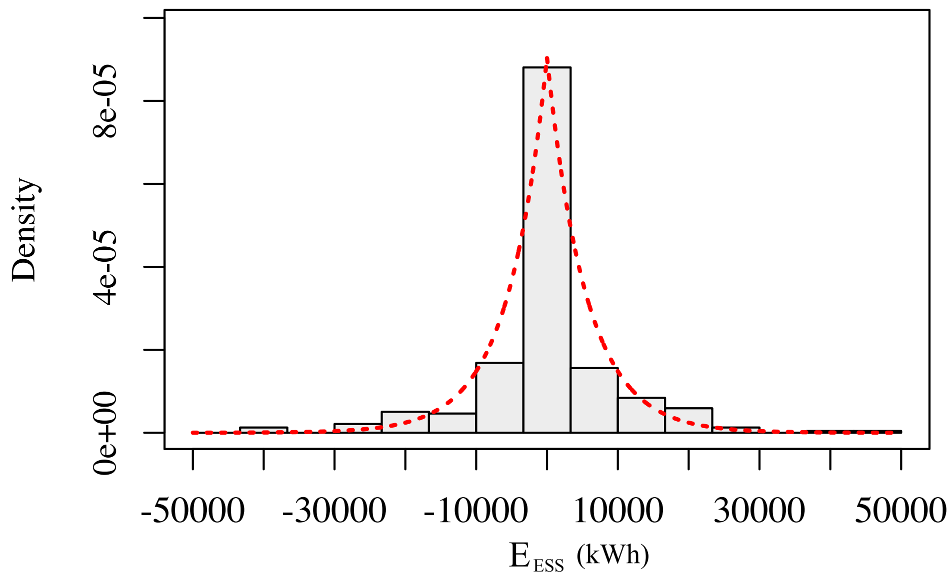

(a) ESS energy histogram

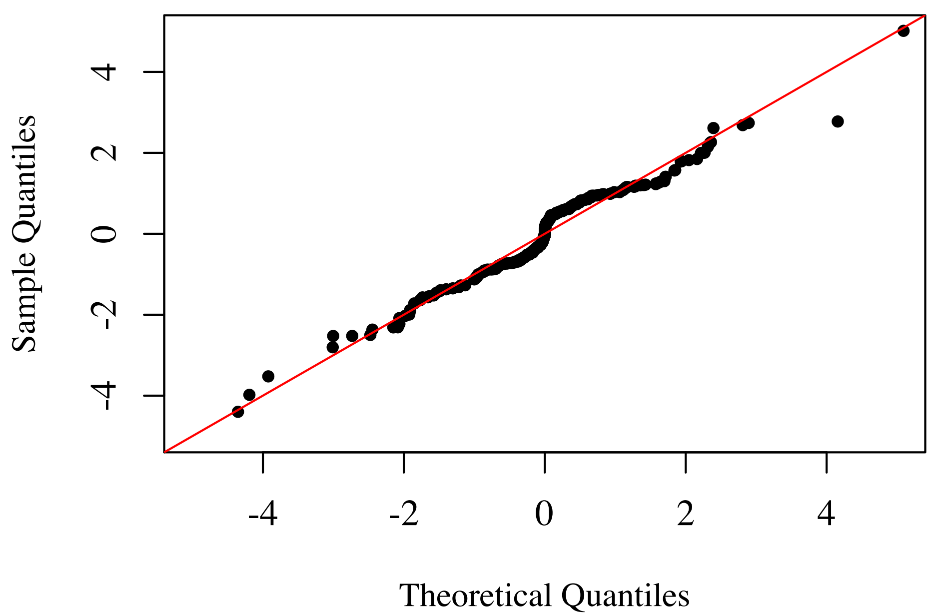

(b) Q-Q plot

Figure 4.7: (a) The histogram of the ESS energy values in kWh and the fitted Laplace distribution, and (b) the Q-Q plot to investigate the goodness of the fit.

Table 4.1: Results for the ESS energy capacities in kWh for the 10-minute wind data using 70-, 80-, 90- and 95%-content tolerance intervals with 90% and 95% confidence intervals.

Time	Method	$1-\alpha=0.9$				$1-\alpha=0.95$			
		P=70%	P=80%	P=90%	P= 95%	P=70%	P=80%	P=90%	P= 95%
	M_{1A}	8,681	11,536	16,435	21,345	8,788	11,667	16,609	21,565
	M_{1B}	4,019	5,343	7,614	9,890	4,071	5,406	7,697	9,995
10-min	M_{1C}	3,651	4,854	6,917	8,985	3,697	4,910	6,993	9,081
	M_2	2,459	3,270	4,661	6,055	2,489	3,307	4,711	6,118
	M_{3A}	2,386	3,171	4,518	5,868	2,416	3,207	4,566	5,928
	M_{3B}	2,389	3,175	4,523	5,875	2,419	3,211	4,572	5,936

and 60-minute averaged wind speed and wind power data. While the patterns of the calculated ESS capacities in the all methods are similar to each other, the capacity sizes vary significantly which can be justified by the impact of the data resolution. Table 4.2 provides a summary of the calculated ESS energy capacities for the hourly averaged data.

Confidence intervals are commonly used in the literature to apply user-selected confidence levels for different applications. However, and in contrast to confidence intervals that provide information concerning the unknowns parameters of the underlying distribution, a tolerance interval provides information on the entire population. In particular, a tolerance interval is an interval for a specific proportion of the sampled population, not its mean, variance, and etc. In confidence intervals, the width of the interval is entirely due to the sampling error where as the sample size goes to infinity, the width of the interval approaches zero. But, the width of the tolerance interval is due to both sampling error and the variance in the population. As the sample size increases, the tolerance interval limits approach to the population percentiles.

Table 4.3 provides a summary of the ESS energy capacities for the presented methods when the methods are repeated using confidence intervals of 90% and 95% instead of the tolerance intervals for the purpose of comparison.

4.7 Chapter summary

We have presented a statistical algorithm for energy storage sizing required to integrate intermittent wind power. The proposed mathematical framework contributes towards generating base-load electricity to a selected confidence level for a wind farm. Three

Table 4.2: Results for the ESS energy capacities in kWh using hourly data using 70-, 80-, 90- and 95%-content tolerance intervals with 90% and 95% confidence intervals.

Time	Method	$1-\alpha=0.9$				$1-\alpha=0.95$			
		P=70%	P=80%	P=90%	P= 95%	P=70%	P=80%	P=90%	P= 95%
	M_{1A}	29,043	38,441	54,606	70,833	29,716	39,267	55,715	72,236
	M_{1B}	13,332	17,611	25,023	32,465	13,620	18,002	25,549	33,130
Hourly	M_{1C}	12,210	16,162	22,960	29,784	12,501	16,519	23,439	30,390
	M_2	7,181	9,532	13,573	17,629	7,338	9,724	13,832	17,956
	M_{3A}	7,615	10,084	14,330	18,492	7,790	10,298	14,618	18,956
	M_{3B}	7,456	9,875	14,034	18,210	7,626	10,083	14,313	18,563

Table 4.3: ESS energy capacities in kWh for 10-minute and hourly data based on $1 - \alpha = 90\%$ and $1 - \alpha = 95\%$ confidence intervals.

Method	10-minute		Hourly	
	90%	95%	90%	95%
M_{1A}	15,556	20,252	49,371	64,233
M_{1B}	7,204	9,373	22,578	29,375
M_{1C}	6,548	8,519	20,717	26,953
M_2	4,419	5,750	12,416	16,154
M_{3A}	4,278	5,566	12,982	16,890
M_{3B}	4,283	5,572	12,726	16,557

methods were proposed based on parametric and nonparametric statistical models using wind resource assessment data and available wind turbine information as well as operational wind power data of a wind farm in North America. Averaged 10-minute and hourly data sets were used to calculate the firm capacity of the wind turbine for each method in the location of study. The size of the storage system was estimated by calculating the energy imbalances in each time interval and the integration over the study time period. To enable applying different desired confidence levels, the probability distributions for the values of the occurred charges and discharges were constructed. The results show that for different stages of the wind farm development, and depending on the available information, the method can properly size the energy storage required to deliver constant power to a user selected confidence level. Moreover, in Chapter 6 the results of this analysis are applied to estimate the cost of wind energy to produce rated power at different confidence levels, which support the cost-effectiveness of proposed approach in base-load generation of wind power.

Chapter 5

Experimental Analysis

This chapter presents a short-duration experimental testing to verify and monitor the degradation of 25 kWh used batteries of PEVs supplied by Electrovaya obtained from a previous electric taxi fleet demonstration in Baltimore in the U.S. For the framework of PEV battery repurposing proposed in this thesis, we investigate the viability of integrating repurposed batteries and wind energy to deliver rated power to a given confidence level. As the model considers battery storage capacity available for repurposing at their EOL, and over their stationary service life, we attempted to add an experimental component that provides an indication of the degradation of repurposed batteries in a stationary service. For the purpose of this testing, we used 2 battery packs of used batteries of electric vehicles with the total capacity of 25 kWh and the approximate DC voltage of 400 V in their "as-is" condition, and performed the profiling of these batteries by charging and discharging to and from the electric grid. The test protocol was to record the charging and discharging of the battery over time while the measurements are digitally stored in a database. The demonstrated project can have other applications such as providing storage to support renewable generation and improve the efficiency of diesel generators. We were able to obtain useful data and an indication of the battery's degradation in spite of the relatively short testing timeline possible at the facility.

5.1 Repurposed battery storage system

When propulsion batteries of PEVs reach their vehicular EOL, they can be repurposed and utilized in stationary applications by providing utility-scale ESS before being recycled. As the interest of this thesis, these batteries can be located at a wind farm to smooth out their capacity and generate a dispatchable output. PEV batteries have a typical 8–10 years of vehicular service with a remainder capacity of approximately 80% at their automotive EOL, and before repurposing [104, 105]. To perform experimental tests of battery degradation in laboratory, we have access to a prototype energy storage system of PEV repurposed batteries. The prototype system is demonstrated at the Manitoba HVDC Research Centre, and is developed through a project by the Clean Energy Fund (CEF) of Canada. The available repurposed batteries supplied by Electrovaya obtained from a previous electric taxi fleet demonstration in the U.S. are in the "as-is" state consisting of electric vehicles battery modules and their battery management systems (BMS). Manitoba HVDC Research Centre has developed the power interface system to operate multiple PEV battery packs. The stationary repurposed ESS consists of 5 bi-directional DC-DC converters individually connected to a BMS forming a battery bank module. Battery bank modules are connected together in parallel and comprise a battery bank collection bus which is by a DC-AC converter system connected to the AC grid. The designed and developed system allows utilizing PEV battery packs obtained from different vendors at different states—may have dif-

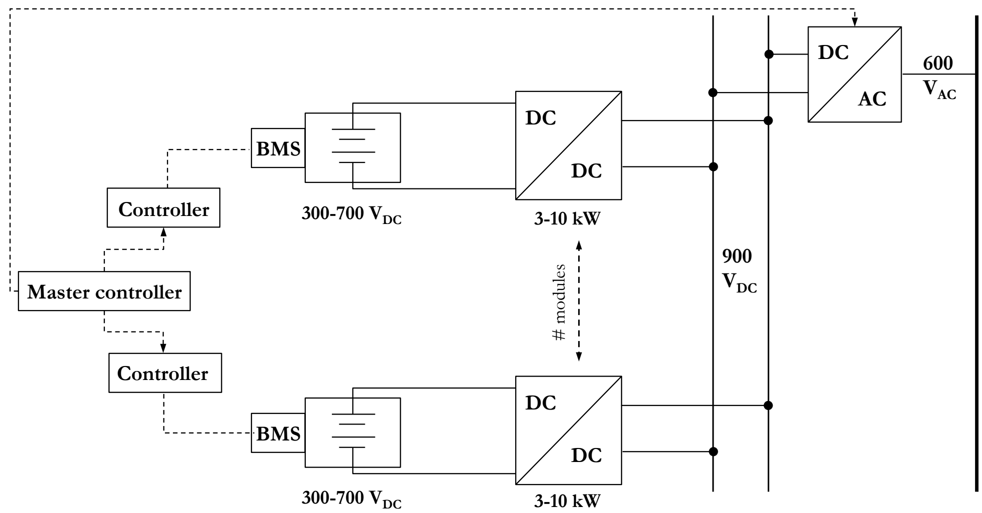

Figure 5.1: Illustration of the overall system configuration of the repurposed battery storage system designed and developed by Manitoba HVDC Research Centre. The system allows different battery types to be interconnected, and provides the flexibility for cogeneration with wind or solar energy, and grid connection [160].

ferent chemistries, capacities, and specifications— to be connected to a common bus to provide flexibility for electric grid interconnection system, or for micro-grids using intermittent renewable energies to smooth out their capacity or diesel generator to increase efficiency. Figure 5.1 illustrates a general configuration of developed system at the centre. The details of the system modules and specifications are presented by the Manitoba Hydro HVDC Centre in [160].

5.2 Experimental system set-up

For the purpose of this experimental study, 2 battery packs are used to perform the tests at different rates in the laboratory. Each battery pack consists of 4 battery modules where 24 battery cells are accommodated in each module. The battery cell's voltage dictates the approximate voltage of each battery pack. Each battery pack is

Figure 5.2: Two battery packs and the BMS interfaces connected to each module. Each pack consists of 4 modules with the approximate DC voltage of 400 V at the Manitoba Hydro HVDC Centre.

connected to a BMS that enables reading battery packs status data such as cell voltages (minimum, maximum and average), battery capacity, values of current, temperature of battery cells, and etc. Figure 5.2 shows two battery packs and the BMS interfaces, where each pack is comprised of 4 modules with the approximate DC voltage of 400 V. While batteries have liquid cooling system and frame in their vehicular service, repurposed batteries in stationary applications shown in this setup are air-cooled.

In the demonstration system, bi-directional DC-DC converters with 5 kW or 10 kW ratings were developed for each battery pack to accommodate battery voltages ranging from 300 V to 700 V. In this design, the constant DC bus collection voltage is 900 V. Each battery system and the associated DC-DC converter form a battery bank module (BBM). Each DC-DC converter and the associated controller form a processing unit accommodated in a cabinet for each battery pack. In each cabinet, the controller in the processing unit protects the systems, and communicates to the BMS and to the master control unit. Figure 5.3 shows two cabinets of the processing units containing the bi-directional DC-DC converter and the controller unit.

Figure 5.3: Two cabinets of the processing units containing the bi-directional DC-DC converter and the controller unit at the Manitoba Hydro HVDC Centre.

In the designed system, a bi-directional DC-AC inverter is used to connect the parallel modules to the AC system. In the developed system, the DC-AC inverter is rated at 100 kW which converts the 900 V DC to three-phase 600 V AC. The designed inverter allows the connection of multiple parallel BBMs.

A master co-ordinator is developed to control the operation and status of the battery systems. This control unit performs the primary supervisory of the system, and allows to set the operation modes and set points , and to start, stop and monitor each DC-DC module. The system is equipped with a Graphical User Interface (GUI) that provides the operator with the ability to configure the system, select operating modes and set-points. The GUI also allows to perform system and alarm monitoring. Figure 5.4 shows a sample screen of the GUI developed for the system.

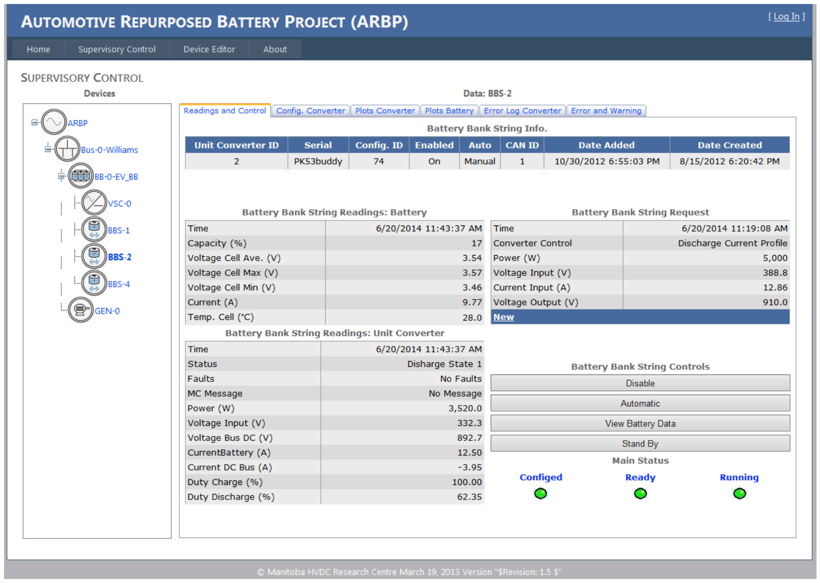

Figure 5.4: A sample screen shot of the multipage graphical user interface developed by the Manitoba Hydro HVDC Centre, that allows for the operator to configure the system, select operating modes and set-points, and to perform system and alarm monitoring.

5.3 Test results

We operated two 388.8 V BBMs of the system for testing the battery capacity, and investigating the degradation of these systems due to charge-discharge cycles. As the battery packs obtained from PEVs are in their "as-is" state, it is important to determine the available capacity in the used batteries. The capacity of a battery can be defined as either the coulometric capacity or the energy capacity. The coulometric capacity of a battery is the electrical charge that can be drawn and is given in ampere-hours (Ah) when the battery is discharged at a certain rate, and is given by [161]

$$\mathbb{C} = \int_0^T I(t)\, dt, \tag{5.1}$$

where $\mathbb{C}$ represents the battery charge/discharge capacity in Ah, $I(t)$ is the instantaneous current in A, and time τ is the test time.

Alternatively, the energy capacity of battery can be used which represents the amount of energy the battery can store, and is given by

$$E = \int_0^{\tau} U(t)\ I(t)\ dt, \tag{5.2}$$

where E is the battery energy content, $U(t)$ is the instantaneous voltage in V, $I(t)$ is the instantaneous current in A, and time τ is the test time.

The nominal energy capacity for each pack of the batteries supplied for this project is 12.5 kWh. To perform the tests, it is required to determine the charge/discharge rate that can be stored at or drawn from the battery. This rate is usually presented in terms of C rate, where 1C is defined as the rate at which a battery is discharged to its maximum capacity in 1 hour. It has been recommended for the battery repurposing demonstration project to follow a conservative approach for the rate of charge/discharge. The battery packs available for this experiment, if were new, would have a 1C rating of 31.25 A, *i.e.*, the rate of charging $\dfrac{12.5 \text{ kWh}}{388.8 \text{ V}}$ in 1 hour. For the developed system, a maximum current of 0.5C and 1C is recommended for the 5 kW and 10 kW DC-DC converters, respectively. Moreover, the battery temperature should be actively monitored not to exceed the maximum allowable cell temperature which is 45°C. Also, the ambient temperature in the lab is frequently monitored by the operator to maintain the test conditions of the battery systems.

To measure the capacity degradation of batteries due charge and discharge cycling, we first determine the capacity of the battery packs in their “as-is” condition. Thus, the initial point for each pack the amount of energy that can be drawn from them when they are fully charged. For this analysis, either of Equations 5.1 or 5.2 can be

Figure 5.5: The set up of battery repurposing project in laboratory where the operator provides test parameters, and performs monitoring and supervisory control via the master co-ordinator interface.

used. To this end, the values of instantaneous current and voltage are stored with the time step of 0.1 sec. To obtain more accurate results and to eliminate one source of measurement error, we use the measured values of the current data using Equation 5.1. The initial capacities measured at the beginning of testing for BBM_1 and BBM_2 are 9.88 Ah and 14.32 Ah, respectively. We were able to perform the tests for more than 60 cycles. For discharging, each BBM can be operated in either power or current control modes. The BBM can be charged by either current control or DC voltage control of the battery side. To calculate the capacity of the battery system at the end of each designated cycle number, BBM_1 which has a 5 kW DC-DC converter was discharged at 12.86 A. Similarly, BBM_2 with a 10 kW DC-DC converter was discharged at 19.29 A. These current rates are equivalent to 0.4C and 0.6C for BBM_1 and BBM_2, respectively. As shown in Figure 5.5, the operator provides test parameters, and performs monitoring and supervisory control via the master co-ordinator interface. To investigate the degradation performance of PEV repurposed batteries, we repeated measuring the capacity of the 2 battery systems for every 8–10 full charge and discharge

Table 5.1: List of parameters of the system and those set by the operator during the tests for investigation of degradation performance of repurposed batteries of PEVs.

#	Parameters	Values
1	Battery bank module ID number selection	1 or 2
2	Battery cell minimum voltage by the system in volts	3.30
3	Battery cell maximum voltage by the system in volts	3.90
4	Battery cell maximum temperature in °C	45
5	Status control mode	Charge or discharge
6	Battery side voltage input in volts	388.8
7	Charge or discharge power ratings in kW	5 or 10
8	Corresponding charge or discharge current ratings in A	12.86 or 19.29

cycles at their designated C rates. To this end, it is also required to ensure the accuracy of capacity calculation at each state point. Therefore, following the last charging half-cycle, and before the full discharge for capacity measurements, we performd a step-charging at lower C rates to top up the charge of each battery system. Table 5.1 lists the input parameters set by the operator during the lab tests.

To obtain the results of the energy capacity at each state point, we also require to perform some data filtering. This step is required due to stoppages during the tests. These incidents may occur by various protection and monitoring operations of parameters such as voltage of the whole battery pack, temperature of the battery, the maximum and minimum allowed voltages of the cells, and communication errors. Each time that this interruption occurs, and as the system is collecting data, the filtering was performed to obtain the correct values of the energy capacities. Table 5.2 presents the results of the measured capacities for each battery system at each state point.

As shown in the table, as the capacities fade in the 2 systems, they are not following similar values. This can be justified by the fact that the supplied battery packs are in their "as-is" condition. Moreover, although 60 cycles only represent a small portion

Table 5.2: Results of the measured capacity values shown for 7 state points (approximately 60 cycles) for each battery system and the corresponding capacity change relative to the previous state point.

State point	Battery Pack 1-BBM$_1$			Battery Pack 2-BBM$_2$		
	Cycles	Capacity (Ah)	Change (%)	Cycles	Capacity (Ah)	Change (%)
1	0	9.88	–	0	14.32	–
2	7	10.71	+2.56	7	14.32	−0.01
3	16	8.48	−6.94	20	13.32	−3.10
4	27	9.02	+1.68	32	13.35	+0.09
5	37	9.39	+1.15	42	13.23	−0.39
6	47	9.72	+1.04	52	13.28	+0.18
7	57	8.61	−3.47	62	13.10	−0.58

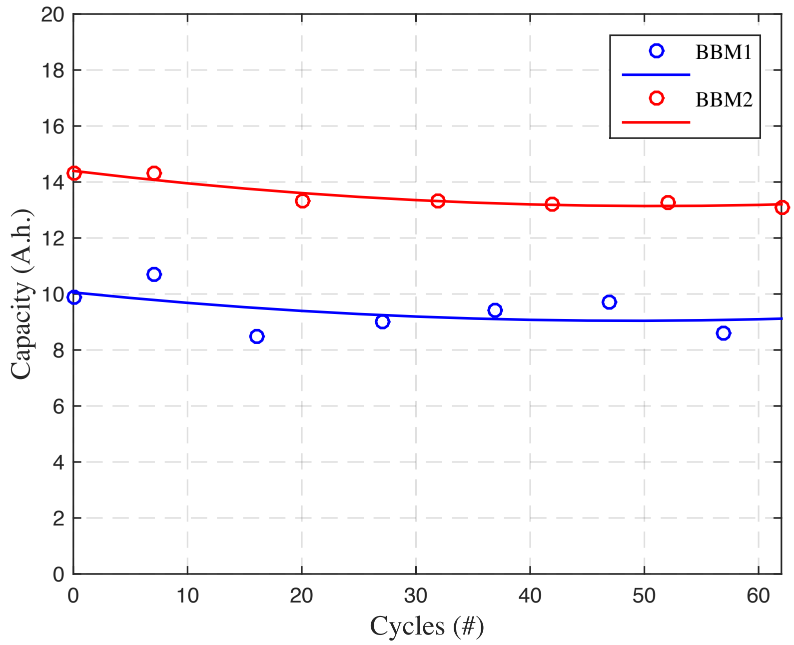

Figure 5.6: Results of measured capacity values for BBM_1 and BBM_2 repurposed Li-ion battery systems at each state point. Although 60 cycles only represent a small portion of the expected life of batteries in stationary applications, the results show a notable change in their capacities. As the batteries are balanced by cycling, this is expected to show less fluctuations and loss over a few thousand cycles.

of the expected life of batteries in stationary applications, the results show a notable change in their capacities. However, and by comparing these results with some degradation results provided by the supplier, fluctuation is expected especially at lower cycle numbers. Within this experimental testing available, these are the results we achieved, but it is expected to show less fluctuations and loss over a few thousand cycles. and follow the expected pattern.

Figure 5.6 graphs the results of measured capacity values for BBM_1 and BBM_2 battery systems at each state point.

5.4 Chapter summary

We have attempted to add an experimental component that provides an indication of the degradation of repurposed batteries. The test apparatus is the PEVs repurposed batteries demonstration system designed and developed by the Manitoba Hydro HVDC Research Centre through the CEF project. The tests were performed in the laboratory to monitor and obtain an indication of degradation of used batteries in stationary applications. The conducted test protocol has been to record the charging and discharging of the battery over time while comparing battery performance over the entire testing. While the results of this experimental study show fluctuations in their measured capacities, it can be justified based on their "as-is" condition and is expected to show a more consistent trend over a few thousand cycles following the expected pattern.

Further study and analysis of the performance of used batteries of PEVs repurposed for stationary applications are required to support a new market for these batteries, and to benefit the electrified transportation and energy sectors.

Chapter 6

Results and Discussion

This chapter provides the results of the model for the proposed framework for a studied case of Canada using the results of ESS sizing algorithm developed and presented in Chapters 3 and 4, followed by the discussion of results.

6.1 Case study

We perform the simulation of the PEV battery repurposing model to investigate the viability and feasibility of the proposed framework for Canada. The simulation considers 2010-2050 for the target study period as PHEVs and BEVs were first mass-produced in the market starting in 2010 [162]. To perform the energy simulation, the repurposing framework first adopts a PEV penetration rate in the Canadian market to calculate the consequent electric energy requirement, and to forecast available storage for repurposing. The model then predicts when the batteries become available on the secondary market and how many hours of storage are available to support the intermittent renewable wind resource. The model finally calculates the annual continuous production of wind power by support of repurposed batteries. The model presents how by addressing the charging requirement of these electric vehicles, new wind power can translate to increase the RER.

For the market penetration forecast, this study applies the results of a penetration model performed at Laval University [163] to predict the number of electric cars as the input to the repurposing model. The penetration model includes criteria such as driven miles by the vehicles, urban or rural driving, gasoline price, electricity price, and vehicles prices. Applying the passenger vehicles sales data [164] to this model projects that PEVs can make about 80% of Canada LDVs new sales in 2050. The model starts with new sales number 1,569,000 vehicles in 2010 and applies a 1% increase in this number to account for the national trend through 2050. To determine the charging load energy demand of PEVs, Equation (2.1) is used to calculate the annual average energy required due to the introduction of PEVs in the Canadian market. The model assumes the rural driving distance coefficient to be 30%, which is met by electricity in BEVs. By inserting the values for the parameters in Equation (2.1), it is calculated that PHEVs and BEVs need 6.5 kWh and 8.45 kWh of electricity per day. To calculate the annual storage capacity available for repurposing, it is assumed that Li-ion batteries retire from their vehicular application when they reach about 80% of their life. The model assumes 20 kWh and 40 kWh as the base capacity of PHEV and BEV batteries respectively, at their introduction in 2010. The model further considers a yearly increase of 2% reflecting likely battery technology advances anticipated through 2050. Another assumption is that PEV batteries are available for a period of 10 years in their stationary application with the initial state of 80% and an avergae yearly drop of 7.5% in their available capacity. This latter assumption translates to 50% at the end

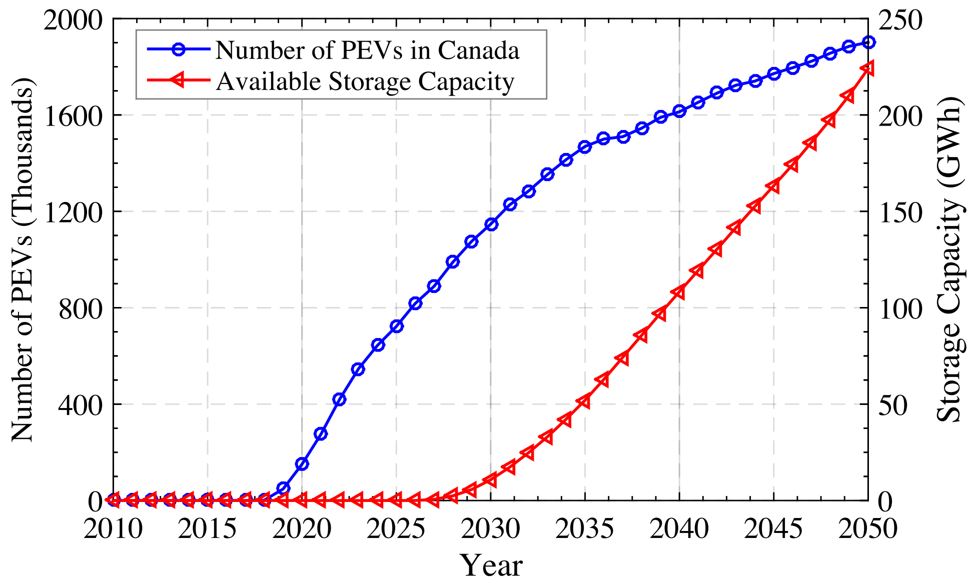

Figure 6.1: Number of the PEVs in Canada through 2050 based on the scenario selected in this study, and the consequent electric storage capacity available from repurposing batteries of these vehicles under the assumptions in this model.

of the 10-year stationary life before being recycled. Table 6.1 presents the parameters and the assigned values for the case study of the repurposing model in Canada.

Figure 6.1 shows the number of new sales of PEVs per year in Canada through 2050, and the annual electric energy storage capacity available from repurposing batteries of these electric vehicles for the described scenario. Table 6.2 presents the values of the annual total calculated storage capacities available from repurposed batteries of PEVs based on the parameters and assumptions described in this section for the period of this study.

Next, the model calculates the storage ratio, S_r, as the required storage capacity in kWh, to generate continuous unit output power in kW. According to the Canadian Wind Energy Association (CanWEA), Canada is benefiting from one of the best wind resources in the world having an average capacity factor of 30% or more [165]. There-

Table 6.1: Parameters values and assumptions used in the PEV battery repurposing models.

#	Parameters	Values
1	Number of light duty vehicles, LDVs, new sales in 2010	1,569,000
2	Yearly increase in the LDV new sales through 2050 in %	1
3	Urban driving distance per day for LDV in a typical North American city in km	32.5
4	Average extra daily driving distance to account for possible rural distances in %	30
5	PEV battery end-of-life capacity in %	80
6	PEV battery vehicular life span in years	8
7	PEV battery post-vehicular life span for stationary applications in years	10
8	PHEV battery base capacity at the technology introduction in kWh	20
9	BEV battery base capacity at the technology introduction in kWh	40
10	PEV battery capacity's technology advances per year in %	2
11	PEV battery degradation rate per year in %	7.5
12	PEV fuel economy (energy consumption) in Wh per km	200

Table 6.2: Total calculated storage capacities available per year from repurposed batteries of PEVs based on the parameters and assumptions from 2030–2050.

Time	Battery storage capacity (GWh)	Number of PEVs
2030	10.78	1,146,974
2035	52.40	1,469,315
2040	108.31	1,613,150
2045	163.32	1,771,837
2050	223.97	1,901,236

fore, a Canadian site is selected where the availability of wind energy is somewhat representative of the country's average capacity factor. The time-domain wind speed data available for the location of study are used in the ESS sizing model. We also use the power curve of a selected GE 1.5 MW turbine with a hub at 80 m height as a typical wind turbine size. The characteristic cut-in, rated, and cut-out wind speeds of the selected turbine are 3.5, 13.5, and 24 m/s, respectively. Based on the methods presented in Chapter 4, and having access to the manufacturer power curve and wind speed data, method M_2 is followed to size of the ESS for this case study.

We use the time-domain wind speed data of this location available from the wind resource assessment. The data set is for a selected year with a sampling rate of 60 sec at 10 m height obtained from the data collected by the station for baseline surface radiation network (BSRN) in Regina, Canada. Figure 6.2 shows the hourly averaged wind speed data for a selected month and the consequent wind power output using the GE 1.5 MW power curve.

As explained earlier, to calculate the size of ESS for the purpose of base-load generation of wind power, p^* needs to be calculated. To this end, we obtain the wind power probability distribution of the wind power values. The firm capacity of the turbine

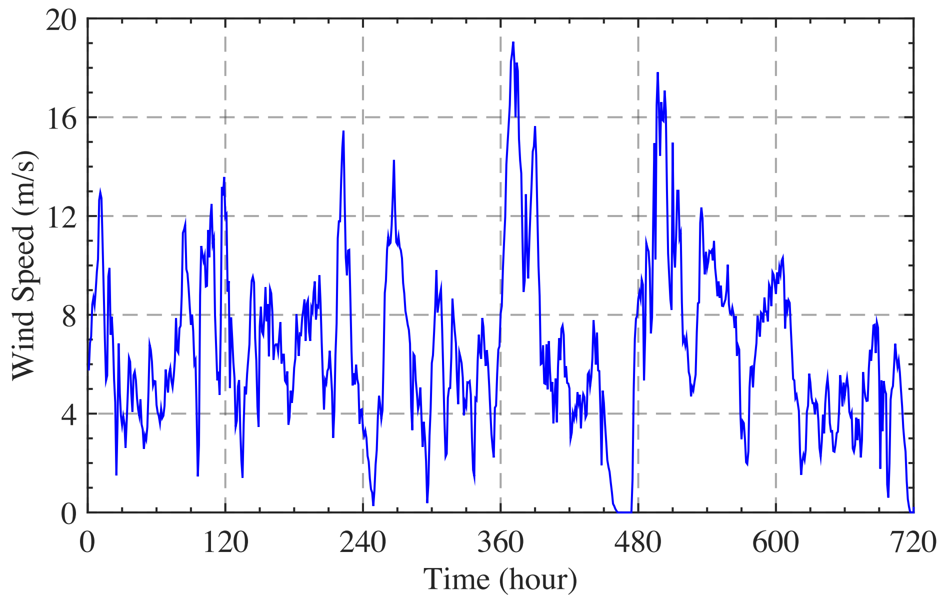

(a)

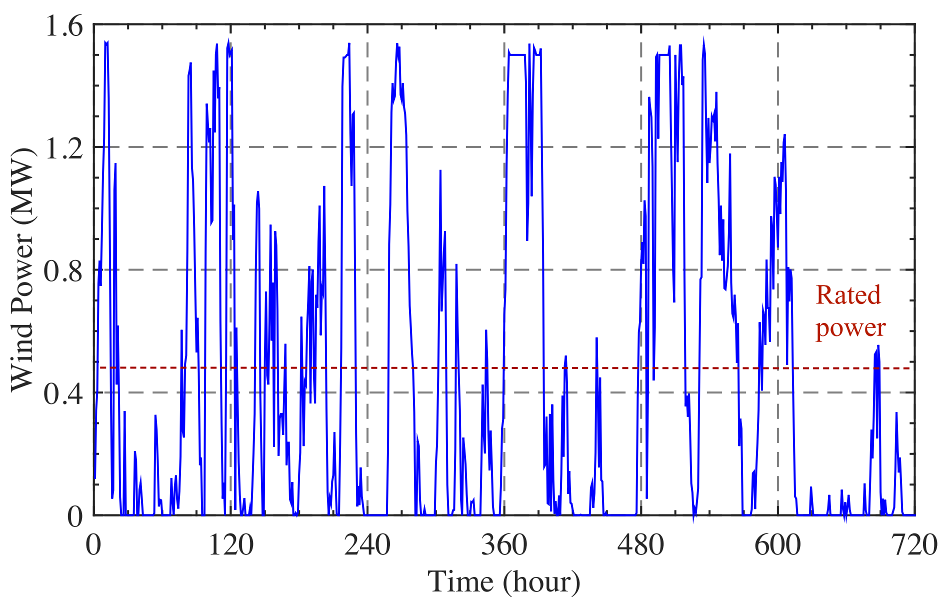

(b)

Figure 6.2: Variability in wind speed, and the output power of a selected 1.5 MW wind turbine. (a) Shows wind speeds for a selected month at the location of study, and (b) shows the corresponding wind power for the same period.

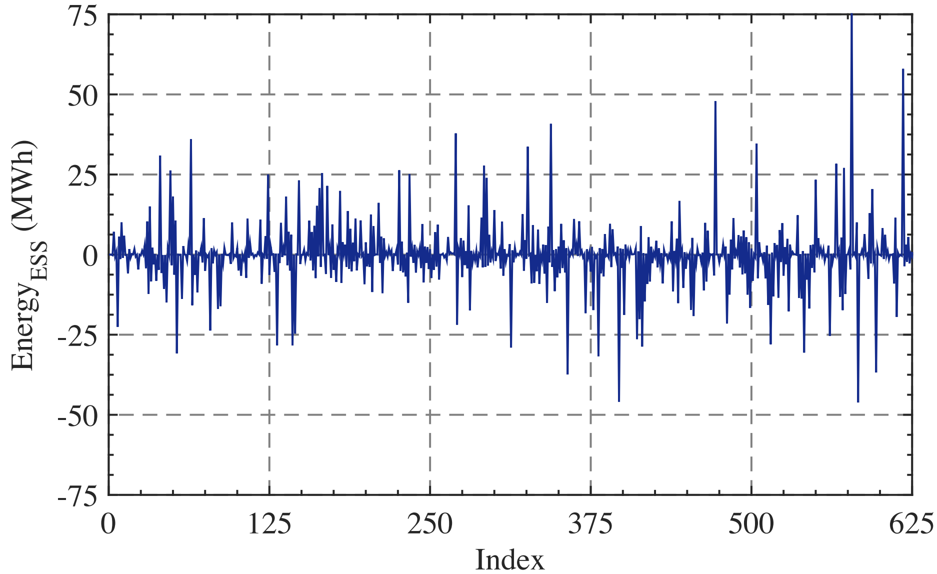

Figure 6.3: The calculated capacities of the occurred energy charges and discharges of the ESS over the study period.

is then computed as the mean value of wind power data using Equation (2.3). By calculating individual energy imbalances using Equation (2.4), the energy charges and discharges of ESS over the time period of study are calculated. Figure 6.3 shows the calculated sizes of the occurred energy charges and discharges for the studied case. Next, the histogram of the calculated energy occurrences of the storage system is next created to enable applying different confidence levels to the calculated energy charges and discharges of ESS. The Laplace distribution shows a better fit for the battery energy values. Figure 6.4 shows the histogram of the ESS calculated energy values fitted with a Laplace distribution, and the corresponding Q-Q plot supporting the well-fitting pattern of the energy values and the Laplace distribution. The parameters of the fitted Laplace distribution are estimated using equations in Chapter 4 and the desired confidence level is applied to obtain the energy capacity of ESS.

Table 6.3 lists the values of the calculated storage ratios required to generate 1 kW base-load power from the intermittent energy source using 70-, 80-, 90- and 95%-

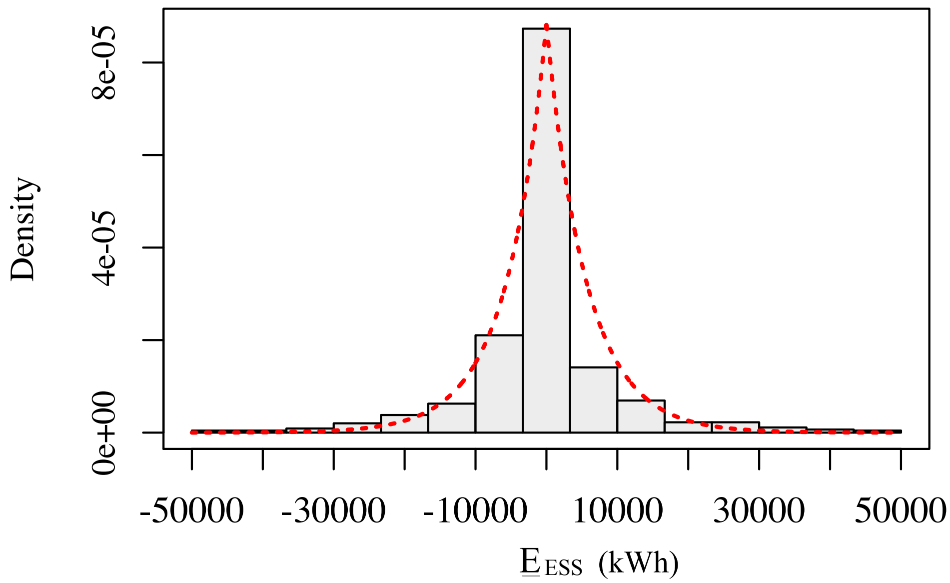

(a)

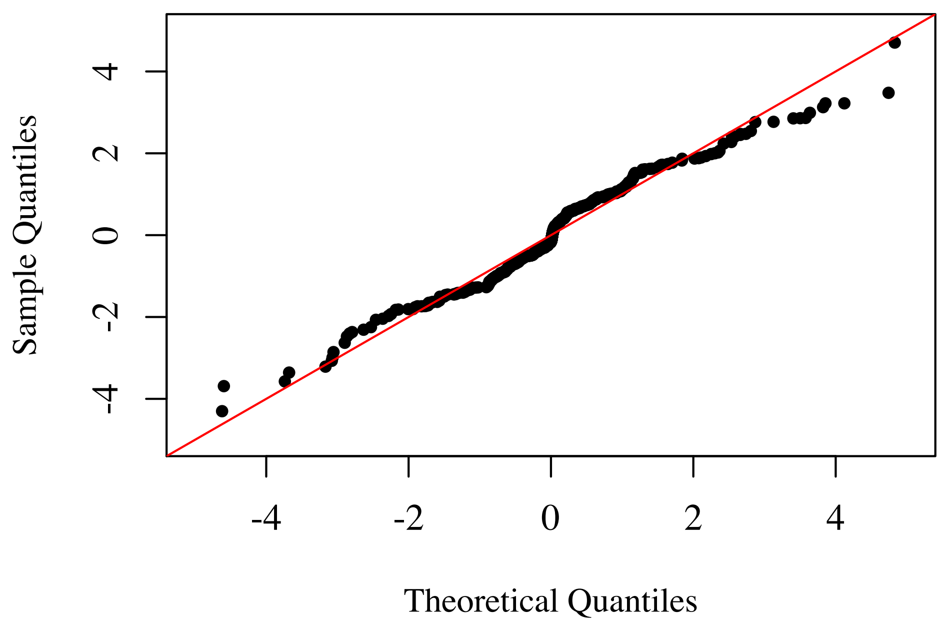

(b)

Figure 6.4: (a) The histogram of the storage system calculated energy values in kWh and the fitted Laplace distribution; and (b) the respective Q-Q plot to assess the goodness of the fitted distribution.

Table 6.3: The values of the calculated storage ratios using 70-, 80-, 90- and 95%-content tolerance intervals with 95% confidence interval.

Confidence level (P) %	Storage ratio (S_r) kWh/kW
95	37.08
90	29.83
80	19.79
70	15.17

content tolerance intervals with the confidence interval $(1 - \alpha)$ is equal to 0.95%.

The framework now investigates how the available storage capacity due to battery repurposing of PEVs can support base-load generations of wind generators, and how the supplemental wind power may address the energy load of the electric vehicles. Figure 6.5 shows this calculated annual energy required for the selected adoption scenario in Canada, and the average wind energy accommodated by support of repurposed batteries per year through 2050.

6.2 Renewable energy sustainability measure

By performing the simulation model for the PEV battery repurposing framework for Canada, we now investigate how the proposed framework can impact the renewable energy performance of Canada. The RER is defined as the ratio of total renewable energy produced to the total primary energy consumed before secondary transformation as follows

$$RER = \frac{Renewable\ Energy}{Primary\ Energy} = \frac{E_{RE}}{E_{RE} + E_{FF}}\,, \tag{6.1}$$

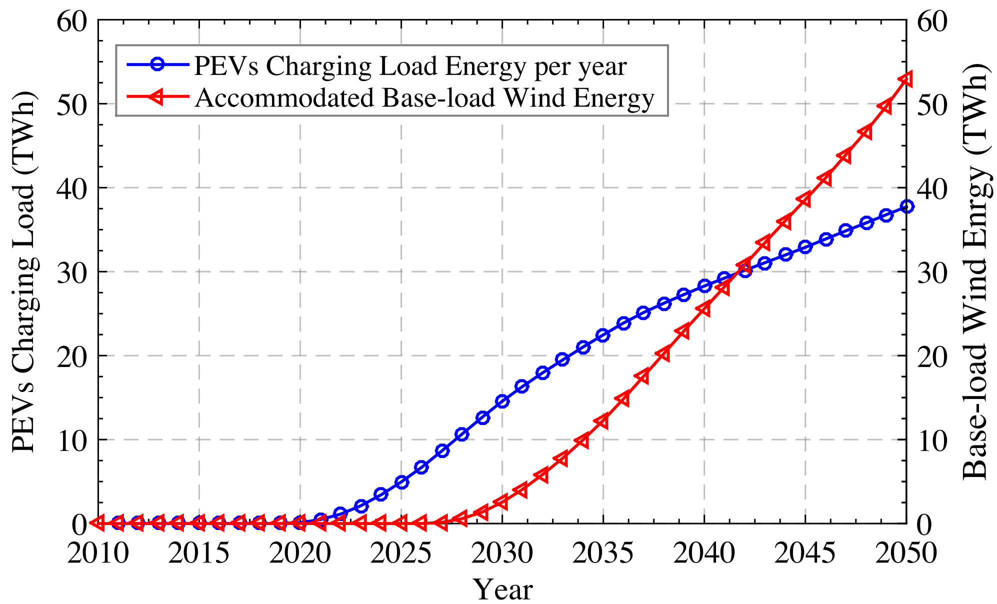

Figure 6.5: Average charging energy demand per year for PEVs based on the selected market adoption scenario for Canada in this study, and the accommodated base-load wind energy per year through 2050.

where E_{RE} is the renewable energy, and E_{FF} is the fossil fuel energy. The proposed ratio is an energy sustainability measure that can be used in a jurisdiction to evaluate its performance in mitigating fossil fuels and address energy drivers simultaneously. By focusing on energy inputs the RER acts as an optimizing tool for policy to achieve a sustainable foundation. To investigate how battery repurposing will support higher RER for Canada, this study compares the RER index with and without adding new base-load wind generation to match the new load. The data for Canada's energy mix and the share of light duty vehicles in the transport sector was obtained from [166, 167]. The available data is extrapolated through 2050 assuming that the trend from 1990 to 2009 will continue in the share of renewable energy, fossil fuels and transportation. Figure 6.6 illustrates the energy flow and the total energy use by major sectors in Canada in 2010. As depicted in this figure, the focus of this analysis is on the LDVs in the Canadian energy mix. To calculate the RER based on these data, it is assumed

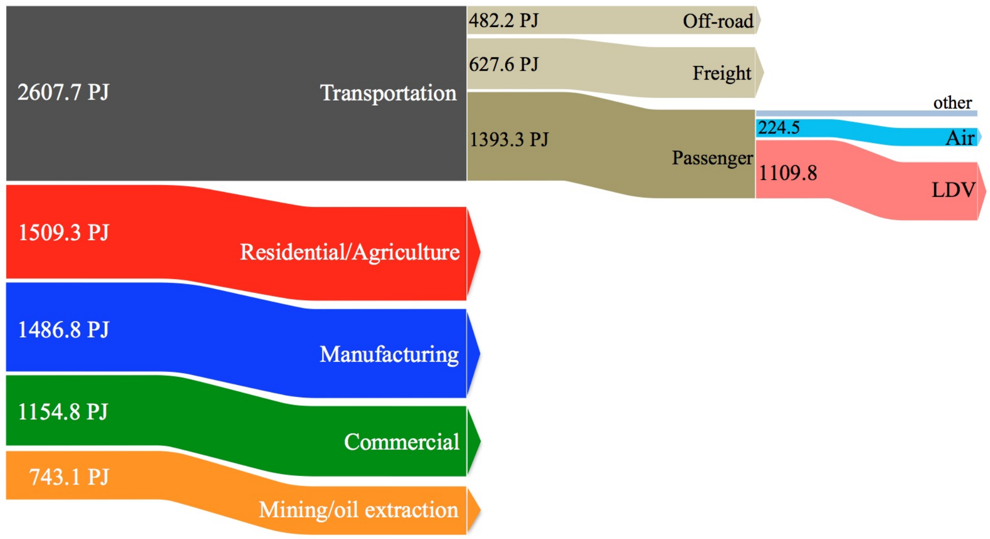

Figure 6.6: The energy flow and the total energy use by different sectors in Canada in 2010. Light duty vehicles in the transport sector are the focus of this study. The values in petajoules (PJ) are obtained from Canada's energy statistics handbook [168].

that LDVs will maintain their current share in transportation's total energy consumption. Also, it is assumed that the increase in energy consumption of LDVs in the transportation sector is solely due to new sales of vehicles. By inserting the values of the energy mix, Equation (6.1) is used to calculate the renewable energy performance of Canada for each year through 2050. Electrification of transportation is the sensible approach that can address energy and environmental issues by replacing the fossil fuels in the transport sector. Therefore, Equation (6.1) can be rewritten

$$RER_1 = \frac{E_{RE}}{E_{RE} + E_{FF,1}} = \frac{E_{RE}}{E_{RE} + (E_{FF} - E_{LDV})}, \tag{6.2}$$

where E_{LDV} is the fossil fuel energy which would be displaced in the energy mix and is proportional to the share of electric vehicles. E_{LDV} can be written as $\Delta E_{Tr} \times N_{LDV} \times N_{PEV}$ where ΔE_{Tr} is the increase in total energy consumption assumed to be solely due to new sales of LDVs, and N_{LDV} and N_{PEV} are the shares of LDVs in the transport energy mix and the share of electric vehicles in LDVs per year, respectively. The displaced fossil fuel energy needs to be replaced by new electrical energy to drive the vehicles. If the new demand of electricity is generated by conventional power plants, the RER formula is rewritten as

$$RER_2 = \frac{E_{RE}}{E_{RE} + E_{FF,2}} = \frac{E_{RE}}{E_{RE} + (E_{FF} - E_{LDV} + E_{PP})}, \tag{6.3}$$

where E_{PP} is the fossil fuel energy that is required to be burnt in conventional power plants to generate the electricity demand by electric vehicles. E_{PP} is obtained by calculating the amount of energy delivered to the wheels of the vehicles divided by the efficiencies for the energy conversions from fossil fuel to electricity as follows

$$E_{PP} = \frac{E_{LDV} \times \eta_{ICE}}{\eta_{EV} \times \eta_{PP}}, \tag{6.4}$$

where η_{ICE} is the ICE vehicles overall efficiency, η_{EV} is the electric vehicles overall efficiency, and η_{PP} is the conventional power plant overall energy conversion efficiency. As can be deduced from Equations (6.3) and (6.4), while electrification of transportation increases the energy efficiency of passenger vehicles from η_{ICE} to $[\eta_{ICE}/\eta_{EV} \times \eta_{PP}]$, it alone may not solve the issues in transportation. To address this problem, we investigate how used batteries of PEVs can be repurposed to support intermittent wind energy to generate base-load power to address the electric load of vehicles. Therefore, with the proposed scenario, the RER can be rewritten as

$$RER_3 = \frac{E_{RE}}{E_{RE} + E_{FF,3}} = \frac{E_{RE} + E_W}{(E_{RE} + E_W) + (E_{FF} - E_{LDV} + E_{PP} - E_{WP})}, \tag{6.5}$$

where E_W is the base-load renewable energy accommodated by the intermittent wind and repurposed batteries, E_{WP} is the equivalent of fossil fuel energy that is displaced from the fossil fuel energy mix by incorporating the accommodated base-load wind

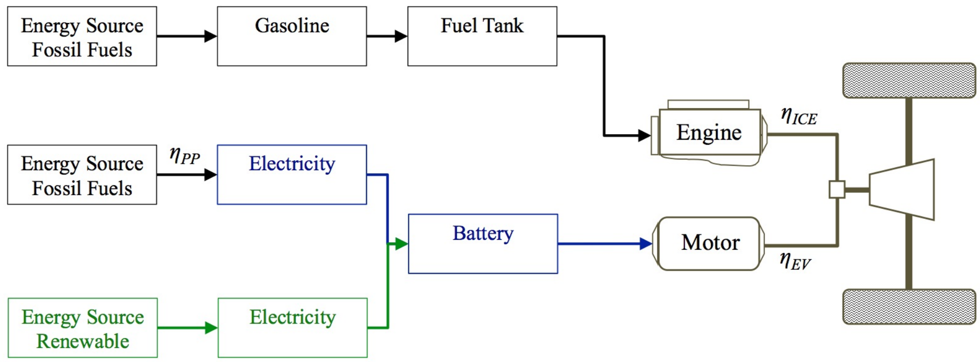

Figure 6.7: Illustration of the proposed sensible approach for the emerging electric vehicles towards a sustainable transportation system. The scenarios to calculate the RER: (i) when the required energy in transportation is from fossil fuels, (ii) when it is the electricity generated from fossil fuels at conventional power plants, or (iii) the required electricity is directly from renewable energy source.

power with repurposed batteries, and is obtained by $E_W \times (\eta_{EV}/\eta_{PP})$. Figure 6.7 shows the concept of energy use in transportation for when it relies on fossil fuels, electricity from fossil fuels, and electricity generated by renewable sources. Based on the described approaches and by setting the parameters values listed in Table 6.4, the energy sustainability performance for Canada is quantified through 2050. Figure 6.8 shows the RER performance in the Canadian energy mix for the three approaches: (i) the business–as–usual where the current trends in the energy mix continue, (ii) electrification of transportation without repurposing, and (iii) electric mobility with implementation of battery repurposing of PEVs. The results of the proposed framework for the approaches described above show that electrification of transportation improves the energy efficiency in the transport sector by increasing the RER by 0.91% for Canada in 2050.

The model then shows that implementation of the battery repurposing of PEVs to support base-load wind power can further increase the RER by 1.65–4.11%, depending the confidence level selected for ESS sizing. Table 6.5 presents the values of the

Table 6.4: Values of the parameters to calculate the RER for Canada in the battery repurposing framework.

#	Parameters	Values
1	Overall efficiency of PEV in %	80
2	Overall efficiency of ICE in %	15
3	Overall efficiency of a typical power plant in %	40
4	Share of LDVs in the total energy consumption in transportation in %	45
5	Total energy consumption in all modes of transportation in 2010 in PJ	2607.7
6	Total energy consumption in passenger transportation in 2010 in PJ	1393.3
7	Total energy consumption in LDVs in 2010 in PJ	1109.8
8	Total renewable energy in 2010 in PJ	1723.28
8	Total fossil fuel energy in 2010 in PJ	8760.10

calculated storage ratios using 70-, 80-, 90- and 95%-content tolerance intervals with the consequent changes of the RER.

Figure 6.9 illustrates the RER performance in the Canadian energy mix for the presented approaches with different confidence levels compared to the business–as–usual and the electrified transportation without repurposing approaches.

6.3 Cost analysis for intermittent renewables

A proper baseline is required to compare capital costs of different renewable energy technologies when they are intermittent sources and energy storage is imposed as part of a sustainable solution. The capital cost can vary considerably if the system is grid connected and intermittency is accommodated by the utility, or if the system operates in isolation and requires storage. Therefore, a general expression for the capital cost of renewable energy sources that includes the cost of storage is desirable. In this section,

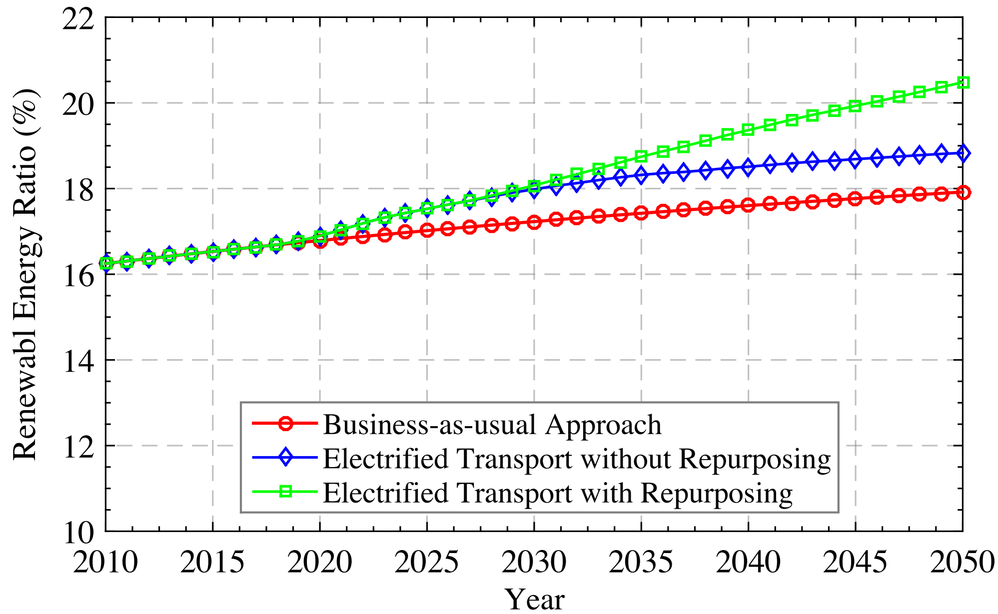

Figure 6.8: The calculated energy sustainability measure, RER, for Canada based to investigate the energy performance in transportation for conventional vehicles, and for electrified transportation with new base-load wind generation (with battery repurposing) and without adding new renewable (without battery repurposing).

we propose this expression to provide a true cost of renewable energy technologies with storage systems, and to show how the cost of storage impacts the technology's large-scale adoption. An alternative approach is to have the utility manage the intermittency. For the current relatively low intermittent generation penetration rates, utilities will attribute interconnection costs for adding new intermittent generation to offset new PEV loads. However, their ability to respond to load variations will decrease as this will reduce dispatchable generation. The long-term sustainable solution is to address the intermittency as part of a transportation policy as that cost needs to be addressed, or impact other scenarios to increase the RER that relies on reducing dispatchable generation.

For fossil fuel power plants, the fuel itself is the storage medium supplying base-loads and often variable loads. Fossil fuel plants tend to operate at relatively high capacity

Table 6.5: Values of the calculated storage ratios using 70-, 80-, 90- and 95%-content tolerance intervals, which result in different values of the RER. The last two columns list the changes of the RER values compared to (a) when the current trends of energy in Canada continue without the electrification of transportation, and (b) when in addition to current trends of energy, transportation is electrified and PEVs are adopted through 2050.

Time	Confidence level	Storage ratio (S_r)	RER	RER change (%)	
	(%)	(kWh/kW)	(%)	(a)	(b)
2050	95	37.08	20.48	2.56	1.65
	90	29.83	20.89	2.97	2.06
	80	19.79	21.96	4.04	3.13
	70	15.17	22.94	5.02	4.11
2030	95	37.08	18.08	0.85	0.10
	90	29.83	18.10	0.87	0.12
	80	19.79	18.15	0.92	0.17
	70	15.17	18.20	0.97	0.22

factors where a decrease in efficiency at partial system loading and shut downs are their main issues in addressing the load. The capital cost per kW, C_p, captures the capital cost of the system where ongoing fuel costs, operational costs, and maintenance costs are in addition to this. Capital costs for renewable energy power stations, in contrast to fossil fuel plants, cannot be calculated based on the rated power generation capacity alone since power generation based on renewable sources is subject to intermittency. The intermittency of the power output affects the reliability of the power generation. The integral effect of intermittency of power generation can be taken into account by defining the capacity factor, C_f, which is the ratio of the actual energy output of a power system to the full rated energy output over a certain period. The capacity factor is always less than one. It is convenient to calculate the cost of effective power

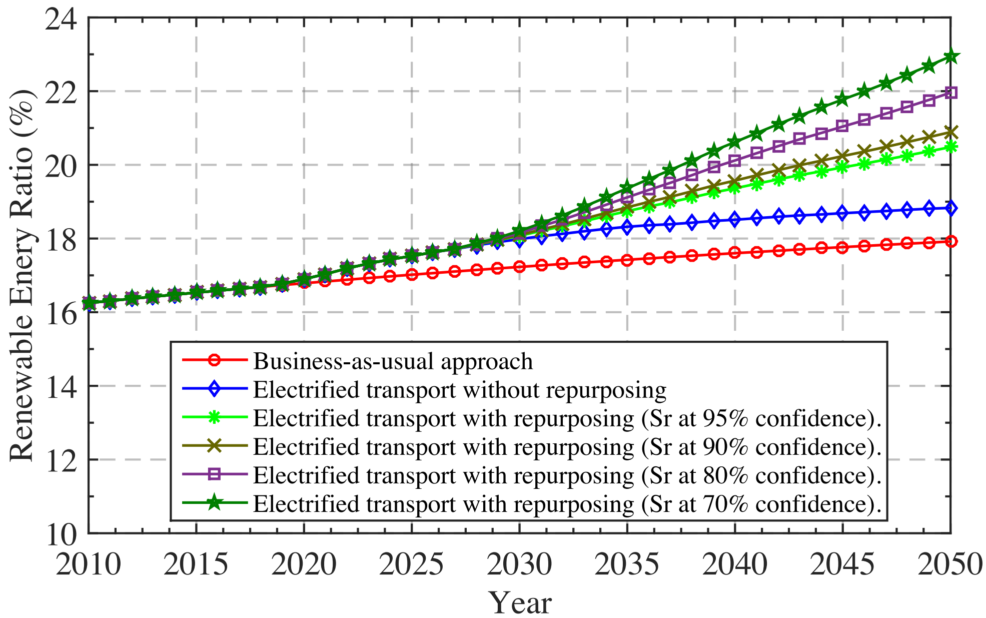

Figure 6.9: Illustration of the energy sustainability performance for Canada, where the electrified transportation is integrated with new base-load wind generation (through battery repurposing using 4 confidence levels) compared to the scenario when the current trends of energy in Canada continue without PEVs, and to the scenario with the electrification of transportation (with PEVs).

generated of an intermittent source, by introducing the capacity factor as

$$C_{eff} = \frac{C_p}{C_f}, \tag{6.6}$$

where C_{eff} is the cost of effective power generation in \$/kW, and C_f is the capacity factor. This effective cost is subject to variability of the local renewable resources, for instance wind, solar or hydro, to obtain the capacity factor for power generation applications. We now consider a continuous unit power output as the simplest load to establish a costing method for comparison. From an energy balance, we propose that the capital cost can be approximated as the following. Addition of a storage system can improve the quality of power generated by removing the effect of intermittency. The total capital cost for generating a continuous power output, C_{con}, is the sum of three cost terms:

$$C_{con} = C_{eff} + C_{loss} + C_{st}\,, \tag{6.7}$$

where C_{eff} is given by Equation (6.6), C_{loss} is the capital cost of generation for the power loss due to charging and discharging the storage system which is reflected on the other two terms, and C_{st} is the storage cost required for every 1 kW of continuous power generation. Rewriting Equation (6.7) by inserting the related terms yields Equation (6.8) where the first term accounts for the cost of effective power generation and the cost of generation for the power loss; and the second term accounts for the storage cost required for continuous power generation:

$$C_{con} = \frac{C_p}{C_f \cdot \eta_c \cdot \eta_d} + \frac{S_r \cdot C_s}{DOD \cdot \eta_d}\,, \tag{6.8}$$

where, C_{con} is the cost of continuous power generation in \$/kW, C_s is the unit cost of storage in \$/kWh, η_c and η_d represent the charging and discharging efficiencies for storage, S_r is the storage ratio or the required storage capacity per effective continuous power generation unit in kWh/kW, and DOD is the depth of discharge of the storage system that indicates the percentage of maximum availability of the storage capacity. The first term considers generation cost subject to the inefficiencies during the storage process. Figure 6.10 shows an example of the hourly output power of a wind generator over the period of one week combined with ESS to generate continuous output. Equation (6.8) can also be used to compare expensive storage technologies like hydrogen and fuel cells, and more cost competitive approaches like pumped hydro storage and compressed air electric storage. The equation demonstrates that the capacity factor and the storage efficiency are coupled into the cost so that significant cost increases will occur if proper care is not taken to select an efficient storage technology when used

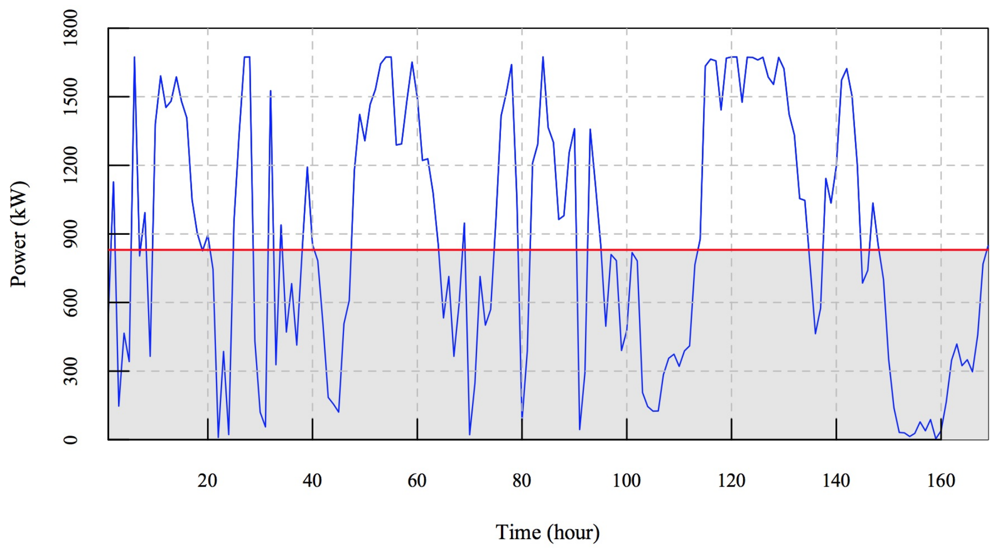

Figure 6.10: An example of the hourly fluctuating output power of a wind turbine combined with an energy storage system to generate constant output of the rated capacity of the turbine.

to support renewables because of the lower C_f compared to fossil fuels. Furthermore, the unit cost of storage, C_s, has a significant influence on the cost of continuous production, C_{con}, as it is multiplied by the storage ratio factor, S_r. These aspects make comparison of intermittent renewables difficult. As this is continuous power delivered to the grid, there are no line losses associated with efficiency of the storage technology used. However, achieving full power 100% of the time is not realistic, as even fossil fuel plants cannot achieve this. The cost of continuous power can be calculated for different confidence levels based on statistical distributions of the calculated charge and discharge occurrences.

By way of example, let the capital cost for the wind name-plate power generation be \$2,000 per kW; using Equation (6.6) the capital cost for generating effective wind power is \$5,715 per kW assuming a capacity factor of 35% in the location of study. To calculate the capital cost of base-load power generation from the intermittent source, a set of values for the parameters are applied in Equation (6.8). Many studies have attempted to forecast the future cost of new Li-ion batteries of PEVs [88, 169, 170]. We apply \$600 per kWh for new batteries which is expected to reach below \$300 per kWh in the future. As presented in Equation (6.8), cost of electric energy storage can significantly raise power generation capital costs from intermittent renewable sources to produce more reliable and uniform power when delivered to the grid. Repurposed PEV batteries at the end of their vehicular life can provide a source of lower cost storage to address this issue. Table 6.6 summarizes the values of the parameters used in Equation (6.8) to compare the capital costs of the base-load power production with new, and with repurposed PEV batteries.

In this example, 10% of the new battery's capital cost is dedicated to the testing and refurbishing process of used batteries. By inserting the values of the parameters associated with each approach, the costs of generating 1 kW of constant wind power are estimated \$29,150 and \$11,750 at 90% confidence level for new and repurposed batteries, respectively.

The comparison in this section shows the significant impact of the storage cost for more base-load wind generation approach. To show the cost-effectiveness of the proposed concept we estimate cost of base-load power generation for a scenario in 2050 using 70-, 80-, 90- and 95% confidence levels. Table 6.7 shows the estimated values when the unit cost of storage system for new and repurposed batteries are assumed \$300 and \$50, respectively, and the capital cost is assumed at \$1000.

As shown in this table, applying a 70% confidence, the cost of base-load power using repurposed batteries reduces to \$5,649 per kW by 2050, as such the current resistance to convert the interment wind energy to a base-load power unit can be overcome.

By way of comparison, and by repeating the cost analysis of base-load wind power

Table 6.6: Values of the parameters used to calculate the capital costs of base-load power generation from intermittent renewable sources using new and repurposed batteries of PEVs at 90% confidence level.

#	Parameters	Values
1	Capital cost for wind name-plate power generation in $ per kW	2,000
2	Capacity factor in the location of study in %	35
3	Storage ratio, S_r, to generate base-load power in kWh per kW at 90% confidence	29.83
4	Depth of discharge, DOD, of the storage system for new batteries in %	90
5	Depth of discharge, DOD, of the storage system for repurposed batteries in %	80
6	Charge efficiency, η_c, of the storage system for new batteries in %	90
7	Discharge efficiency, η_d, of the storage system for new batteries in %	90
8	Charge efficiency, η_c, of the storage system for repurposed batteries in %	80
9	Discharge efficiency, η_d, of the storage system for repurposed batteries in %	80
10	Cost of storage, C_s, of the storage system for new PEV batteries in $ per kWh	600
11	Cost of storage, C_s, of the storage system for repurposed PEV batteries in $ per kWh	60

Table 6.7: Estimated cost of wind power base-load generation for a scenario in 2050 using 70-, 80-, 90- and 95%-content tolerance intervals and 95% confidence interval. For this calculation, the unit cost of storage system for new and repurposed batteries are assumed \$300 and \$50, respectively, and the capital cost estimated at \$1000.

Battery type	Confidence level (%)	Storage ratio (S_r) (kWh/kW)	Base-load cost (\$/kW)
New	95	37.08	17,261
	90	29.83	14,575
	80	19.79	10,857
	70	15.17	9,146
Repurposed	95	37.08	7,361
	90	29.83	6,795
	80	19.79	6,010
	70	15.17	5,649

with fuel cell storage system, the results show a significant increase to produce 1 kW base-load. Using the case of 95% confidence level which requires 37.08 kW of storage, and assuming a fuel cell storage system with 50% charge and discharge efficiencies, full depth of discharge (DOD = 1), and \$800 for the cost of storage per kWh, the calculated base-load cost is \$70,757. This example is based on available data in the literature, and highlights the cost effectiveness of the proposed concept of using Li-ion batteries versus fuel cell storage systems. Moreover, Appendix A discusses why EVs and not fuel cells derived from electrolysed hydrogen is mathematically a more suitable choice, in line with the RED objectives. When bringing sustainability to transportation, FCVs don not compete with EVs as their efficiency is approximately 4 times less than the EV's. This Appendix contains an analysis of the energy conversion efficiency and a primer for various powertrains and energy losses during the secondary conversion processes assemble from data found in the literature and presented to highlight the key points to understand the root of electric mobility as a sustainable approach for transportation.

6.4 Discussion

It is imperative to implement strategic policies towards a sustainable future of the world's energy, and mitigate risks from the current approach. These policies should focus on inputs to the global energy system rather than looking at the system outputs like GHG's. The sensible approach is addressing energy drivers simultaneously by displacing fossil fuels with new renewable energy generation to solve energy and environmental issues in transportation effectively rather than looking at aspects in isolation. The battery repurposing concept is therefore proposed in this thesis, to study the integration of base-load wind power and electrified transportation at low cost without depletion of dispatchable power. The developed model can be used as a policy tool to investigate how different scenarios and parameters can effectively meet the challenges of sustainability in the energy and transportation sectors when the ultimate objective is to simultaneously displace fossil fuels with new generation of renewable energy. However, the presented concept contains forward-looking statements, scenarios, parameters and assumptions which involve uncertainties. Therefore, the outcome of the proposed framework model is subject to a diverse array of factors and circumstances in the future. For instance, the emerging market of PEVs is growing rapidly, but projections remain uncertain. Technology advancements of electric vehicles and their propulsion batteries are happening at a fast pace. The price of battery systems for PEV is decreasing significantly. The process of acquiring, refurbishing, and distributing of the repurposed batteries is complex, and its cost remains difficult to estimate. The energy mix of the future lactic grids is uncertain and depends on several scenarios that may or may not happen. These factors may make it difficult to picture a more realistic future for the proposed concept. Nonetheless, this analysis shows that the battery repurposing model can be used, and advanced, to investigate the influence of various future outcomes. Furthermore, the study shows that integration of electrified transpiration and renewable energy through battery repurposing of PEVs is an effective approach to improve the energy performance towards a sustainable transportation system.

As we strive to a more sustainable future, the ESS sizing algorithm presented in Chapter 4 addresses circumstances to overcome society's stringent inertia to replace fossil fuel generation with intermittent renewable wind generation. While large utilities are presently not planning for high penetration of wind energy, the presented methods in this thesis can contribute towards the goal of converting intermittent renewable energy to base-load generation in future electric grids. Most robust grid systems today, no matter what the supply mix is, can likely accommodate 25% intermittent sources such as wind power without major changes to the grid. Integrating beyond 25% and up to 50% wind may require some grid changes such as energy storage or demand response, and added system inertia for stability purposes. Areas that may have access to base-load renewable energy power generation like hydro, geothermal or biomass can look to accommodate 100% renewables by adding wind or solar at lower penetration *e.g.*, up to 25% with no storage or other grid enhancements. The future electric grid can be made 100% renewable with utilizing intermittent renewables like wind and solar, that are available just about anywhere in the world, if the wind or solar are converted to behave like base-load generation by the addition of an appropriate amount of energy storage. Economics of wind power generation compared to today's other base-load generation, and its viability in the future with further storage system cost reductions make this concept even more favorable. Thus, it is anticipated that a future grid in 2030+ will likely economically accommodate more wind and solar power. In summary, following is the list of possible applications to build a wind farm at a known confidence level for base-load power generation.

- Building a wind farm at a known confidence level for base-load power generation can also be used to remove diesel generation in remote locations.

- This can also be used by utilities that are not limited by generation or capacity but have environmental constraints and are capped out in emissions. As such they require analysis to use larger penetration rates of wind as a need to evaluate alternatives.

- An independent power producer can also achieve a higher price for less intermittent power generation. As this is dictated by market conditions, the independent power producer has to be able to prove a confidence level of power delivery to the financial institution and the utility.

- The proposed method can also be utilized in net-zero buildings that require to be self-sufficient in their energy and have access to a good wind resource.

There are several parametric and nonparametric methods that can be used to model wind turbine power curves. Examples of these models include segmented linear models, polynomial regression, four- or five-parameter logistic distributions; and neural networks, fuzzy logic methods, and data mining methods approaches. In this thesis, we made a contribution by presenting novel methods for wind power curve modeling. The developed methods are easier to implement compared with the mentioned methods. These methods can be used for on-line monitoring of power curves for detecting anomalies in a wind turbine power generation process. This feature will provide the opportunity of enhanced wind turbine monitoring.

Chapter 7

Conclusions and Future Work

This chapter provides a summary of the accomplishments of the research work presented in thesis. Herein, the thesis is concluded by providing the outline of the suggested future work that can be followed upon this research to achieve a low-cost sustainable transportation.

7.1 Summary of accomplishments

We presented the battery repurposing of PEVs that can effectively integrate the emerging electric vehicles and intermittent renewable energy. The potential viability of the proposed framework to increase the share of renewable energy by incorporating more renewable sources and relinquishing the reliance on fossil fuels was investigated. We introduced a new cost model for the comparison of the capital costs of base-load power generation from intermittent energy sources. The proposed approach shows that adding used batteries of electric vehicles at their vehicular EOL to wind turbines yields a potential cost-effective solution to produce base-load and dispatchable renewable power. The simulation also shows that the proposed approach for the studied case of Canada can further improve the energy sustainability performance by increasing the renewable energy ratio by 1.65–4.11% in 2050, in addition to electrifying transportation and depending the confidence level selected for ESS sizing. Moreover, such a scenario makes base-load power generation from intermittent wind energy an economic reality. When using fossil fuels, one achieves 100% flexibility as fossil fuels store the energy in the fuel, and are available on-demand. We have shown a cost-effective method to rely on repurposed batteries and low-cost intermittent wind energy to replace fossil fuels, and still accessing the advantages of fossil fuels to be able to store energy.

In the framework, we developed a statistical algorithm to calculate the capacity of an energy storage system required for delivering base-load electricity for a wind farm in the future electric grids. The developed algorithm contributes towards the goal of utilizing low-cost intermittent wind energy to base-load power generation in the future electric grids. The introduced algorithm presents three methods to perform the sizing calculations each representing a scenario associated with the stages of the wind energy industry.

While applications of the statistical models for obtaining probability distribution functions, expected value, truncated and inflated distributions exist in the field of science, the main contribution of the author is presenting a practical algorithm using these models for predicting the storage capacity when the ultimate goal is generating constant output power of the wind farm. This is an essential step in the integration of wind power systems with energy storage in the future electric power systems with higher penetration of renewable energy.

The results show that for different stages of the wind farm development, and depending on the available information, the method can properly size the energy storage required to deliver constant power to a user selected confidence level. The results were applied to estimate the cost of wind energy to produce rated power using different confidence levels. Using the analysis in Section 6.3, the total cost of 70% confidence level with ESS will be $5,649 per kW. As such, utilities can be interested in less intermittency on their systems to allow more capacity credit—a measure to assess the reliability of wind power plants in replacing conventional power plants [171]—for wind energy as part of proper supply planning with larger penetrations of renewables.

Furthermore, advanced parametric and nonparametric models were applied to estimate the power curve of wind turbines based on the available operational wind power data. While the application of regression models for wind power curve modeling and estimating the output power of wind turbines is not new, advanced statistical methods utilized in this thesis are applied for more accurate estimations of power curves based on operational power data. As no one fitting approach dominates all other techniques over all possible observations obtained from different wind turbines, polynomial regression was studied as a benchmark parametric method for power curve fitting. While this method has been extensively used in the literature, the author makes a significant contribution to the filed by applying advanced statistical techniques to improve the performance of the power curve estimation. It is shown in this thesis that non-parametric methods are more flexible, less sensitive to anomalies within the set of observations, easier to implement, and computationally more feasible compared to other methods in the literature.

Finally, a short-duration experimental testing was performed in laboratory to investigate the capacity degradation of used batteries of PEVs in stationary applications using a 25 kWh repurposed energy storage system. Within this experimental testing available, the obtained state points of the battery systems show fluctuations in their measured capacities. This can be justified based on their "as-is" condition, and also is expected to show less fluctuations and loss over a few thousand cycles following the expected pattern.

The author has attempted to show the proof of concept and include an indication of the degradation of used batteries. The main contribution has been using the set up for the specific purpose of monitoring the degradation of repurposed batteries of PEVs under a specific charging and discharging protocol. The author has been responsible for operating the systems, collecting the data, and data processing to calculate the state of energy after certain number of cycles described in Chapter 5. The battery packs were the first demonstration of repurposed batteries available for testing designed at the Manitoba Hydro HVDC Research Centre.

7.2 Future work

The suggested future work in this thesis are presented in the following directions:

7.2.1 Battery repurposing framework

A novel energy model was presented for the integration of PEVs and wind energy to investigate how using repurposed batteries of electric vehicles can support greater penetration of wind power and improve the RER performance. The presented concept, however, contains future-looking statements, scenarios, assumptions and parameters which involve uncertainties. Therefore, the outcome of the proposed framework model involves uncertainties over a diverse array of factors and circumstances in the future. For instance, input parameters to the model may include technologies and designs of PEVs, battery cost, cost of electricity, driving patterns, availability of charging infrastructures, cost of petroleum, PEV consumer acceptance, automakers investments, PEV charging load, and electric energy generation mix. Therefore, effective implementation of this model requires enhancing the comprehensive model through identifying realistic aspects of the interaction between the energy and transport sectors, understanding the technical and economic factors, and applying these parameters to the comprehensive model. The proposed numerical method will predict optimum scenarios for the future of the Canadian energy system by incorporating the pertinent parameters. This approach will provide the policymakers with a strategy tool that can govern technology implementation with the target of maximizing fossil fuel displacement, clean energy incorporation and emissions abatement.

Following is the list of suggested works in this direction:

- Enhancement of the simulation model by incorporating more realistic scenarios and applicable parameters to the framework. This may require a more detailed review of the state-of-the-art of electric vehicles technologies and market, automakers investments, energy market status, renewable energy technologies, GHG emissions, and government policies.

- Performing a classical sensitivity analysis to identify the impact of different input parameters to the energy framework model. This analysis will help to develop different "what-if" scenarios for the future of energy systems in a jurisdiction.

- Developing an optimization algorithm for the presented model to investigate economic and environmental sustainable scenarios which can govern energy related policy implementations.

- Developing a more extensive experimental testing of battery degradation and analysis of pertinent parameters on the overall performance of batteries; and, using operational wind data to emulate the charging and discharging frequencies of an intermittent renewable source for the system.

7.2.2 Wind energy and storage sizing algorithm

In the wind energy industry, wind turbine power curves are used to study the relationship between the electrical power generated by a wind turbine and the wind speed at the machine over the period of power generation. These curves can also be used to forecast wind power, to assess wind turbine performance and turbine condition monitoring, and also to estimate the energy storage system capacity required to improve the quality and reliability of the intermittent wind power. However, available methods in the literature for wind turbine power curve modeling primarily focus on parametric and nonparametric approaches using frequentist methods (*e.g.*, maximum likelihood method, least squares method, etc.), and usually consider wind speed as the only auxiliary information for the purpose of modeling. Therefore, it is suggested to extend the results in Chapter 3 to multiple auxiliary information and improve wind turbine power curve modeling by including some other environmental factors such as air density, humidity, wind direction, and turbulence intensity in the estimation process to more realistically capture the nonlinear relationships between these environmental factors and the generated wind power.

The other suggested work in this research direction is to incorporate Bayesian and robust Bayesian ideas in power curve modeling, and use the results to develop more robust algorithms for estimating wind resource potentials based on area specific data, and a statistical algorithm for sizing the energy storage system required for delivering base-load electricity to a selected confidence level for a wind farm. This allows to incorporate expert opinion knowledge into the statistical inference process. The idea is to extend the results in Chapter 4 where the methods introduced are based on specific parametric assumptions about the statistical distribution of the wind speed in the location of study (*i.e.*, a Weibull(α, β) for the wind speed values). Using nonparametric methods prevents imposing any pre-specified model assumption and provides more realistic results over parametric models. However, these methods usually require a large amount of data to deliver the desired outcome, need longer data collection time, and are more costly. Therefore, it is usually more desirable, especially in industrial applications, to use benchmark parametric methods. In many cases, there are valuable extra information about the underlying problem that can be obtained from similar studies or from expert-opinion knowledge. These extra information can be formulated in terms of prior distributions on the parameters of the underlying parametric models. For example, for the underlying location of study, after consulting with experts and using historical wind speed data, one may conclude that wind speed data follow a Weibull(α, β) distribution, while α and β are also random variables taking values in specific ranges with some probability distributions. In such cases, we suggest to use the Bayesian approach to incorporate the extra information about the parameters of the wind speed distribution into the study.

Following is the list of suggested works in this direction which can be built upon this research:

- *Wind turbine performance monitoring and power curve modeling*

1. Applying the developed methods in this study to perform energy storage sizing for solar power.
2. Performance monitoring of wind turbines to investigate the icing phenomenon of the turbine blades based on operational power data.
3. Optimization analysis for the selection of wind turbines of a wind farm and the site location when the objectives are the capacity and cost of base-load power generation .
4. Optimal selection of a wind site location based on the objective of base-load power generation
5. Developing algorithms for estimating wind resource potentials based on area specific data.

- *Energy storage sizing algorithm for intermittent renewable energy*

1. The work will be extrapolated so that the approach can address a variable load for net zero buildings and remote communities
2. Technical and economic study of replacing diesel generation in communities with wind and solar energy when their capacity is smoothed out by integrating adequate battery storage.
3. Economic analysis of base-load wind generation and the comparison with other base-load power generation sources.
4. Investigating how PEV battery repurposing can economically support base-load power generation of intermittent wind.
5. Analysis of the influence of long-term wind data and operational power data on the proposed algorithm.
6. Analysis of the land requirements for the large-scale integration of batteries for base-load power generation.

7. Comparing the the results of ESS capacity requirement for base-load generation with operational ESS capacity available to a wind farm/region to investigate/obtain a practical coefficient of conversion from the worst-case capacity requirement and a common cap used.

Appendix A

EVs *vs.* FCVs

With the emergence of various electric vehicles, many publications and even automakers have discussed the viability of using hydrogen as the alternative and clean fuel for the future transportation. Fuel cell electric vehicles consume electrolysis-derived hydrogen to drive the vehicle. Hydrogen has a very high energy density compared to many other energy carriers, which makes the technology very attractive to many stakeholders. However, towards a sustainable transportation, and in line with RED approach, the concept should be looked at as whole not in isolation.

We present an analysis of the energy conversion efficiency and a primer for various powertrains and energy losses during the secondary conversion processes assemble from data found in the literature and presented to highlight the key points to understand the root of electric mobility as a sustainable and economic approach for transportation.

Table A.1 presents the results of the analysis, and highlights the key points to electrified transportation as a sustainable approach for transportation.

Table A.1: Comparison of energy density (Wh/kg) for various powertrains.

Attributes	Powertrain type		
	ICE	EV	FCV
Energy density in Wh/kg	12000	200	35000
Drivetrain efficiency in %	0.2	0.9	0.3
Effective energy density in Wh/kg	2400	180	10500
Fuel capacity in kg	40	300	3
Total available energy in Wh	96000	54000	31500
Drivetrain total weight in kg	450	350	750
Drivetrain energy density in Wh/kg	213	154	42

APPENDIX B

Electric Vehicles Drivetrains

Hybrid electric vehicles

HEVs can have different hybridization configurations depicted in Figure B.1 which can be categorized as parallel, series, and power-split configuration [46]. In the parallel HEVs the electric motor and the engine can both drive the transmission system. In the series HEV an electric motor propels the vehicle while using the engine to drive a generator to power the electric motor and store energy in battery when required. The power-split HEV has a combination of the series and parallel characteristics.

Plug-in hybrid electric vehicles

PHEVs can have two different hybridization configurations: parallel, and series configurations. In the parallel PHEV the electric motor and the engine can both drive

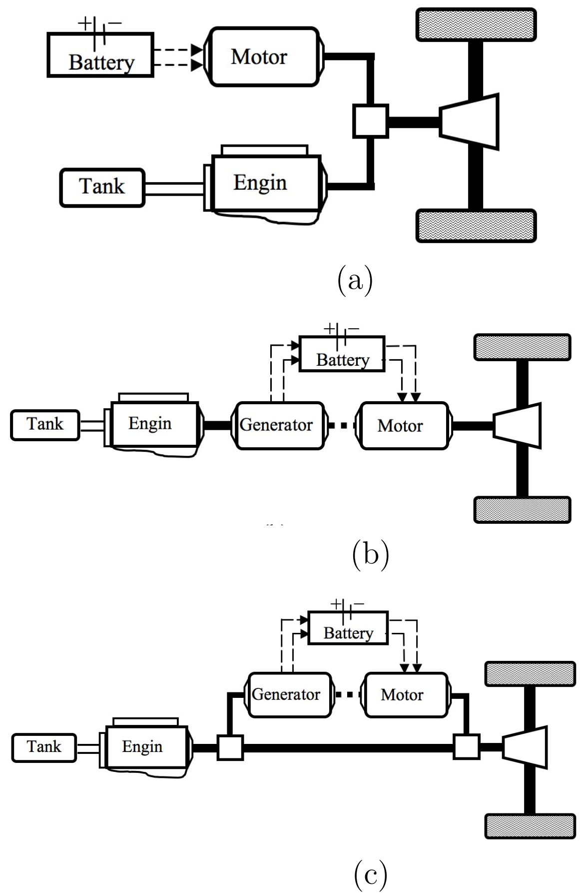

Figure B.1: HEVs can have different hybridization configurations which can be categorized as (a) parallel, (b) series, and (c) power-split configuration. In the parallel HEVs the electric motor and the engine can both drive the transmission system. In the series HEV an electric motor propels the vehicle while using the engine to drive a generator to power the electric motor and store energy in battery when required. The power-split HEV has a combination of the series and parallel characteristics.

the transmission system. In the series PHEV the electric motor propels the vehicle and the engine is used to solely drive the generator. The larger battery capacity in PHEVs, varying from 5 to 22 kWh [8], extends their all-electric range (AER) through reducing the reliance on the ICE. In the series hybrid configuration, the engine is used to solely power the generator [72]. Figure B.2 illustrates the configuration of parallel and series PHEVs.

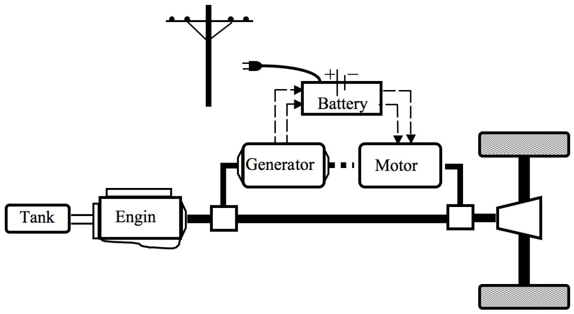

(a)

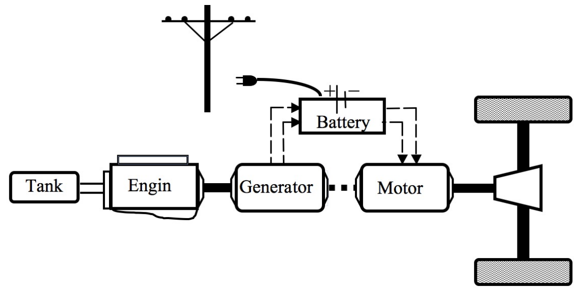

(b)

Figure B.2: PHEVs can have two different hybridization configurations named as (a) parallel, and (b) series configurations. In the parallel PHEV the electric motor and the engine can both drive the transmission system. In the series PHEV the electric motor propels the vehicle and the engine is used to solely drive the generator.

Battery electric vehicles

BEVs are pure electric vehicles with no engine onboard. Figure B.3 shows a simple configuration of BEVs which exclusively are powered through electricity stored in their battery.

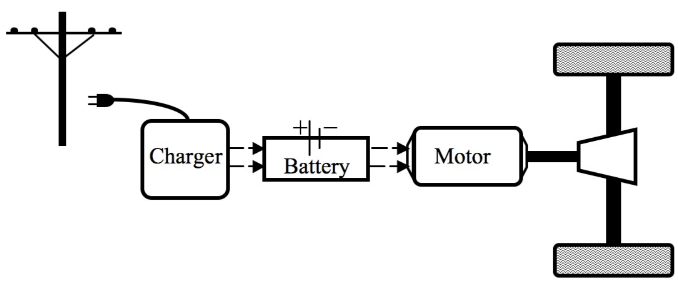

Figure B.3: The configuration of BEVs where the vehicle is equipped with a larger battery, and is propelled solely with an electric motor through the electricity stored in their battery.

Bibliography

[1] International Energy Agency (IEA), "World Energy Investment Outlook–2014," Technical. Report, Paris, 2014.

[2] International Energy Agency (IEA), "World Energy Outlook–2012," Technical Report, Paris, 2012.

[3] International Energy Agency (IEA),"Global EV Outlook: Understanding the Electric Vehicle Landscape to 2020," Technical Report, Paris, 2013.

[4] International Energy Agency (IEA), "Tracking Clean Energy Progress–2012," Technical Report, Paris, 2012.

[5] International Energy Agency (IEA), "Energy Technology Perspectives 2012: Pathways to A Clean Energy System," Technical Report, Paris, 2012.

[6] A. Emadi, "Transportation 2.0," *Power and Energy Magazine, IEEE*, vol. 9, no. 4, pp. 18–29, July 2011.

[7] R. Reisinger and A. Emadi, "Sensible Transportation Electrification : Get Rid of Inefficient Powertrain Designs." *Electrification Magazine, IEEE*, vol. 1, no. 2, pp. 6–12, Dec 2013.

[8] International Energy Agency (IEA), "Technology Roadmap: Electric and Plug-in Hybrid Electric Vehicles," Technical Report, Paris, 2011.

[9] Natural Resources Canada, "Electric Vehicle Technology Roadmap for Canada," Technical Report, Ottawa, 2010.

[10] World Wind Energy Association (WWEA), "World Wind Energy Report–2012," Technical Report, Bonn, 2013.

[11] International Energy Agency (IEA), "Technology Roadmap–Wind Energy," Technical Report, Paris, 2013.

[12] International Energy Agency (IEA),"World renewable energy outlook–2013," Technical Report, Paris, 2013.

[13] International Energy Agency (IEA), "World energy outlook–2013," Technical Report, Paris, 2013.

[14] Bloomberg, "Fossil Fuels Just Lost the Race Against Renewables," [Online]. Available: http://www.bloomberg.com/news/articles/2015-04-14/fossil-fuels-just-lost-the-race-against-renewables, accessed: 2015-06-20.

[15] Lazard, "Lazard's Levelized Cost of Energy Analysis - Version 8.0," 2014. [Online]. Available: http://www.lazard.com/PDF/Levelized%20Cost%20of%20Energy%20-%20Version%208.0.pdf

[16] J. Conti, P. Holtberg, J. Diefenderfer, S. Napolitano, A. Schaal, J. Turnure, and L. Westfall, "Annual Energy Outlook 2014 with Projections to 2040," *US Energy Information Administration*, 2014.

[17] U. Bossel, Ph. D, B. Eliasson, Ph. D, and G. Taylor, "The Future of the Hydrogen Economy: Bright or Bleak?" *Cogeneration and Distributed Generation Journal*, vol. 18, no. 3, pp. 29–70, 2003.

[18] U. Bossel, "Does A Hydrogen Economy Make Sense?" *Proceedings of the IEEE*, vol. 94, no. 10, pp. 1826–1837, 2006.

[19] C. Chan, "The State of the Art of Electric, Hybrid, and Fuel Cell Vehicles," *Proceedings of the IEEE*, vol. 95, no. 4, pp. 704–718, 2007.

[20] B. K. Sovacool and R. F. Hirsh, "Beyond Batteries: An Examination of the Benefits and Barriers to Plug-in Hybrid Electric Vehicles (PHEVs) and A Vehicle-to-Grid (V2G) Transition," *Energy Policy*, vol. 37, no. 3, pp. 1095–1103, 2009.

[21] E. Bibeau, "Repurposing PEV Batteries: Supporting Renewables; Meet the Drivers," in *PHEV 2009 - Plug-In Hybrids and Electric Vehicles Conference, Montreal, Canada*, 2009.

[22] E. Bibeau, "Increasing the Renewable Energy Ratio of Northern Communities," in *Canadian Meteorological and Oceanographic Society – 44th Annual Congress, Ottawa, Canada*, 2010.

[23] E. Tara, S. Shahidinejad, S. Filizadeh, and E. Bibeau, "Battery Storage Sizing in A Retrofitted Plug-in Hybrid Electric Vehicle," *Vehicular Technology, IEEE Transactions on*, vol. 59, no. 6, pp. 2786–2794, July 2010.

[24] A. Ipakchi and F. Albuyeh, "Grid of the Future," *Power and Energy Magazine, IEEE*, vol. 7, no. 2, pp. 52–62, March 2009.

[25] A. Kusiak, A. Verma, and X. Wei, "Wind Turbine Capacity Frontier from Scada," *Wind Systems Magazine*, vol. 3, no. 9, pp. 36–39, 2012.

[26] A. Benatiallah, L. Kadia, and B. Dakyob, "Modelling and Optimisation of Wind Energy Systems," *JJMIE*, vol. 4, no. 1, 2010.

[27] Z. Zhang, Q. Zhou, and A. Kusiak, "Optimization of Wind Power and Its Variability with A Computational Intelligence Approach," *Sustainable Energy, IEEE Transactions on*, vol. 5, no. 1, pp. 228–236, Jan 2014.

[28] M. Duvall, E. Knipping, M. Alexander, L. Tonachel, and C. Clark, "Environmental Assessment of Plug-in Hybrid Electric Vehicles," *Electric Power Research Institute (EPRI), Palo Alto, CA*, July, 2007.

[29] P. Balducci, "Plug-in Hybrid Electric Vehicle Market Penetration Scenarios," *PNNL-17441 Report. Pacific Northwest National Laboratory. Richland, WA*, 2008.

[30] J. Cochran, T. Mai, and M. Bazilian, "Meta-Analysis of High Penetration Renewable Energy Scenarios," *Renewable and Sustainable Energy Reviews*, vol. 29, pp. 246–253, 2014.

[31] D. Palchak and P. Denholm, "Impact of Generator Flexibility on Electric System Costs and Integration of Renewable Energy," NREL/TP-6A20-62275. Golden, CO: National Renewable Energy Laboratory. Accessed September 4, 2014: http://www. nrel. gov/docs/fy14osti/62275. pdf, Tech. Rep., 2014.

[32] S. Shokrzadeh, M. Jafari-Jozani, E. Bibeau, and T. Molinski, "A Statistical Algorithm for Predicting the Energy Storage Capacity for Baseload Wind Power Generation in the Future Electric Grids," *Energy*, 2015.

[33] S. B. Peterson, J. Apt, and J. Whitacre, "Lithium-ion Battery Cell Degradation Resulting from Realistic Vehicle and Vehicle-to-Grid Utilization," *Journal of Power Sources*, vol. 195, no. 8, pp. 2385–2392, 2010.

[34] A. Ritchie, "Recent Developments and Likely Advances in Lithium Rechargeable Batteries," *Journal of Power Sources*, vol. 136, no. 2, pp. 285–289, 2004.

[35] K. Smith, M. Earleywine, E. Wood, J. Neubauer, and A. Pesaran, "Comparison of Plug-in Hybrid Electric Vehicle Battery Life Across Geographies and Drive Cycles," SAE Technical Paper, Tech. Rep., 2012.

[36] R. Spotnitz, "Simulation of Capacity Fade in Lithium-ion Batteries," *Journal of Power Sources*, vol. 113, no. 1, pp. 72–80, 2003.

[37] H. J. Ploehn, P. Ramadass, and R. E. White, "Solvent Diffusion Model for Aging of Lithium-ion Battery Cells," *Journal of The Electrochemical Society*, vol. 151, no. 3, pp. A456–A462, 2004.

[38] K. Smith, T. Markel, and A. Pesaran, "PHEV Battery Trade-Off Study and Standby Thermal Control," in *26th Int. Battery Seminar & Exhibit, Fort Lauderdale, FL*, 2009.

[39] Statistics Canada, "Canada Year Book–2012," 2012.

[40] Transport Canada, "Transportation in Canada 2013 – Overview Report," 2013.

[41] J. Neubauer and A. Pesaran, "The Ability of Battery Second Use Strategies to Impact Plug-in Electric Vehicle Prices and Serve Utility Energy Storage Applications," *Journal of Power Sources*, vol. 196, no. 23, pp. 10 351–10 358, 2011.

[42] A. Brooker, M. Thornton, and J. Rugh, "Technology Improvement Pathways to Cost-Effective Vehicle Electrification," SAE Technical Paper, 2010.

[43] M. O'Keefe, A. Brooker, C. Johnson, M. Mendelsohn, J. Neubauer, and A. Pesaran, *Battery Ownership Model: A Tool for Evaluating the Economics of Electrified Vehicles and Related Infrastructure*. National Renewable Energy Laboratory, 2010.

[44] J. S. Neubauer, A. Pesaran, B. Williams, M. Ferry, and J. Eyer, "A Techno-Economic Analysis of PEV Battery Second Use: Repurposed-Battery Selling Price and Commercial and Industrial End-User Value," SAE Technical Paper, 2012.

[45] E. Cready, J. Lippert, J. PIHL, I. Weinstock, and P. SYMONS, "Technical and Economic Feasibility of Applying used EV Batteries in Stationary Applications," Sandia National Labs., Albuquerque, NM (US); Sandia National Labs., Livermore, CA (US), Tech. Rep., 2003.

[46] C. Narula, R. Martinez, O. Onar, M. Starke, and G. Andrews, "Final Report Economic Analysis of Deploying Used Batteries in Power Systems," *Oak Ridge National Laboratory, Oak Ridge, TN*, 2011.

[47] A. Emadi, "Advanced Electric Drive Vehicles," *CRC Press*, 2014.

[48] L. James and L. John, "Electric Vehicle Technology Explained," *John Wiley & Sons*, 2003.

[49] M. H. Westbrook, *The Electric Car: Development and Future of Battery, Hybrid and Fuel-Cell Cars*. Iet, 2001, no. 38.

[50] N. Research, "Global Forecasts for Light Duty Hybrid, Plug-in Hybrid, and Battery Electric Vehicles 2012-2020," Technical Report, Boulder, 2012.

[51] Battery University, "The Future Battery," http://batteryuniversity.com/learn/article/the_future_battery, accessed: 2013-05-10.

[52] K. Fell, K. Huber, B. Zink, R. Kalisch, D. Forfia, D. Hazelwood, N. Dang, D. Gionet, M. Musto, W. Johnson *et al.*, "Assessment of Plug-In Electric Vehicle Integration with ISO/RTO Systems," *KEMA, Inc. and ISO/RTO Council*, 2010.

[53] R. Graham *et al.*, "Comparing the Benefits and Impacts of Hybrid Electric Vehicle Options," *Electric Power Research Institute (EPRI), Palo Alto, CA, Report*, vol. 1000349, 2001.

[54] M. Duvall, M. Alexander, A. Maitra, D. Saucedo, B. Jungers, J. Halliwell, R. Entriken, M. Davis, and K. Davis, "Transportation Electrification—A Technology Overview," 2011.

[55] Hybrid Cars, "Hybrid Cars, Auto Alternatives for the 21st Century," http://www.electricdrive.org/index.php?ht=d/sp/i/20952/pid/20952, accessed: 2011-08-26.

[56] Nissan Motor Company, "Nissan Leaf Smashes 50,000 Global Sales Milestone."

[57] Mitsubishi Motor Company, "Mitsubishi Facts and Figurs."

[58] Hybrid Cars, "December 2012 dashboard," http://www.hybridcars.com/december-2012-dashboard, accessed: 2013-03-10.

[59] A. Bandivadekar, K. Bodek, L. Cheah, C. Evans, T. Groode, J. Heywood, E. Kasseris, K. Kromer, and M. Weiss, "On the Road in 2035: Reducing Transportation's Petroleum Consumption and GHG Emissions," *lLaboratory for Energy and the Environment*, Massachusetts Institute of Technology, 2008.

[60] K. Sikes, T. Gross, Z. Lin, J. Sullivan, and T. Cleary, "Plug-in Hybrid Electric Vehicle Market Introduction Study: Final Report," Technical Report, 2010.

[61] B. M. Al-Alawi and T. H. Bradley, "Review of Hybrid, Plug-in Hybrid, and Electric Vehicle Market Modeling Studies," *Renewable and Sustainable Energy Reviews*, vol. 21, pp. 190–203, 2013.

[62] D. Hurst and J. Gartner, "Electric Vehicle Market Forecasts: Global Forecasts for Light Duty Hybrid, Plug-in Hybrid, and Battery Electric Vehicles, 2013-2020," *California. Prepared for the California Air Resources board, University of Delaware, Green Mountain College, AC Propulsion, Inc., and UC Berkeley*, 2013.

[63] J. Ford, G. Khowailed, J. Blackburn, and K. Sikes, "A Comparative Study on Emerging Electric Vehicle Technology Assessments," Oak Ridge National Laboratory (ORNL), Technical Report, 2011.

[64] Society of Automotive Engineers (SAE), "SAE Electric Vehicle and Plug in Hybrid Electric Vehicle Conductive Charge Coupler," *J1772_201210*, 2012.

[65] K. Morrow, D. Karner, and J. Francfort, "Plug-in Hybrid Electric Vehicle Charging Infrastructure Review," *US Department of Energy-Vehicle Technologies Program*, 2008.

[66] K. Parks, P. Denholm, and A. J. Markel, *Costs and Emissions Associated with Plug-in Hybrid Electric Vehicle Charging in The Xcel Energy Colorado Service Territory.* National Renewable Energy Laboratory Golden, CO, 2007.

[67] J. Taylor, A. Maitra, M. Alexander, D. Brooks, and M. Duvall, "Evaluations of Plug-in Electric Vehicle Distribution System Impacts," in *Power and Energy Society General Meeting, 2010 IEEE.* IEEE, 2010, pp. 1–6.

[68] E. Sortomme, M. M. Hindi, S. J. MacPherson, and S. Venkata, "Coordinated Charging of Plug-In Hybrid Electric Vehicles to Minimize Distribution System Losses," *Smart Grid, IEEE Transactions on*, vol. 2, no. 1, pp. 198–205, 2011.

[69] S. Shahidinejad, S. Filizadeh, and E. Bibeau, "Profile of Charging Load on the Grid due to Plug-in Vehicles," *Smart Grid, IEEE Transactions on*, vol. 3, no. 1, pp. 135–141, 2012.

[70] S. W. Hadley and A. A. Tsvetkova, "Potential Impacts of Plug-in Hybrid Electric Vehicles on Regional Power Generation," *The Electricity Journal*, vol. 22, no. 10, pp. 56–68, 2009.

[71] A. Ashtari, E. Bibeau, S. Shahidinejad, and T. Molinski, "PEV Charging Profile Prediction and Analysis based on Vehicle Usage Data," *Smart Grid, IEEE Transactions on*, vol. 3, no. 1, pp. 341–350, 2012.

[72] A. A. Pesaran, "Choices and Requirements of Batteries for EVs, HEVs, PHEVs," *National Renewable Energy Laboratory (NREL)*, 2011.

[73] D. Rastler, "Electricity Energy Storage Technology Options: A White Paper Primer on Applications, Costs and Benefits," *Electric Power Research Institute*, 2010.

[74] A. de Guibert, "Innovation in Industrial Technologies: The Case of Batteries," in *Industrial Technologies, Aarhus, Denmark*, 2012.

[75] P. G. Bruce, B. Scrosati, and J.-M. Tarascon, "Nanomaterials for Rechargeable Lithium Batteries," *Angewandte Chemie International Edition*, vol. 47, no. 16, pp. 2930–2946, 2008.

[76] R. Spotnitz, "Advanced EV and HEV Batteries," in *Vehicle Power and Propulsion, 2005 IEEE Conference.* IEEE, 2005, pp. 4–pp.

[77] H. A. Kiehne, “Battery Technology Handbook,” *by D. Berndt.* CRC Press, 2003, vol. 60.

[78] J. Eyer and G. Corey, “Energy Storage for the Electricity Grid: Benefits and Market Potential Assessment Guide,” *Sandia National Laboratories*, 2010.

[79] M. Safari, M. Morcrette, A. Teyssot, and C. Delacourt, “Multimodal Physics-based Aging Model for Life Prediction of Li-ion Batteries,” *Journal of The Electrochemical Society*, vol. 156, no. 3, pp. A145–A153, 2009.

[80] International Energy Agency (IEA), “World Energy Outlook–2010,” Technical Report, Paris, 2010.

[81] International Energy Agency (IEA), “Energy Technology Perspectives–2014,” Technical Report, Paris, 2014.

[82] J. Walker and N. Jenkins, “Wind Energy Technology,” *John Wiley & Sons Canada*, 1997.

[83] G. L. Johnson, “Wind Energy Systems,” *Prentice-Hall Englewood Cliffs*, (NJ), 1985.

[84] P. Jain, “Wind Energy Engineering,” *McGraw-Hill Education*, 2010.

[85] International Energy Agency (IEA), “Energy Technology Perspectives: Scenarios and Strategies to 2020,” Technical Report, Paris, 2008.

[86] International Energy Agency (IEA), “Technology Roadmap–Wind Energy,” Technical Report, Paris, 2010.

[87] M. Bolinger, “2008 Wind Technologies Market Report,” *Lawrence Berkeley National Laboratory*, 2010.

[88] US EIA, “Annual Energy Outlook 2012,” *US Energy Information Administration, Washington, DC*, 2012.

[89] J. Baker and A. Collinson, “Electrical Energy Storage at the Turn of the Millennium,” *Power Engineering Journal*, vol. 13, no. 3, pp. 107–112, 1999.

[90] B. K. Parsons, M. Milligan, J. C. Smith, E. DeMeo, B. Oakleaf, K. Wolf, M. Schuerger, R. Zavadil, M. Ahlstrom, and D. Y. Nakafuji, *Grid Impacts of Wind Power Variability: Recent Assessments from a Variety of Utilities in the United States.* National Renewable Energy Laboratory, 2006.

[91] E. Hittinger, J. Whitacre, and J. Apt, “What Properties of Grid Energy Storage Are Most Valuable?” *Journal of Power Sources*, vol. 206, pp. 436–449, 2012.

[92] B. V. Mathiesen, H. Lund, and K. Karlsson, "100% Renewable Energy Systems, Climate Mitigation and Economic Growth," *Applied Energy*, vol. 88, no. 2, pp. 488–501, 2011.

[93] M. Z. Jacobson and M. A. Delucchi, "Providing All Global Energy with Wind, Water, and Solar Power, Part I: Technologies, Energy Resources, Quantities and Areas of Infrastructure, and Materials," *Energy Policy*, vol. 39, no. 3, pp. 1154–1169, 2011.

[94] M. A. Delucchi and M. Z. Jacobson, "Providing All Global Energy with Wind, Water, and Solar Power, Part II: Reliability, System and Transmission Costs, and Policies," *Energy Policy*, vol. 39, no. 3, pp. 1170–1190, 2011.

[95] S. Becker, B. A. Frew, G. B. Andresen, M. Z. Jacobson, S. Schramm, and M. Greiner, "Renewable Build-Up Pathways for the US: Generation Costs Are Not System Costs," *Energy*, vol. 81, pp. 437–445, 2015.

[96] M. Z. Jacobson, M. DeLucchi, G. Bazouin, Z. A. Bauer, C. C. Heavey, E. Fisher, S. B. Morris, D. J. Piekutowski, T. A. Vencill, and T. W. Yeskoo, "100% Clean and Renewable Wind, Water, and Sunlight (WWS) All-Sector Energy Roadmaps for the 50 United States," *Energy & Environmental Science*, 2015.

[97] Sustainable Canada Dialogues, "Acting on Climate Change: Solutions from Canadian Scholars," Technical Report, 2015.

[98] L. Ahmadi, M. Fowler, S. B. Young, R. A. Fraser, B. Gaffney, and S. B. Walker, "Energy Efficiency of Li-ion Battery Packs Re-Used in Stationary Power Applications," *Sustainable Energy Technologies and Assessments*, vol. 8, pp. 9–17, 2014.

[99] A. Pesaran, C. Ban, A. Dillon, J. Gonder, J. Ireland, M. Keyser, G.-H. Kim, K.-J. Lee, D. Long, J. N. S. Santhanagopalan *et al.*, "FY2011 Annual Report for NREL Energy Storage Projects," *Contract*, vol. 303, pp. 275–3000, 2012.

[100] L. Ahmadi, A. Yip, M. Fowler, S. B. Young, and R. A. Fraser, "Environmental Feasibility of Re-Use of Electric Vehicle Batteries," *Sustainable Energy Technologies and Assessments*, vol. 6, pp. 64–74, 2014.

[101] W. Kempton and J. Tomić, "Vehicle-to-Grid Power Fundamentals: Calculating Capacity and Net Revenue," *Journal of power sources*, vol. 144, no. 1, pp. 268–279, 2005.

[102] S. Shahidinejad, E. Bibeau, and S. Filizadeh, "Statistical Development of A Duty Cycle for Plug-in Vehicles in A North American Urban Setting Using Fleet Information," *Vehicular Technology, IEEE Transactions on*, vol. 59, no. 8, pp. 3710–3719, 2010.

[103] J. Neubauer and A. Pesaran, "PHEV/EV Li-ion Battery Second-Use Project," in *Conference paper presented at the Advanced Automotive Batteries Conference (AABC)*, 2010.

[104] C. A. Rosenkranz, "Modern Battery Systems for Plug-in Hybrid Electric Vehicles," *Power*, vol. 1, no. 10, p. 100, 2007.

[105] J. Axsen, A. Burke, and K. S. Kurani, "Batteries for Plug-in Hybrid Electric Vehicles (PHEVs): Goals and the State of Technology Circa 2008," *Institute of Transportation Studies*, 2008.

[106] R. Gasch and J. Twele, "Wind Power Plants: Fundamentals, Design, Construction and Operation," *Electrical Engineering Springer*, 2011.

[107] J. F. Manwell, J. G. McGowan, and A. L. Rogers, "Wind Energy Explained: Theory, Design and Application," *2nd Ed., John Wiley & Sons*, 2009.

[108] C. Carrillo, A. O. Montaño, J. Cidrás, and E. Díaz-Dorado, "Review of power curve modelling for wind turbines," *Renewable and Sustainable Energy Reviews*, vol. 21, no. 0, pp. 572 – 581, 2013.

[109] M. Lydia, S. S. Kumar, A. I. Selvakumar, and G. E. P. Kumar, "A Comprehensive Review on Wind Turbine Power Curve Modeling Techniques," *Renewable and Sustainable Energy Reviews*, vol. 30, no. 0, pp. 452 – 460, 2014.

[110] A. Kusiak, H. Zheng, and Z. Song, "On-line Monitoring of Power Curves," *Renewable Energy*, vol. 34, no. 6, pp. 1487 – 1493, 2009.

[111] M. Hollander, D. Wolfe, and E. Chicken, "Nonparametric Statistical Methods," *Wiley Series in Probability and Statistics*, 2013.

[112] M. G. Khalfallah and A. M. Koliub, "Suggestions for Improving Wind Turbines Power Curves," *Desalination*, vol. 209, no. 1-3, pp. 221 – 229, 2007, the Ninth Arab International Conference on Solar Energy (AICSE-9), Kingdom of Bahrain.

[113] P. Giorsetto and K. F. Utsurogi, "Development of A New Procedure for Reliability Modeling of Wind Turbine Generators," *Power Apparatus and Systems, IEEE Transactions on*, vol. PAS-102, no. 1, pp. 134–143, Jan 1983.

[114] R. Chedid, H. Akiki, and S. Rahman, "A Decision Support Technique for the Design of Hybrid Solar-Wind Power Systems," *Energy conversion, ieee transactions on*, vol. 13, no. 1, pp. 76–83, 1998.

[115] M. Lydia, A. Selvakumar, S. Kumar, and G. Kumar, "Advanced Algorithms for Wind Turbine Power Curve Modeling," *Sustainable Energy, IEEE Transactions on*, vol. 4, no. 3, pp. 827–835, July 2013.

[116] A. Marvuglia and A. Messineo, "Monitoring of Wind Farms' Power Curves Using Machine Learning Techniques," *Applied Energy*, vol. 98, no. 0, pp. 574 – 583, 2012.

[117] T. Üstüntaş and A. D. Şahin, "Wind Turbine Power Curve Estimation based on Cluster Center Fuzzy Logic Modeling," *Journal of Wind Engineering and Industrial Aerodynamics*, vol. 96, no. 5, pp. 611–620, 2008.

[118] A. Kusiak, H. Zheng, and Z. Song, "Models for Monitoring Wind Farm Power," *Renewable Energy*, vol. 34, no. 3, pp. 583 – 590, 2009.

[119] T. J. Hastie and R. J. Tibshirani, "Generalized Additive Models," *Chapman & Hall, London*,1990.

[120] B. Ai, H. Yang, H. Shen, and X. Liao, "Computer-Aided Design of PV/Wind Hybrid System," *Renewable Energy*, vol. 28, no. 10, pp. 1491 – 1512, 2003.

[121] S. Diaf, D. Diaf, M. Belhamel, M. Haddadi, and A. Louche, "A Methodology for Optimal Sizing of Autonomous Hybrid PV/Wind System," *Energy Policy*, vol. 35, no. 11, pp. 5708 – 5718, 2007.

[122] T. Ackermann and L. Soder, "Wind Energy Technology and Current Status: A Review," *Renewable and Sustainable Energy Reviews*, vol. 4, no. 4, pp. 315 – 374, 2000.

[123] T. Ackermann, "Wind Power in Power Systems," *Wiley and Sons, Hoboken, NJ*, 2012.

[124] A. Betz, "Das maximum der theoretisch moglichen ausnutzung des windes durch windmotoren, the maximum of the theoretically possible exploitation of the wind by wind motors," *Z. Gesamte Turbinenwesen*, vol. 26, 1926.

[125] W. S. Cleveland and S. J. Devlin, "Locally Weighted Regression: An Approach to Regression Analysis by Local Fitting," *Journal of the American Statistical Association*, vol. 83, pp. 596–610, 1988.

[126] W. S. Cleveland, "Robust Locally Weighted Regression and Smoothing Scatterplots," *Journal of the American Statistical Association*, vol. 74, pp. 829–836, 1979.

[127] T. J. Hastie, R. J. Tibshirani, and J. H. Friedman, *The Elements of Statistical Learning : Data Mining, Inference, and Prediction*, *Springer, New York*, 2009.

[128] V. Thapar, G. Agnihotri, and V. K. Sethi, "Critical Analysis of Methods for Mathematical Modelling of Wind Turbines," *Renewable Energy*, vol. 36, no. 11, pp. 3166 – 3177, 2011.

[129] G. Wahba, "Spline Models for Observational Data," *Society for Industrial and Applied Mathematics (SIAM)*, Philadelphia, PA: 1990, vol. 59.

[130] J. H. Friedman and B. W. Silverman, "Flexible Parsimonious Smoothing and Additive Modeling," *Technometrics*, vol. 31, no. 1, pp. 3–21, 1989.

[131] D. Ruppert, "Selecting the Number of Knots for Penalized Splines," *Journal of Computational and Graphical Statistics*, vol. 11, no. 4, pp. 735–757, 2002.

[132] IEC-61400-12-1, "Power Performance Measurements of Electricity Producing Wind Turbines," International Standard, Technical Report, 61400-12-1, December 2005.

[133] S. Li, D. Wunsch, E. O'Hair, and M. Giesselmann, "Using Neural Networks to Estimate Wind Turbine Power Generation," *Energy Conversion, IEEE Transactions on*, vol. 16, no. 3, pp. 276–282, Sep 2001.

[134] Z. Liu, W. Gao, Y.-H. Wan, and E. Muljadi, "Wind Power Plant Prediction by Using Neural Networks," in *Energy Conversion Congress and Exposition (ECCE), 2012 IEEE*, 2012, pp. 3154–3160.

[135] A. Kusiak and X. Wei, "A Data-Driven Model for Maximization of Methane Production in A Wastewater Treatment Plant." *Water Science & Technology*, vol. 65, no. 6, 2012.

[136] J. Barton and D. Infield, "Energy Storage and Its Use with Intermittent Renewable Energy," *Energy Conversion, IEEE Transactions on*, vol. 19, no. 2, pp. 441–448, June 2004.

[137] H. Lund and B. V. Mathiesen, "Energy System Analysis of 100% Renewable Energy Systems? The Case Of Denmark in Years 2030 And 2050," *Energy*, vol. 34, no. 5, pp. 524–531, 2009.

[138] M. Korpaas, A. T. Holen, and R. Hildrum, "Operation and Sizing of Energy Storage for Wind Power Plants in A Market System," *International Journal of Electrical Power & Energy Systems*, vol. 25, no. 8, pp. 599–606, 2003.

[139] H. Lund, "Large-Scale Integration of Wind Power into Different Energy Systems," *Energy*, vol. 30, no. 13, pp. 2402–2412, 2005.

[140] W. F. Hederman, "IEEE Report to DOE Quadrennial Energy Review on Priority Issues," 2014.

[141] P. Alotto, M. Guarnieri, and F. Moro, "Redox flow batteries for the storage of renewable energy: a review," *Renewable and Sustainable Energy Reviews*, vol. 29, pp. 325–335, 2014.

[142] A. Castillo and D. F. Gayme, "Grid-Scale Energy Storage Applications in Renewable Energy Integration: A Survey," *Energy Conversion and Management*, vol. 87, pp. 885–894, 2014.

[143] P. Denholm and M. Hand, "Grid Flexibility and Storage Required to Achieve Very High Penetration of Variable Renewable Electricity," *Energy Policy*, vol. 39, no. 3, pp. 1817–1830, 2011.

[144] C. Justus, W. Hargraves, A. Mikhail, and D. Graber, "Methods for Estimating Wind Speed Frequency Distributions," *Journal of applied meteorology*, vol. 17, no. 3, pp. 350–353, 1978.

[145] S. E. Tuller and A. C. Brett, "The Characteristics of Wind Velocity That Favor the Fitting of A Weibull Distribution in Wind Speed Analysis," *Journal of Climate and Applied Meteorology*, vol. 23, no. 1, pp. 124–134, 1984.

[146] K. Conradsen, L. B. Nielsen, and L. P. Prahm, "Review of Weibull Statistics for Estimation of Wind Speed Distributions," *Journal of Climate and Applied Meteorology*, vol. 23, no. 8, pp. 1173–1183, 2014/03/10 1984.

[147] N. Johnson, S. Kotz, and N. Balakrishnan, "Continuous Univariate Distributions," *Applied Probability and Statistics, Wiley & Sons*, 1995, no. v. 2.

[148] J. P. Hennessey Jr, "A Comparison of the Weibull and Rayleigh Distributions for Estimating Wind Power Potential," *Wind Engineering*, vol. 2, pp. 156–164, 1978.

[149] A. N. Celik, "A Statistical Analysis of Wind Power Density Based on the Weibull and Rayleigh Models at the Southern Region of Turkey," *Renewable Energy*, vol. 29, no. 4, pp. 593 – 604, 2004.

[150] M. Stevens and P. Smulders, "The Estimation of the Parameters of the Weibull Wind Speed Distribution for Wind Energy Utilization Purposes," *Wind engineering*, vol. 3, pp. 132–145, 1979.

[151] A. Garcia, J. Torres, E. Prieto, and A. de Francisco, "Fitting Wind Speed Distributions: A Case Study," *Solar Energy*, vol. 62, no. 2, pp. 139 – 144, 1998.

[152] L. M. Le Cam, "On Some Asymptotic Properties of Maximum Likelihood Estimates and Related Bayes' Estimates," *University of California Press*, 1953, vol. 1, no. 11.

[153] B. Dodson, "The Weibull Analysis Handbook," *ASQ Quality Press*, 2006.

[154] T. J. Ypma, "Historical development of the Newton–Raphson Method," *SIAM review*, vol. 37, no. 4, pp. 531–551, 1995.

[155] C. G. Justus, W. R. Hargraves, and A. Yalcin, "Nationwide Assessment of Potential Output from Wind-Powered Generators," *Journal of Applied Meteorology*, vol. 15, no. 7, pp. 673–678, 2014/03/10 1976.

[156] J. P. Hennessey, "Some Aspects of Wind Power Statistics," *Journal of Applied Meteorology*, vol. 16, no. 2, pp. 119–128, 1977.

[157] S. Shokrzadeh, M. Jafari Jozani, and E. Bibeau, "Wind Turbine Power Curve Modeling Using Advanced Parametric and Nonparametric Methods," *Sustainable Energy, IEEE Transactions on*, vol. 5, no. 4, pp. 1262–1269, Oct 2014.

[158] S. Kotz, T. Kozubowski, and K. Podgorski, *The Laplace Distribution and Generalizations: A Revisit with Applications to Communications, Exonomics, Engineering, and Finance.* Springer, 2001, no. 183.

[159] L. Bain, J. Eastman, M. Engelhardt, A. R. L. (U.S.), and M. U. ROLLA., "A Study of Life-Testing Models and Statistical Analyses for the Logistic Distribution," Defense Technical Information Center, 1973.

[160] R. Wachal, F. Mosallat, D. Williams, A. Chevrefils, W. Erickson, A. Darbandi, and R. Yonza, "Stationery Energy Storage System Using Second Life EV Batteries," in *2014 CIGRÉ Canada Conference*.

[161] H. A. Kiehne, *Battery Technology Handbook.* CRC Press, 2003, vol. 60.

[162] Electric Drive Transportation Association, "Electric drive sales dashboard." http://www.electricdrive.org/index.php?ht=d/sp/i/20952/pid/20952, accessed: 2014-08-26.

[163] J. Eaves and Z. Bizhuang, "A Dynamic Forecasting Model of PHEV and BEV Diffusion when Drivers Are Economically Motivated," *Working Paper, Laval University.*

[164] CANSIM Statistics Canada, "New Motor Vehicle Sales, Canada." http://www.electricdrive.org/index.php?ht=d/sp/i/20952/pid/20952, accessed: 2014-08-26.

[165] Canadian Wind Energy Association (CanWEA), "Wind Vision 2025," *Canadian Wind Energy Association, Technical Report*, 2008.

[166] Office of Energy Efficiency–Natural Resources Canada, "Energy efficiency trends in Canada, 1990 to 2009," Technical Report, Ottawa, 2011.

[167] Office of Energy Efficiency–Natural Resources Canada, "Energy Use Data Handbook, 1990 to 2007," Tech. Rep., Ottawa, 2010.

[168] Statistics Canada, "Energy Statistics Handbook – First Quarter 2012," Technical Report, Ottawa, 2012.

[169] Navigant Research, "Electric Vehicle Batteries," Technical Report, Boulder, 2014.

[170] R. Hensley, S. Knupfer, and D. Pinner, "Electrifying Cars: How Three Industries Will Evolve," *McKinsey Quarterly*, vol. 3, no. 2009, pp. 87–96, 2009.

[171] M. R. Milligan, "Modelling Utility-Scale Wind Power Plants. Part 2: Capacity Credit," *Wind Energy*, vol. 3, no. 4, pp. 167–206, 2000.